Embryonic and foetal germ cell development in the marmoset monkey: comparative *in situ* and cell culture studies

Dissertation

for the award of the degree
"Doctor rerum naturalium"
of the Georg-August University Göttingen
within the doctoral program "Biology"
of the Georg-August University School of Science (GAUSS)

Submitted by

Eva Wolff (née Grün)

from Kaiserslautern, Germany

Göttingen 2018

Members of the Thesis Committee:

Prof Dr Rüdiger Behr
Platform Degenerative Diseases
German Primate Center

Prof Dr Sigrid Hoyer-Fender
Department of Developmental Biology
Johann-Friedrich-Blumenbach-Institute for Zoology und Anthropology
Georg-August University Göttingen

Members of the Examination Board:

Referee: Prof Dr Rüdiger Behr
              Platform Degenerative Diseases
              German Primate Center

2nd Referee: Prof Dr Sigrid Hoyer-Fender
              Department of Developmental Biology
              Johann-Friedrich-Blumenbach-Institute for Zoology und Anthropology
              Georg-August University Göttingen

Further Members of the Examination Board:

Prof Dr Susann Boretius
Functional Imaging Laboratory
German Primate Center

Prof Dr Gregor Bucher
Department of Evolutionary Developmental Biology
Johann-Friedrich-Blumenbach-Institute for Zoology und Anthropology
Georg-August University Göttingen

Dr Ufuk Günesdogan
Department of Developmental Biology
Johann-Friedrich-Blumenbach-Institute for Zoology und Anthropology
Georg-August University Göttingen

Dr Christian Roos
Primate Genetics Laboratory
German Primate Center

Date of oral examination: 15th October 2018
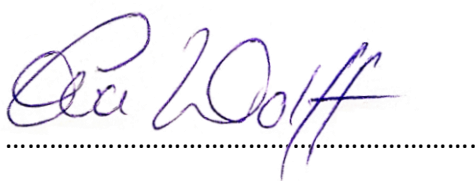
Affidavit & Disclosure

This project was conducted at the Research Platform Degenerative Diseases (formerly Stem Cell Biology Unit) of the German Primate Center in the group of Prof Dr Rüdiger Behr from April 2015 to September 2018.

I hereby declare that I conducted the described experiments on my own, with no other materials, references and aids than quoted.

Parts of this work were already presented at the 9th International Meeting of the Stem Cell Network North Rhine Westphalia, Münster, Germany in May 2017, at the 7th DVR-Kongress, Munich, Germany in December 2017 and the 20th European Testis Workshop, Obidos, Portugal in May 2018.

A manuscript entitled "Primordial germ cells do not migrate along nerve fibres in marmoset monkey and mouse embryos" was submitted for publication in the Journal *Reproduction* and after the peer-review process invited for resubmission with only minor revisions. The data are expected to be published within the course of this year.

Göttingen, 17th September 2018

………………………………………………………….
Eva Wolff

Acknowledgements

I also owe my gratitude to several collaborators inside and outside of the DPZ: Prof Henrik Kaessmann and his group in Heidelberg for performing the single cell transcriptome analyses. Prof Christoph Viebahn for teaching me embryo microdissection; Prof Hubert Schorle and his group in Bonn for showing me their PGC culture and generously providing feeder cells; Dr Jessica Nolte and Dr Nadine Mellies for providing mouse ESCs; Dr Berit Neumann for helping me with the FACS; the caretakers at the MPI and ENI animal facilities where we obtained mice; the Hormone Laboratory for the blood analyses and especially the technicians of the Infection Pathology Laboratory for all the small services to make our histology run smoothly!

Representative for the many employees of the DPZ who make this a great place to work, I want to thank our animal caretakers, the ladies at human resources and the IT-guys (without whom we scientists would all be lost ;).

I would also like to thank my husband, my parents and the rest of my family and friends for the enormous support you gave me throughout all my studies, and for making my life happy!

Last but not least, I want to thank Selma, Ohbi and all the other "furry employees" for making me one of the few lucky people that are actually looking forward to come to work on Monday mornings.

Table of Contents

Abbreviations

AF-488	AlexaFluor-488
AP	Alkaline Phosphatase
bFGF	Basic fibroblast growth factor
BMP	Bone morphogenic protein
BSA	Bovine serum albumin
C.j.	*Callithrix jacchus*
CRL	Crown-Rump-Length
CS	Carnegie stage
DAB	3,3'-Diaminobenzidine
DMEM	Dulbeco's modified eagle medium
dNTPs	Deoxyribonukleoside triphosphates
DPZ	Deutsches Primatenzentrum
E	Embryonic day
EAA	Essential amino acids
ECL	Enhanced chemiluminescence
EDTA	Ethylenediaminetetraacetic acid
EGC	Embryonic germ cell
ESC	Embryonic stem cell
ESM	Embryonic stem cell medium
EtOH	Ethanol
FACS	Fluorescence activated cell sorting
FCS	Foetal calf serum
GD	Gestational day
(U)GR	(Uro-) Genital ridge
GSK	Glycogen synthase kinase
HE	Haematoxylin and eosin
HRP	Horseradish peroxidase
ICM	Inner cell mass
IF	Immunofluorescence
IHC	Immunohistochemistry

iPSC	Induced pluripotent stem cell
IWR1	Inhibitor of Wnt response 1
kDa	Kilo-Dalton
LIF	Leukaemia inhibitory factor
MACS	Magnetism associated cell sorting
MAP2	Microtubule-associated protein 2
MEF	Mouse embryonic fibroblast
MEK	MAP-Kinase/Erk kinase
MN	Mesonephros
N.D.	Not determined
NEAA	Non-essential amino acids
NHP	Non-human primate
NLS	Nuclear localisation sequence
OCT4	Octamer-binding transcription factor 4
PBS	Phosphate buffered saline
(q)PCR	(quantitative) Polymerase chain reaction
PFA	Paraformaldehyde
PGC	Primordial germ cells
PGF2α	Prostaglandin $F_{2\alpha}$
PSC	Pluripotent stem cell
P/S	Penicillin/Streptomycin
RA	Retinoic acid
RT	Reverse transcription *or* Room temperature
SCF	Stem cell factor
SDS	Sodium dodecyl sulfate
TAE	Tris base, acetic acid and EDTA
Tris	Tris(hydroxymethyl)-aminomethan
TUBB3	Beta-tubulin type 3

List of Figures

List of Tables

Abstract

Primordial germ cells (PGCs) are the precursors of sperm and egg cells. They arise early in mammalian embryonic development and have to translocate from their extraembryonic tissue of specification over a significant distance to reach the prospective gonads. The development of mammalian PGCs has been investigated mostly in rodents due to the broad availability of mouse embryos and the genetic tools established in this species. However, results obtained in mice cannot be directly transferred onto the human and other species, and many questions remain concerning PGC specification and migration mechanisms. Therefore, this project aimed at investigating germ cell development in a non-human primate animal model, the common marmoset monkey (*Callithrix jacchus*). One goal was the *in situ* characterisation of PGCs in marmoset embryo tissue sections and identification of new PGC specific marker proteins. This led to the discovery of Aminopeptidase N (ANPEP) expression on the cell surface of marmoset PGCs.

A study on human embryos demonstrated a close spatial relationship between migrating PGCs and peripheral nerves, suggesting a guiding function of the neurons. Therefore, I tested the hypothesis that this might be a conserved strategy in mammalian PGC development by analysing sections of mouse and common marmoset monkey embryos via immunohistochemical double staining. In both investigated species, no spatial association between neurons and migrating PGCs could be detected, and the PGCs had reached the gonads before neurons could be detected in the gonads' vicinity.

Pluripotent stem cells (PSCs) form the basis of emerging therapies to degenerative diseases since they can develop into all tissues of the adult body. PGCs can be considered as potentially pluripotent cells, and the culture of mouse and human PGCs was reported to result in the derivation of PSC lines, so called embryonic germ cells (EGCs). Therefore, it was the second aim of this study to establish EGC lines of the marmoset monkey, and compare them with already available marmoset embryonic stem cells and induced pluripotent stem cells. For this purpose, PGCs were isolated from marmoset embryos of defined developmental stages and cultured according to published protocols. Even after testing several culture approaches, no EGCs could be derived from marmoset PGCs.

This work provides new insights into PGC translocation in mammals and identifies ANPEP as a novel PGC surface protein in the marmoset monkey. However, for the conversions of PGCs to EGCs additional cell culture conditions need to be tested.

1. Introduction

1.1 The Marmoset Monkey and Other Non-Human Primate Animal Models

1.1.1 The common marmoset monkey (*Callithrix jacchus*)

The common marmoset monkey (*Callithrix jacchus*) is a New World monkey that belongs to the family of Callithrichidae, together with other marmosets, tamarins and lion tamarins (**Figure I**). The feature that sets the members of Callithrichidae apart from other New World monkeys is their possession of claw-like nails known as tegulaes on most of their fingers, which are used for climbing and scratching tree bark. They originate from the north-eastern coast of Brazil[1]. Marmosets are arboreal animals that eat insects, fruit, seeds and bird eggs, but mostly rely on plant exudates such as gum, sap and latex for their diet[1]. They live in stable family groups of around nine animals with only one dominant breeding pair to avoid incest[2]. The breeding pair relies on the help of the other family members in raising the offspring, which are typically born twice per year typically in twin pairs[3].

Like human embryos, marmoset embryos can be classified into 23 developmental stages, so-called Carnegie stages (CS), based on somite- and limb development[4]. The embryonic development of the marmoset is strongly delayed compared to humans or other non-human primates[5-7]. At the gestational day (GD) of implantation (~GD 12), this delay between marmoset and human is approx. 5 days, and at CS 11 approx. 25 days[6]. Between CS 11 and 23, however, the speed of development is comparable, meaning that the delay at CS 23 is still 25 days. After this the development accelerates and the delay is made up for during foetal development so that the total gestation time in marmosets is 143 days[6] (compared to approx. 267 days in humans). At birth marmosets are particularly locomotorily well-developed in order to cling to the parents' back fur. Marmoset offspring are weened after approx. 3 months and reach adult size and sexual maturity with approx. 15 months of age[8]. Healthy adult common marmosets in captivity weigh between 350 and 550 grams, with males being slightly larger than females. Their small body size makes housing and handling of common marmosets relatively easy and affordable. There are also no known zoonoses that can be transmitted to humans.

Marmosets have become an important model species in biomedical research. As mentioned, housing and handling of marmosets is relatively easy compared to other non-human primates (NHP), while they still exhibit representative primate biology. They are used to investigate basic principles of - among others - genetics[9], immunology[10], neurology[11], stem cell biology[12-14], embryology[15, 16] and reproduction[17, 18], but have also become a popular animal model of human diseases such as Alzheimer's[19] or autism[20]. Also, the first New World monkey genome sequenced was that of a female common marmoset[21].

1.1.2 Macaques as non-human primate animal models

Macaques are a genus of Old World monkeys of the subfamily Cercopithecinae (**Figure I**), with its 23 species distributed all over the world, making macaques the most widespread primate genus apart from humans. Some well-known species include the Barbary macaque (*Macaca sylvanus*) which lives in northern Africa and the Rock of Gibraltar, the Japanese macaque (*M. fuscata*), the lion-tailed macaque (*M. silenus*), the cynomolgus monkey (*M. fascicularis*) and the rhesus monkey (*M. mulatta*). The last two species are of special interest since they are popular animal models in biomedical research[22]. As can be seen in **Figure I**, old world monkeys are relatively closely related to humans. Some research questions and medical applications make it indispensable to have an animal model that resembles the human as closely as possible, for example for the development of vaccines. Since animal experiments on apes are ethically difficult and forbidden in many countries including the EU, macaques are the best-established alternative for such a model organism. Especially the rhesus monkey is well characterised and widely used in neuroscience and infection research as well as transplantation studies and drug testing[23]. In contrast to the common marmoset, however, rhesus monkeys have some disadvantages. They only produce one offspring per year and take 4 years to reach sexual maturity. They are bigger and more aggressive so that, unless they are trained, most handling and treatment actions on the animals require anaesthesia, and, most importantly, they can carry zoonoses such as Herpes B, which can be lethal for humans[24, 25].

Lemurs (Lemuriformes)	Loris (Lorisidae)	Tarsiers (Tarsiiformes)	**New World monkeys** (Platyrrhini)	Colobines (Colobinae)	**Cheek pouch monkeys** (Cercopithecinae)	Gibbons (Hylobatidae)	Great apes incl. Humans (Hominidae)
106 species	35 species	11 species	175 species	78 species	82 species	20 species	7 species

20 Mio years

23 Mio years

Tailed Old World monkeys (Cercopithecoidea)

Apes (Hominoidea)

32 Mio years

Old World monkeys (Catarrhini)

46 Mio years

Simians (Simiiformes)

64 Mio years

57 Mio years

Wet-nosed primates (Strepsirrhini)

Dry-nosed primates (Haplorrhini)

68 Mio years

Flying lemurs (Dermoptera)

Primates

86 Mio years

Figure I | Primate evolution. A family tree of primate evolution. The years at the split branches indicate the last common ancestor. (Source: https://www.dpz.eu/en/info-center/knowledge/primates/evolution-and-diversity-of-primates.html. Layout: Luzie Almenräder. All images taken from internal resources or the Wikimedia foundation under Creative Commons license (https://commons.wikimedia.org)).

1.1.3 Gametogenesis in primates

Male gametes, the spermatozoa, are constantly produced in the seminiferous tubules of the adult testis. During embryonic development, after the germ cell precursors have reached the gonadal anlage, they proliferate and in males differentiate into gonocytes and then eventually to spermatogonia. The process of spermatogenesis starts after puberty and involves several steps that happen gradually from the basement membrane of a tubule towards the lumen (**Figure II**). Spermatogonia are found in direct contact to the basement membrane and multiply via a species-specific number of mitotic divisions[26], leading to self-renewal as well as differentiation into primary spermatocytes. Primary spermatocytes enter meiosis I to form secondary spermatocytes and upon completion of meiosis II form the so-called round spermatids[27]. During spermiogenesis, the spermatids elongate and mature into the spermatozoa or sperm cells, which are released from the germinal epithelium into the tubular lumen. Some seasonality in sperm production might occur, for example in the rhesus macaque[28], as adaptation to seasonal female oestrus. However, the marmoset as well as the human do not show any signs of reproductive seasonality.

21
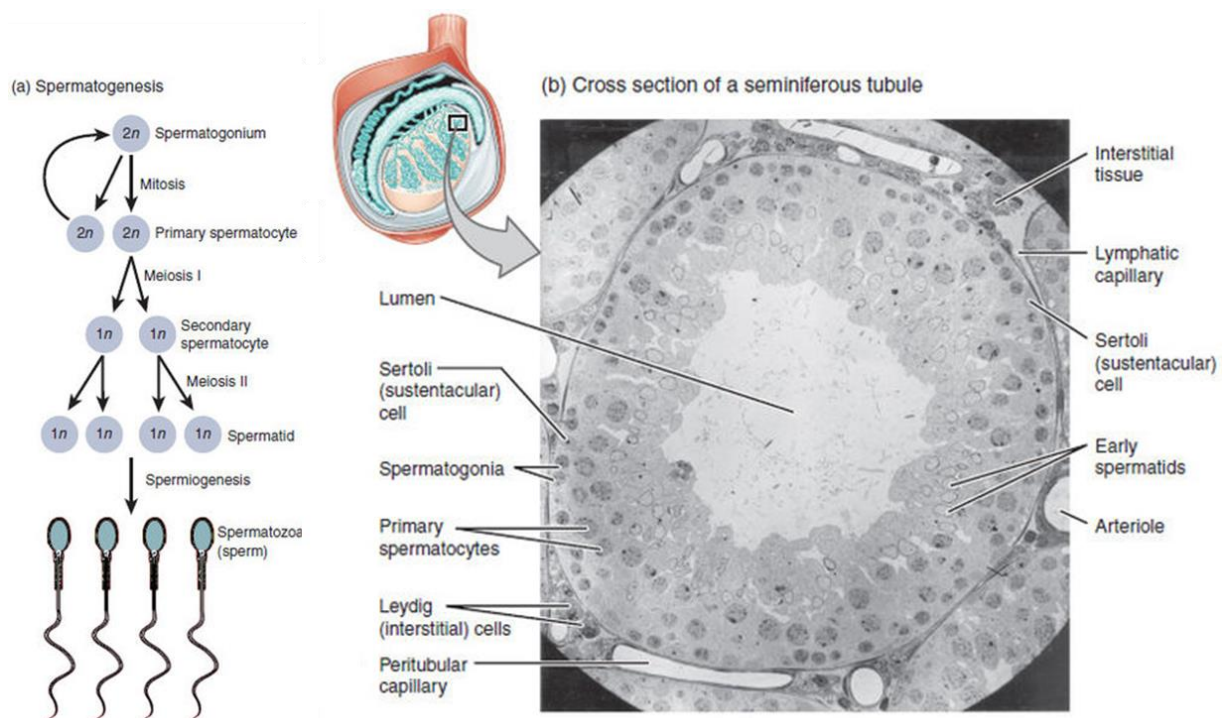
Figure II | Spermatogenesis. A) Schematic representation of spermatogenesis in humans and non-human primates. B) Histological cross-section of a seminiferous tubule and indication of different cell types. (Source: https://commons.wikimedia.org/wiki/File:Figure_28_01_04.jpg)

Female meiotic germ cells, so called oocytes, are found in the ovaries. During embryonic development, after the germ cell precursors have reached the gonadal anlage, they proliferate and in females differentiate into oogonia and then oocytes. The immature oogonia enter meiosis, thereby becoming primary oocytes, but arrest in meiosis I before birth and remain in this arrested state for several years. After puberty, only one oocyte becomes mature during each reproductive cycle, finishes the first meiotic division, enters meiosis II and becomes competent for fertilisation. Only after fertilisation occurs, meiosis II will be completed. The gamete pool of female primates is thus defined during foetal development before birth, and no neo-oogenesis seems to occur in adult females. In contrast to humans and rhesus monkeys, the neonatal ovary of the marmoset, however, still harbours substantial numbers of pre-meiotic oogonia[29]. This allows investigating primate pre-meiotic oocyte development in a non-human primate model by making them more easily accessible than in human foetuses.

1.2 Pluripotent Stem Cells

Totipotency is defined as the potential of a cell to give rise to a new organism, whereas pluripotent cells can differentiate into tissues of all three germ layers (ectoderm, endoderm, mesoderm), but not the extraembryonic structures. *In vivo*, totipotency only occurs in the fertilised zygote and after its division in the individual daughter cells up to at least the 4-cell-stage embryo[30-32]. After this, the cells diverge until the blastocyst stage, where the trophectoderm cells will form the extra-embryonic tissues such as the placenta and only the pluripotent cells of the inner cell mass (ICM) will develop into the embryo proper[33]. This was demonstrated by injection of epiblast cells into genetically different mouse blastocysts and resulting chimaera-formation[34]. The culture of ICM cells under appropriate culture conditions leads to the maintenance of this pluripotent state also *in vitro* in indefinitely self-renewing cell lines. These ICM-derived cell lines were termed embryonic stem cells (ESCs). ESC derivation was first achieved in mice in 1981[35, 36], in the rhesus monkey in 1995[37], in the common marmoset in 1996[38] and in humans in 1998[39]. The pluripotent state of ESCs can be confirmed by their expression of pluripotency factors (namely OCT4A and NANOG), the potential to differentiate into tissues of the three germ layers *in vitro* and *in vivo* via teratoma formation, and by their ability to contribute to a chimeric animal, although this is of course not feasible for human ESCs. The discovery of pluripotent stem cells (PSCs)

heralded a new age in biomedical research. Since it is theoretically possible to obtain all cell types of an organism by directed differentiation of PSCs into the target tissue, they form the basis for the development of new cell replacement therapies and tissue engineering strategies. Many degenerative diseases are currently untreatable, and it is the hope that with PSCs, lost tissue can be replaced, for example heart muscle cells after myocardial infarction[40], neurons in degenerative diseases such as Parkinson's[41], or retina cells in macular degeneration[42]. However, the use of ESCs for clinical applications comes with ethical concerns since the destruction of embryos is necessary for their derivation. There are also some technical issues such as the tumorigenic potential of PSCs and the immune rejection of the donor tissue by the host[43].

Apart from ESCs, a second pluripotent stem cell type is now available. So called induced pluripotent stem cells (iPSCs) were discovered in 2006[44]. It was hypothesised that genes important for ESCs, early embryo development and teratoma formation, might be able to re-induce pluripotency in differentiated adult cells upon external delivery and gene expression. In a laborious but elegant approach, an initial set of 24 ESC-relevant genes was identified and delivered into mouse fibroblasts via retro-viral vectors. This resulted in the emergence of ESC-like colonies with unlimited proliferative potential. Step by step, one factor was removed from the pool of the 24 genes and the ability of the remaining 23 to induce ESC-like cells was tested. This way, Yamanaka *et al*. identified four factors necessary and together sufficient for the creation of iPSCs: OCT4, SOX2, C-MYC and KLF4[44]. These iPSCs can form viable chimeric mice and can contribute to the mouse germ line, thus fulfilling the gold standard of pluripotency[45]. Even more impressive, fully iPSC-derived mice were generated using the tetraploid complementation method[46]. Human iPSCs were first derived by two groups. While the group around Yamanaka used the same four factors as for mouse iPSCs[47], the group around Thomson, who also derived the first human ESCs, used OCT4, SOX2, NANOG and LIN28 for successful reprogramming of human fibroblasts[48]. iPSCs can now be derived from a variety of adult tissues, such as skin fibroblasts, peripheral blood[49] and renal epithelial cells in the urine[50], so that there are no ethical concerns about the source of the cells potentially used for therapy. It is also possible to derive patient-specific iPSCs so that an autologous cell replacement therapy without immune rejection would be possible.

For the marmoset monkey, several embryonic stem cell as well as induced pluripotent stem cell lines were established and characterised in our lab and are available for further research[13, 14].

Before iPSCs were available, embryos were the only source for pluripotent stem cell derivation. It was therefore attempted by many researchers to find a more accessible and less controversial way to obtain PSCs. Several reports were published on the successful derivation of pluripotent cells from the neonatal mouse testis[51], and even spermatogonia-derived PSC from the adult mouse testis were cultured successfully[52, 53]. These were the first reports that show the potential of post-natal germ cells to convert back into a pluripotent state if they are cultured under the appropriate conditions. Studies on the derivation of pluripotent cells from human spermatogonia followed soon after[54-57], as did reports on adult ovary-derived pluripotent cells[58]. They are, however, strongly debated as of today. After the publication of human spermatogonia-derived PSCs, this was also attempted for the common marmoset monkey. While adult spermatogonia could be identified and maintained in culture, no pluripotent stem cells appeared[59]. As mentioned above, the neonatal marmoset ovary - in contrast to humans - still contains oogonia that express pluripotency factors[29]. Therefore, also neonatal ovary culture was attempted. It resulted in the appearance of possible oocyte-like cells, but not in the derivation of pluripotent stem cells[60].

1.3 Primordial Germ Cells

1.3.1 Definition, epigenetic reprogramming and pluripotency factor expression

Primordial germ cells (PGCs) arise early in embryonic development and are the undifferentiated precursors of sperm and egg cells[61]. They are fundamental in reproduction since they are the only cells during embryonic development able to relay their genetic information to the next generation. PGCs are considered unipotent since they only give rise to the gametes, however they are the only cells in the body which finally form a totipotent cell. Germ cells are present during the entire life span of an animal and the germ cell cycle closes with the fusion of a spermatozoon and an oocyte to create the zygote. In mammals, after the first cell divisions, PGCs arise in the newly formed organism via inducing paracrine

signals and translocate to their final destination, the forming gonadal ridges[62]. These will then develop into immature ovaries and testes around mid-gestation.

While in a differentiated cell the epigenome essentially remains the same over the lifespan throughout mitosis/meiosis, PGCs undergo significant epigenetic reprogramming via histone modification and DNA methylation changes[63]. During embryonic development, after implantation of the blastocyst the somatic cells gradually acquire a somatic epigenetic profile[63]. This includes inactivation of one X-chromosome in female cells. The DNA in the specified PGCs, however, becomes globally demethylated until even the marks on imprinted genes are erased, and it also comes to the reactivation of the X-chromosome in female PGCs[63]. Re-establishment of maternal or paternal imprinting in the respective gametes starts around birth[63].

In mammals, the available information about PGCs was gathered mostly in the mouse model. In mouse PGCs it was shown that shortly after their specification, pluripotency genes are re-upregulated and that, although their function in the germ line remains unclear, OCT4, SOX2 and NANOG are necessary for germ cell survival[64-66]. This dependency on pluripotency factors led to the hypothesis that PGCs can actually be considered as potentially pluripotent, and that in fact there is a latent cycle of pluripotency, from the inner cell mass over PGCs and through fertilisation over the zygote back to the ICM, which is sustained by a common transcription factor network[67]. Furthermore, mouse PGCs express the surface marker SSEA-1, which can be used to select and purify the cells[68], but do not seem to express other known ESC markers such as SSEA-3, -4, TRA-1-60 or TRA-1-81[69]. While in mice the investigation of PGCs is now relatively easy due to possibilities of transgenesis and reporter-genes, the identification of primate PGCs is still based on morphological criteria and immunohistochemical detection of PGC marker proteins.

Due to the actual lack of early human embryonic material, studies on human PGCs are rare and some important studies even date back as far as the early twentieth century[70, 71]. During that time, only histological observations were possible. Human PGCs could be identified in the yolk sac at the base of the allantois by the end of the third week of gestation, showing already at that time their extra-gonadal origin[70, 71]. From there, they are incorporated into the gut epithelium, where they can be found in gestational week four, invade the gut mesenchyme in week five and can be found in the developing genital ridges from the sixth week of gestation onward[61, 72]. Apart from the early description of human

PGC tissue locations, only little information was available for a long time. In 1953, the expression of Alkaline Phosphatase (AP) was detected on human PGCs[73]. As for the surface markers expressed on human ESCs, human PGCs also seem to express SSEA-1, -3 and -4, c-Kit and CXCR4, but not TRA-1-60 or TRA-1-81[74, 75]. More recently, attractive cell culture systems have become available as an alternative for *in vivo* human PGCs to make up for the lack of information on the molecular mechanisms behind human germ cell development[76, 77].

For the marmoset monkey, there is only one recent study available on PGCs. Aeckerle *et al*. investigated marmoset embryos of different developmental stages and confirmed that marmoset PGCs can be identified via the expression of the pluripotency factors OCT4A, LIN28, NANOG and SALL4, and also express the germ cell marker VASA[16]. A study by Sasaki *et al*. published in 2016 investigated PGCs in embryos of the cynomolgus monkey (*Macaca fascicularis*)[7]. In cynomolgus monkeys, the late embryonic Carnegie stages (CS) 17-23 are already formed between gestational day (GD) 35 – GD 55, which is in strong contrast to the common marmoset, where GD 50 approximately corresponds to CS 10, and CS 18 is reached approximately around GD 75[16]. During this developmental period, PGCs of the cynomolgus monkey (cyPGCs) are found in the embryonic gonad and express the transcription factors BLIMP1 and TFAP2C, the known pluripotency factors (OCT4, SALL4, NANOG, LIN28), germ cell specific proteins DDX4 (VASA) and DAZL, as well as the surface proteins TRA-1-60, TRA-1-81, D2-40 and c-KIT[7]. Gonadal cyPGCs also express SOX17. In contrast to its role in pluripotency and embryonic stem cells, and in contrast to mouse PGCs, primate PGCs do not seem to express SOX2[7, 78, 79].

1.3.2 PGC specification

In animals, there are two mechanisms by which germ cells are specified. One way is via so-called germ plasm[80]. The unfertilised oocyte of most animals exhibits an asymmetrical distribution of mRNAs and proteins, and therefore after cell division the daughter cells inherit a different fate via the differential presence of signal molecules. The daughter cells which inherited the cytoplasmic portion of the oocytes that made up the germ plasm will therefore become germ cells. In birds and mammals, however, the unfertilised oocyte is rather symmetric or, in other words, no equivalent of germ plasm has been identified so far, and the initial cell divisions result in equivalent totipotent daughter cells that all have the

potential to become germ cells. Therefore, PGCs have to be specified via inducing signals of neighbouring cells that will set them apart from somatic cells. In mice, PGCs are specified via inducing signals from cells of the proximal posterior epiblast starting at embryonic day (E) 6.0[62], and an initial population of 30 – 50 PGCs expressing distinctive markers has formed in the extra-embryonic mesoderm by E 7.25[81]. The signalling cascade in mouse PGCs is believed to start with bone morphogenic protein 2 (BMP2) and BMP4, which induce the expression of B-lymphocyte-induced maturation protein 1 (BLIMP1, also known as PR domain-containing 1 (PRDM1)), closely followed by PRDM14, which finally leads to the upregulation of PGC-specific genes *Tfap2c*, *fragilis* and *stella*. All of these markers can be detected in early mouse PGCs, as can the expression of Tissue Nonspecific Alkaline Phosphatase (TNAP)[82].

The knowledge about mammalian PGC specification was obtained mainly in mice. These results can however not be translated directly onto humans and other primates. For example, the tissues involved in mouse PGC specification, namely the extraembryonic ectoderm, seem to have no clear counterpart in humans[75]. Due to the lack of suitable human embryonic material, pluripotent stem cell culture studies are currently the only alternative to investigate human PGCs. Irie *et al*. in 2015 managed to derive human PGC-like cells (hPGCLC) from human pluripotent stem cells *in vitro* and thus were able to investigate the molecular mechanisms behind human PGC specification[76]. They found that SOX17, which is a critical transcription factor for the endodermal germ layer[83, 84], is also the key regulator for human PGC induction. SOX17 is detectable in hPGCLCs even before BLIMP1[76]. The role of BLIMP1 in hPGCLCs seems to be the suppression of endodermal and other somatic genes downstream of SOX17, which is different from its role in mice, where BLIMP1 seems to be the key regulator of PGC fate[85].

Until recently, no *in vivo* data was available on primate PGC specification. The earliest data available on human and primate PGCs described them during the migratory phase in gestational weeks 3-4, where they were initially found in the yolk sac endoderm. As described above, Sasaki *et al*. investigated PGC specification in embryos of the cynomolgus monkey and shed first light on the involved tissues and mechanisms[7]. After establishing a panel of gonadal cyPGC markers, the combinatorial detection of these validated markers allowed them to identify also migrating PGCs, and they finally traced them back to their origin in early post-implantation embryos of GD 11 to GD 17. It was shown that

SOX17/TFAP2C-double positive PGCs arise in the dorsal posterior amnion prior to gastrulation, and no PGCs were detected within the epiblast[7].

1.3.3 PGC migration

It has been known for a long time even for humans that although the final location of the PGCs is the genital ridges, these cells are of extra-gonadal origin[61, 70-72]. In mice, after the PGCs are specified in the proximal epiblast, they have to transit via the hindgut endoderm and the dorsal mesentery towards their destination, the urogenital ridges. Between E 9.5 and E 10.5 the PGCs reach the genital ridges developing laterally to the aorta where they form the embryonic gonads[86]. As described above, in primate embryos PGCs seem to arise in the amnion[7] and they, too, translocate to the genital ridges via the dorsal/caudal wall of the yolk sac, the hindgut endoderm and the dorsal mesentery. In the cynomolgus monkey, they showed that most markers detected on the gonadal PGCs are also already present on the migrating PGCs, with the exception of DDX4 (VASA) and DAZL[7]. For the marmoset, so far only one study on migrating PGCs is available. While it confirms the translocation route via hindgut and mesentery, it also shows a wide spatio-temporal distribution of PGCs during embryonic development, and proposes a translocation model which is based on morphogenetic changes of the tissues containing the PGCs rather than long-range PGC migration[16].

The exact mechanism of this PGC translocation from their ventral extraembryonic tissue of specification towards the dorsal body wall of the developing embryo is indeed still debated. Passive movement of the cells via morphogenetic changes of the surrounding tissues may play an important role in transporting the PGCs closer to their destination[16, 87]. However, in order to move from the hind- and midgut to the gonadal ridges, active PGC migration has to be involved. Images of human PGCs published by Politzer as early as 1933 show cytoplasmic protrusions on the cells, suggesting an amoeboid migratory movement[72]. Molyneaux et al.[88] tagged Oct4 with GFP in genetically modified mice and thus were able to visualise and take time-lapse videos of PGCs during the stages of their migration. They showed that the PGCs exhibit active locomotion, however this does not seem to be an intrinsically directed movement. Rather, it was proposed that the PGCs have to follow contact guidance clues or chemotactic signals in order to find the way to their site of function. Factors

proposed to be involved in chemotaxis of PGCs include tumour growth factor β (TGFβ)[89], stromal-derived factor 1 (SDF1 or CXCL12)[90, 91] and stem cell factor (SCF; or kit ligand)[92, 93].

It was first suggested by Hoyer *et al.* that human PGCs might not be guided only by gradients of signalling molecules, but also by anatomical structures, namely nerve fibres. This was based on a strong spatial association of human PGCs with autonomic nerve fibres of the dorsal mesentery in a study on c-Kit and SCF distribution in human embryos[93]. This hypothesis was further investigated by Møllgard *et al.*[94]. In 4 – 8 weeks post conception (pc) human embryos they identified migrating PGCs and neurons and found that indeed, a large proportion of PGCs were located within bundles of autonomic nerve fibres on their route from the dorsal mesentery to the gonadal ridges. They also observed by immunohistochemical marker staining that the innervation of the human gonadal ridges starts between 29 and 33 days pc, the same time that the first PGCs arrive at their destination. They concluded from their data that in human embryos the PGCs preferentially follow peripheral autonomic nerve fibres during their translocation from the dorsal mesentery to the gonads[94].

1.4 Primordial Germ Cell Culture and Embryonic Germ Cell Derivation

1.4.1 Mouse EGCs

On feeder cells, isolated mouse PGCs proliferate for several days but eventually cease their proliferation and decrease in cell number[95, 96]. Mouse embryonic germ cells (EGCs) were initially discovered as a result of long-term PGC culture experiments. Two groups around Matsui *et al.* and Resnick *et al.* discovered at approximately the same time that the combination of several growth factors is required to maintain PGC proliferation and that this leads to the formation of pluripotent cell colonies[97, 98]. These were termed EGCs in analogy to the term embryonic stem cells (ESCs), which are derived from the inner cell mass of the blastocyst. To be more specific, it was known that the cytokine leukaemia inhibitory factor (LIF) stimulates PGC proliferation in culture[95] and that the membrane-bound form of stem cell factor (SCF) is required for PGC survival *in vitro*[99, 100]. But only the addition of basic fibroblast growth factor (bFGF) induced long-term PGC proliferation[97, 98].

It was soon accepted that under the appropriate culture conditions, PGCs will spontaneously reprogram and convert back to a pluripotent state, which led to the publication of several

detailed culture protocols[68, 101, 102]. From the beginning, it was known that mouse PGCs express the enzyme Alkaline Phosphatase (AP) and that AP-expression is also a hallmark of pluripotent stem cells, which is why AP-detection served as a tool to identify PGCs and EGCs[97]. While PGCs cannot contribute to chimaera-formation, the injection of mouse EGCs into blastocysts will lead to incorporation of these cells into the new organism and they even contribute to the germ line, this being the ultimate proof of their pluripotent potential[103].

1.4.2 Human EGCs

Not long after the discovery of mouse EGCs, the same protocols were tested for human PGCs, leading to the establishment of human EGCs[104-106]. Same as the mouse EGCs, human EGCs are derived by dissociation of the embryonic genital ridges and then plating the cells on mouse feeder cells expressing membrane-bound SCF. AP-positive colonies appear and can be expanded and passaged as EGCs. Human EGCs apparently are generated relatively easy, however, in contrast to initial claims, it seems difficult to maintain them as a stable cell-line through extended passage[105, 106].

Nevertheless, there have been some promising reports on the therapeutical use of human EGCs. Kerr *et al*. reported in 2003 that human EGC-derived cells could restore motor neuron function in paralysed rats[107]. Frimberger *et al*. reported increased regeneration of injured rat bladders after hEGC transplantation[108], and Yu *et al*. differentiated human EGCs into cardiomyocytes and used them to treat acute myocardial infarction in rats[109].

Apart from human and mouse, also EGC lines of rat, buffalo, pig and goat were reported[68]. The EGC derivation of rabbit, sheep, cow and baboon was intended, but no successful EGC line was established[68].

1.5 Rationale and Aim of the Study

Part I

As explained in chapter 1.3.3, the mechanisms behind mammalian PGC migration are still debated. A study by Møllgard *et al*. reported that in human embryos, PGCs are guided towards their destination by peripheral nerve fibres[94]. One aim of the present study was therefore to investigate whether this method of PGC guidance and transition could be

observed also in other mammalian species and whether it might represent an evolutionary conserved, i.e. general strategy of mammalian germ cell development. In order to answer the study question, I investigated embryos of different developmental stages from the mouse and a non-human primate, the marmoset monkey, covering the phase from early PGC migration to their arrival in the gonadal ridge. Embryo sections were immunohistochemically co-stained for tubulin beta-3 chain (TUBB3) to visualise neurons and Octamer-binding protein 4 (OCT4) as marker for PGCs, and the distance between each PGC and the closest detectable neuron was measured in order to make a statement about their spatial relationship.

Investigating primate germ cell development is of interest under several aspects, for example for reproductive medicine. As described above, the study of human germ cell development is difficult, and the marmoset monkey might be a valuable alternative. While much is known about mouse PGCs, there is only paper available on the common marmoset PGC development, describing four intracellular markers for their identification[16]. It was therefore another goal of this study to test the expression of several candidate proteins including surface markers of PGCs in the marmoset embryo. One candidate is the transcription factor SOX17. While SOX17's functions in the formation and maintenance of definitive endoderm[83], vascular endothelium[110], and foetal hematopoietic stem cells[111] are well established, its role in germ cells is less clear. A recent publication reported it to be the key regulator of germ cell fate in the human[76], and so its expression in (early) marmoset germ cells was investigated.

Part II

As described in chapter 1.3, PGCs can be considered to be inherently pluripotent due to their expression of pluripotency factors. Their close relationship to embryonic stem cells is corroborated by their potential, as has been shown convincingly at least in the mouse, to spontaneously form pluripotent cell lines under the appropriate culture conditions, which are then termed embryonic germ cells (EGCs). As explained above, pluripotent stem cells (PSCs) are highly interesting for the prospect of using them in cell replacement therapies, and PSCs of different origins might have different advantages and disadvantages, probably depending on their epigenetic properties. Embryonic stem cells (ESCs) as well as induced pluripotent stem cells (iPSCs) of the common marmoset monkey (*Callithrix jacchus*) are

already available in our laboratory. It was therefore my aim to establish a third pluripotent stem cell type from marmoset PGCs, characterise the resulting EGC lines and compare them to the already available ESCs and iPSCs with regard to their potential use as a source for cell replacement therapies. As described above, human and mouse EGCs can be derived from genital ridge culture and protocols are available in the literature. Since there are no recent human EGC culture reports, and the culture method is similar for both species, I based my experiments on publications by Durcova-Hills *et al.*[101], De Miguel *et al.*[68] and Leitch *et al.*[102].

2. Results

2.1 Part I – *In situ* studies of PGC development

2.1.1 PGCs do not migrate along nerve fibres in marmoset monkey and mouse embryos

2.1.1.1 PGC localisation in the common marmoset monkey (*Callithrix jacchus*)

Eight common marmoset embryos of different developmental stages (gestational day (GD) 65, 68, 72, 75, 90) were analysed in this study, approximately representing the Carnegie stages 15-23. A list of the specimens used for this part of the project is given in **Table 1**. A total of 853 PGCs were counted on 30 histological sections.

The PGCs were first grouped according to the anatomical compartment they were found in (**Figures 1 and 2**). Looking at the total cells, approx. 3 % of PGCs were detected in the epithelium of the gut, 12 % either in the gut mesenchyme, the dorsal mesentery or the peri-aortic region and 14 % of PGCs were attributed to the dorsal body wall. With 71 % the majority of PGCs was located in the developing genital ridges, or the mesonephros and gonadal precursors in more developed embryos (i.e. GD 75 onwards). Separating the sections according to the gestational day of the embryos, the proportion of PGCs that have reached the gonad expectedly increased from 13.7 % on GD 65 over 47.7 % on GD 72 to 93.3 % on GD 90.

Table 1 | Marmoset monkey (*Callithrix jacchus*) embryos used in this study.

Embryo	Gestational day	CRL (mm)	BPD (mm)	FROD (mm)	Sex	Sectioning plane
1	65	9.1	2.5	3.9	female	Sagittal
2	65	9.2	2.8	4.1	male	Sagittal
3	68	10.0	2.9	4.4	female	Transversal
4	68	9.1	2.7	3.6	male	Sagittal
5	72	10.5	3.0	4.7	male	Sagittal
6	72	9.2	2.2	4.7	female	Sagittal
7	75	N.D.	N.D.	N.D.	female	Sagittal
8	90	27.5	10.6	11.9	male	Sagittal

CRL: Crown-rump-length; BPD: biparietal diameter; FROD: fronto-occipital diameter; N.D.: Not determined.

34
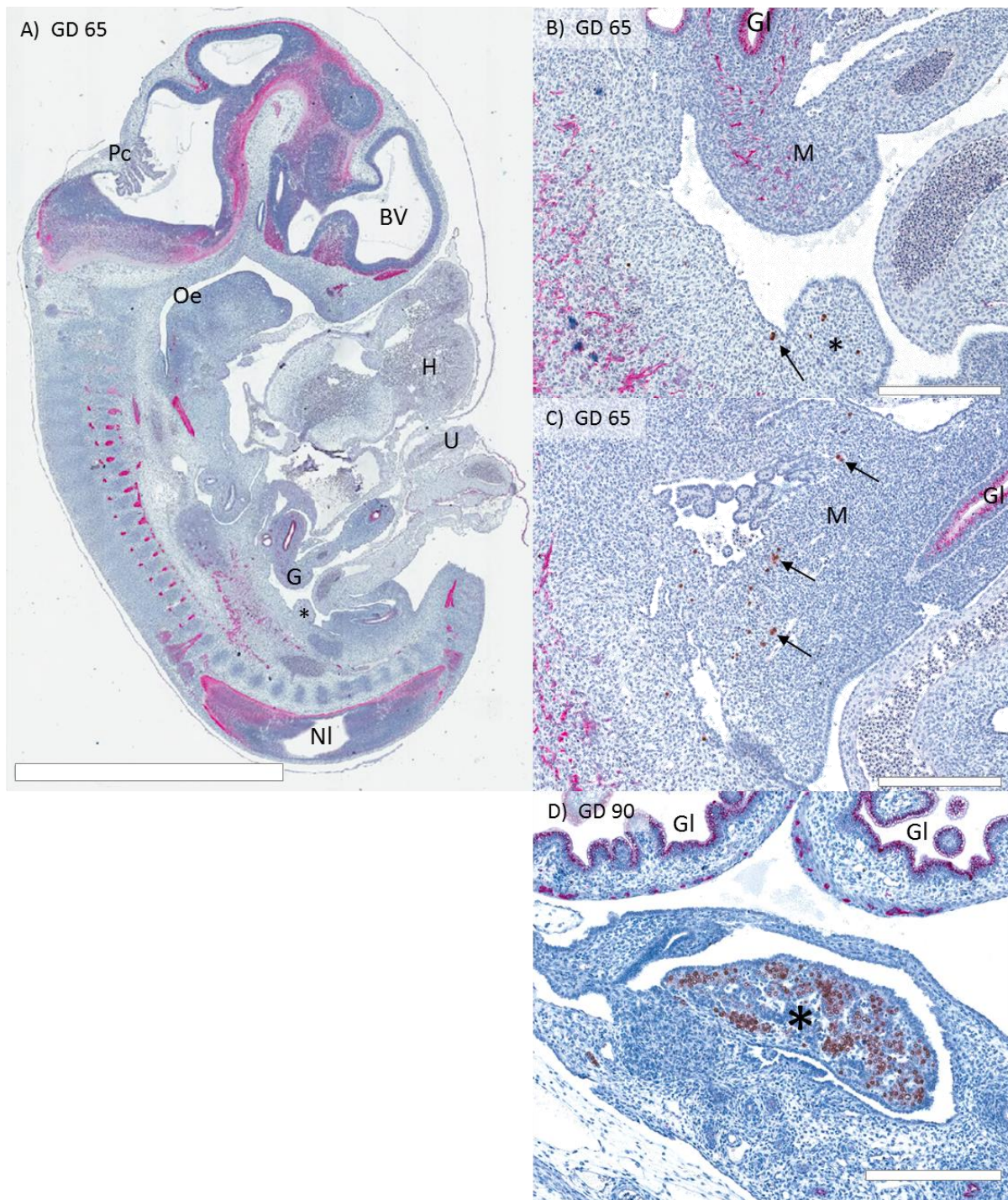
Figure 1 | PGC locations in the common marmoset monkey embryo. Immunohistochemical double staining of OCT4A (brown) and TUBB3 (pink). **A)** Representative sagittal overview section of a GD 65 embryo. **B)** Higher magnification of area of prospective gonad in A). **C)** Sagittal section of a GD 65 embryo (different than shown in A). Black arrows highlight migrating PGCs in the gut mesenchyme. **D)** Developing gonad in a GD 90 embryo containing post-migratory PGCs. Bv: Brain vesicle, G(l): Gut (lumen), H: Heart, M: Mesenchyme, Nt: Neural tube, Nl: Neural lumen, Oe: Oesophagus, Pc: Plexus choroideus, U: Umbilical cord. The asterisks mark the developing genital ridge. Scale bar ≙ 3 mm (A), 300 µm (B-D).

Figure 2 | Graphical representation of PGC locations in the common marmoset monkey embryo. Tissue locations of PGCs in all investigated slides, separately analysed for each gestational day, n = number of cells available for analysis.

From each detected PGC the distance to the closest neuron was measured and the results divided into three groups: (I) Cells more than 50 µm away, (II) cells that were found between 50 – 20 µm from the nearest neuron and (III) cells with a distance of less than 20 µm.

The main finding of my examination was that for over 96 % of the total detected PGCs no nerve cells could be detected within a distance of 50 µm. 1.64 % of the total PGCs were found in the distance range of 50 – 20 µm and only 1.75 % (15 cells total) less than 20 µm away. Of these 15 cells only two were found in direct contact with a neuron (**Figure 3**). Sub-dividing the data according to the gestational day of the embryos does not reveal any differences in the PGC-neuron distance: at least 95.3 % of PGCs were found at a distance > 50 µm (GD 72), 0.8 – 2.8 % are found in the 50 – 20 µm distance range, and only max. 3.9 % of PGCs could be detected less than 20 µm from the closest neuron (GD 72) (**Figure 4**).
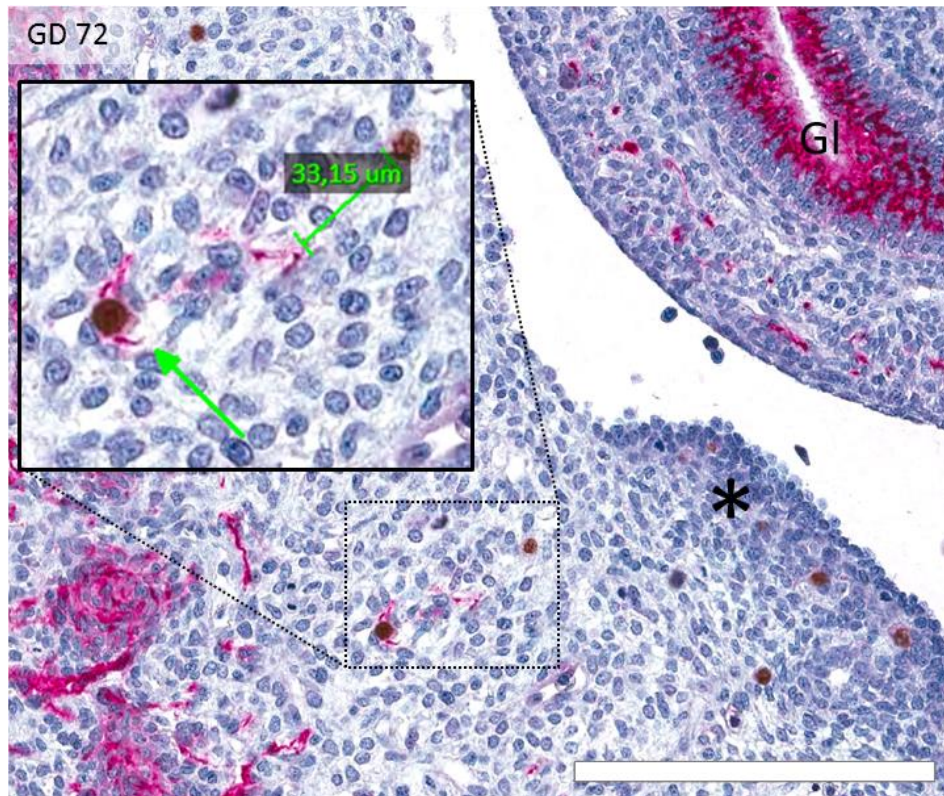
Figure 3 | PGC-neuron distance in the common marmoset monkey embryo. Representative sagittal section of a GD 72 marmoset monkey embryo. Immunohistochemical double staining of OCT4A (brown) and TUBB3 (pink). Inlay shows an exemplary distance measurement of a migratory PGC to the closest neuron. Green arrow highlights a PGC in direct contact with a neuron. Scale bar ≙ 200 µm.
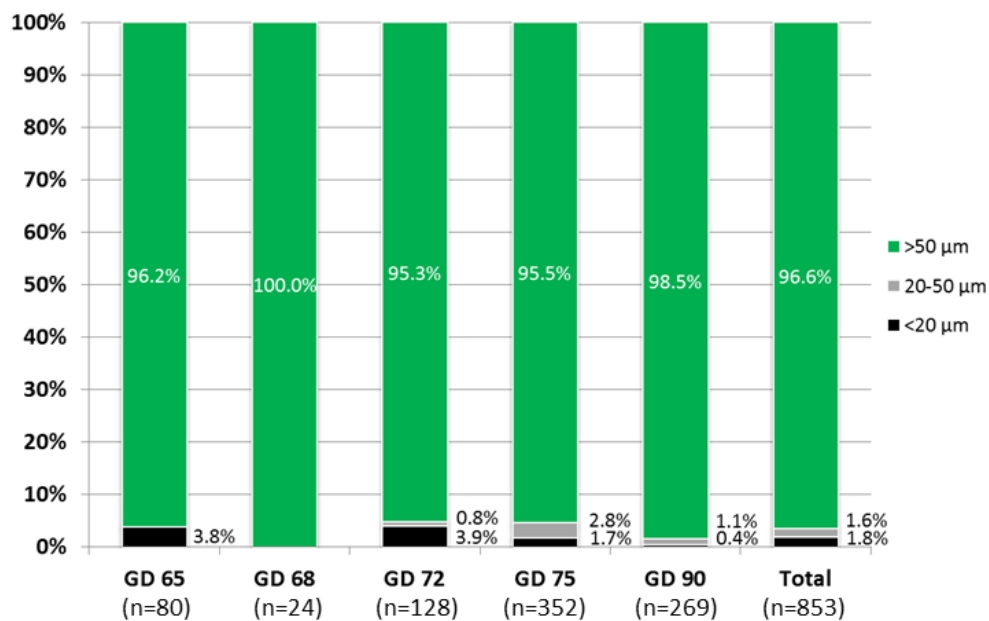
Figure 4 | Graphical representation of the PGC-neuron distance in the marmoset embryo. The distance between the observed PGCs and the respectively closest detectable neuron, separately analysed for each gestational day, n = number of cells available for analysis.

2.1.1.2 PGC localisation in the mouse embryo

In the mouse, a total of 3482 PGCs were counted on 64 sections of 8 embryos of consecutive embryonic days (E 8.5 – E 11.5). The list of mouse samples for this study can be found in **Table 2**. Looking at mouse embryos provided the advantage of a more systematic investigation of PGC migration, as migration happens over a shorter time than in the marmoset. The developmental span of E 8.5 – E 11.5 covers almost the entire range of PGC migration. Additionally, it allowed to better follow the neuronal development and draw conclusions on potential interactions with PGC migration. This observation could not be made in the marmoset embryos since the neuronal development (but not the PGC translocation!) in the earliest investigated stage (GD 65) had already progressed further than that in the oldest investigated mouse embryo (E 11.5).

Table 2 | Mouse embryos used in this study.

Embryo	Embryonic day	CRL (mm)	Sex	Sectioning plane
1	8.5	2.4	N.D.	Sagittal
2	8.5	N.D.	N.D.	Transversal
3	9.5	2.9	N.D.	Sagittal
4	9.5	N.D.	N.D.	Transversal
5	10.5	4.6	N.D.	Sagittal
6	10.5	N.D.	N.D.	Transversal
7	11.5	5.4	Female	Sagittal
8	11.5	N.D.	Male	Transversal

CRL: Crown-rump-length; N.D.: Not determined. Where possible, sex was determined by SOX9-IHC on embryonic gonads.

Again, PGCs were first classified according to their tissue location (**Figures 5 and 6**). On E 8.5 98.25 % of PGCs were found either in the gut epithelium or the mesenchyme surrounding the gut. On E 9.5 the majority of PGCs (84.77 %) were migrating through the gut mesenchyme and the mesentery. 7.28 % were found in the gut epithelium and 7.95 % had already reached the location where the genital ridges started to form. By E 10.5 the genital ridges were clearly distinguishable from the surrounding tissue, and while they now harboured most of the detected PGCs (84.67 %), 9.17 % of PGCs were found in the gut mesenchyme, the mesentery or the region surrounding the aorta. By E 11.5 by far the most of the PGCs (> 90 %) had reached the developing gonads. The remaining cells were detected mostly in the peri-aortic region or the mesentery. These findings reflect the PGC migration / translocation process.

38
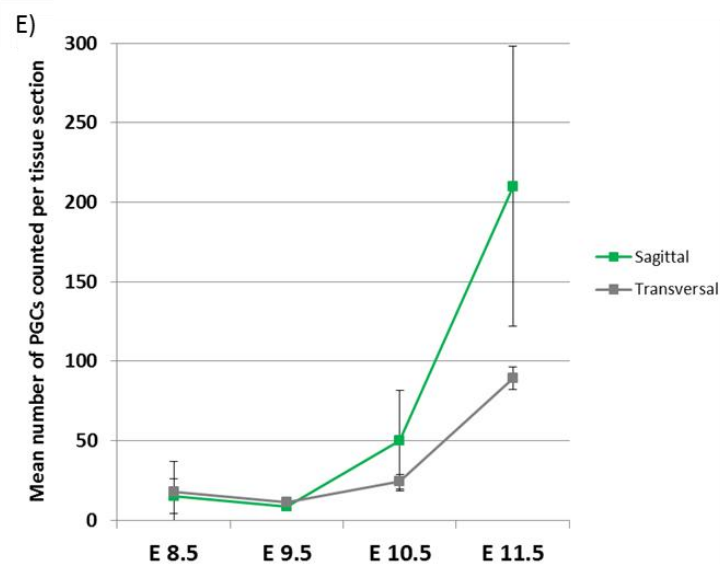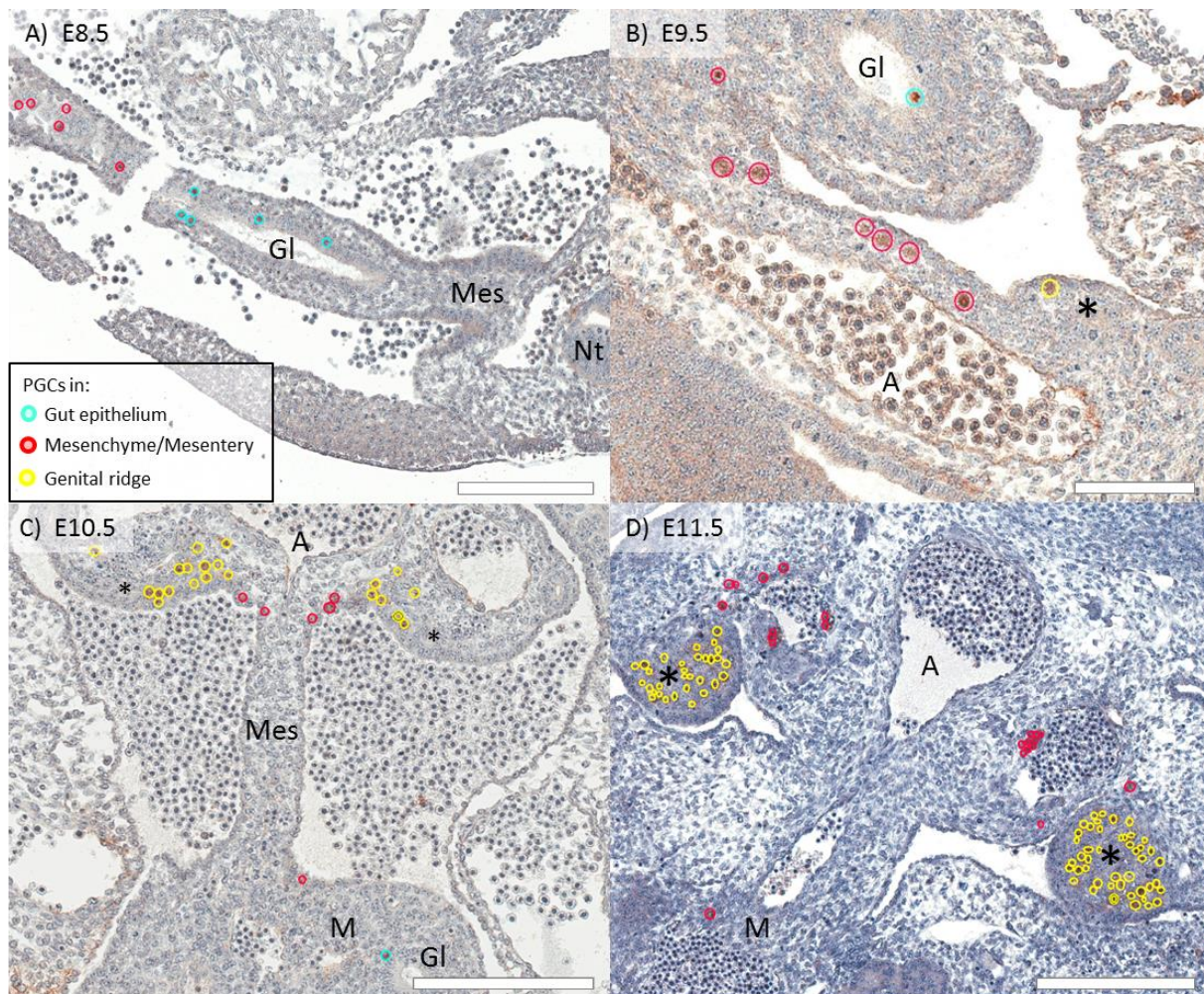
Figure 5 | PGC tissue locations in the mouse embryo. A-D) Sections of different embryonic stages immunohistochemically stained for OCT4. **A)** Representative transversal section of an E 8.5 embryo. **B)** Representative sagittal section of an E 9.5 embryo. **C)** Representative transversal section of an E 10.5 embryo. **D)** Representative transversal section of an E 11.5 embryo. A: Dorsal aorta, Gl: Gut lumen, M: Mesenchyme, Mes: Mesentery, Nt: Neural tube. The asterisks mark the developing genital ridge. PGCs are highlighted and colour-coded according to the tissue they were detected in. Scale bar ≙ 90 µm (B),

200 μm (A, C, D). **E)** Graphical representation of PGC numbers in the mouse embryo. Number of detectable PGCs per tissue section in all investigated slides, separately analysed for each embryonic day.

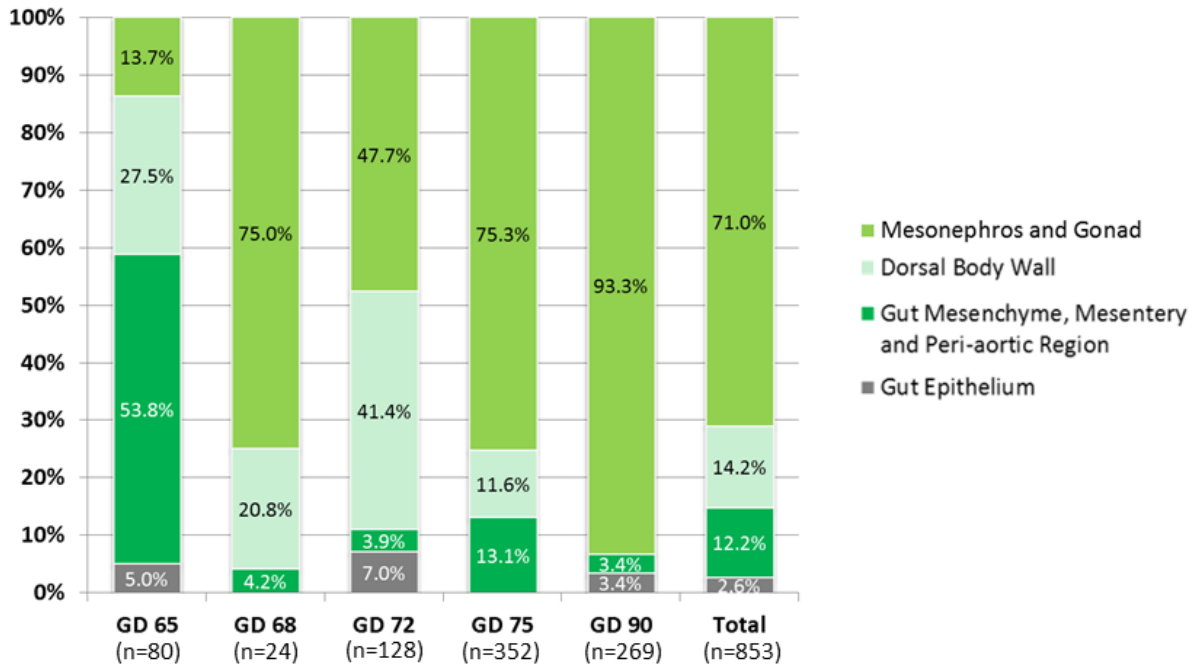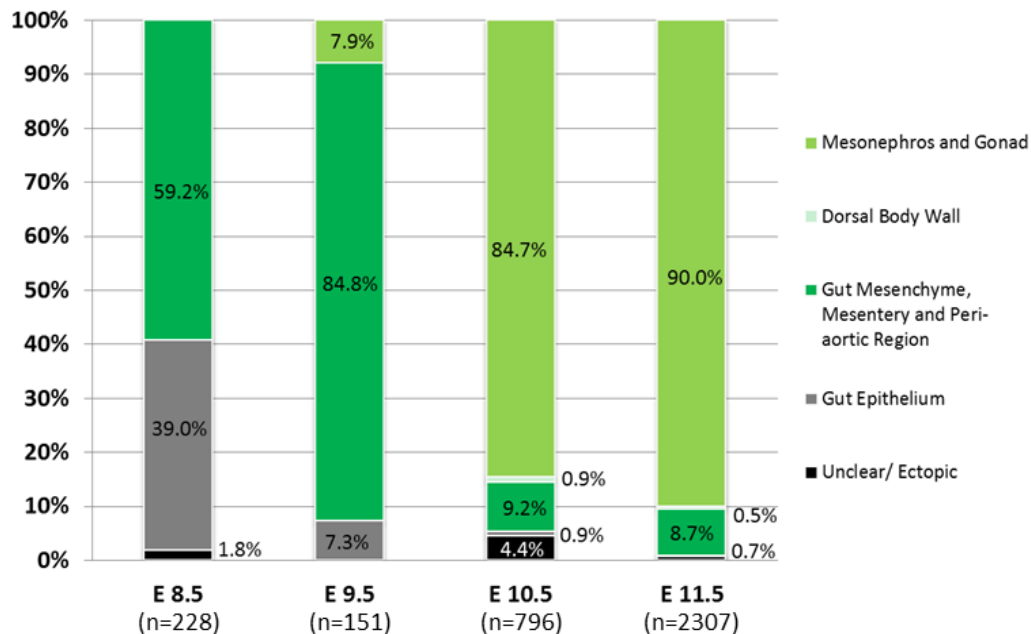**Figure 6 | Graphical representation of PGC tissue locations in the mouse embryo.** Tissue locations of PGCs in all investigated slides, separately analysed for each embryonic day, n = number of cells available for analysis.

Approximately 2 % of total PGCs were also found at ectopic regions (regions that deviate from the "normal" migration route) such as the neural tube.

Measuring the distance of each PGC to the closest neuron revealed results similar to those obtained in the marmoset embryos (**Figures 7 and 8**): On E 8.5 only 0.88 % of cells were found at a distance of less than 20 μm from a neuron and 0.44 % in the distance range of 50 – 20 μm (2 and 1 cell in total, respectively). 98.68 % of cells were more than 50 μm away. This percentage even increased in the data obtained on E 9.5, where not a single PGC was detected within a 50 μm distance of a neuron. On E 10.5 and E 11.5 the results remained similar, with 98.12 % and 95.02 % of cells detected in the > 50 μm distance category, respectively. On E 11.5 the proportion of PGCs that were found closer to a neuron increased slightly, with 2.8 % and 2.9 % per category, respectively.

In the mouse embryos we observed a strong increase in PGC number between E 10.5 and E 11.5 (for comparison see **Figure 5 C/D**), which indicates the onset of intense PGC proliferation. Clusters of several PGCs could be found outside the gonad on E 11.5, whereas only single cells were observed on the days before. The increase in PGC numbers is also quantified in **Figure 5 E**.
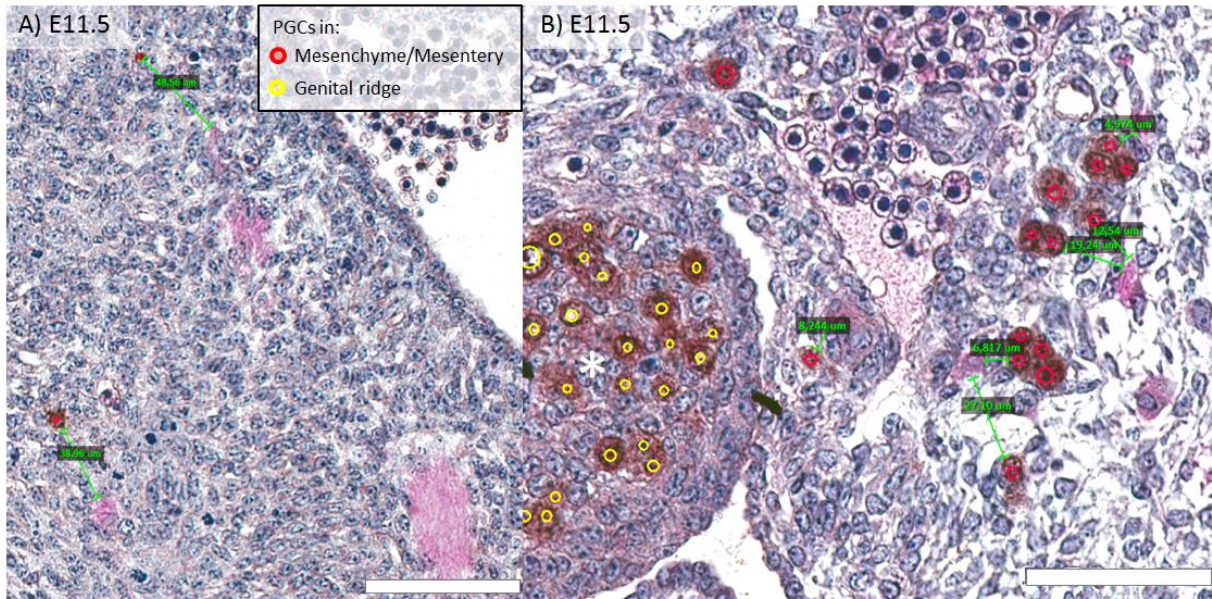
Figure 7 | PGC-neuron distance in the mouse embryo. A+B) Sagittal and transversal section of E 11.5 mouse embryos immunohistochemically double stained for OCT4 (brown) and TUBB3 (pink). Exemplary distance measurements between representative PGCs and the respectively closest detectable neuron. Scale bar ≙ 80 μm (A), 60 μm (B). Asterisk marks the prospective gonad. PGCs are highlighted and colour-coded according to the tissue they were detected in.
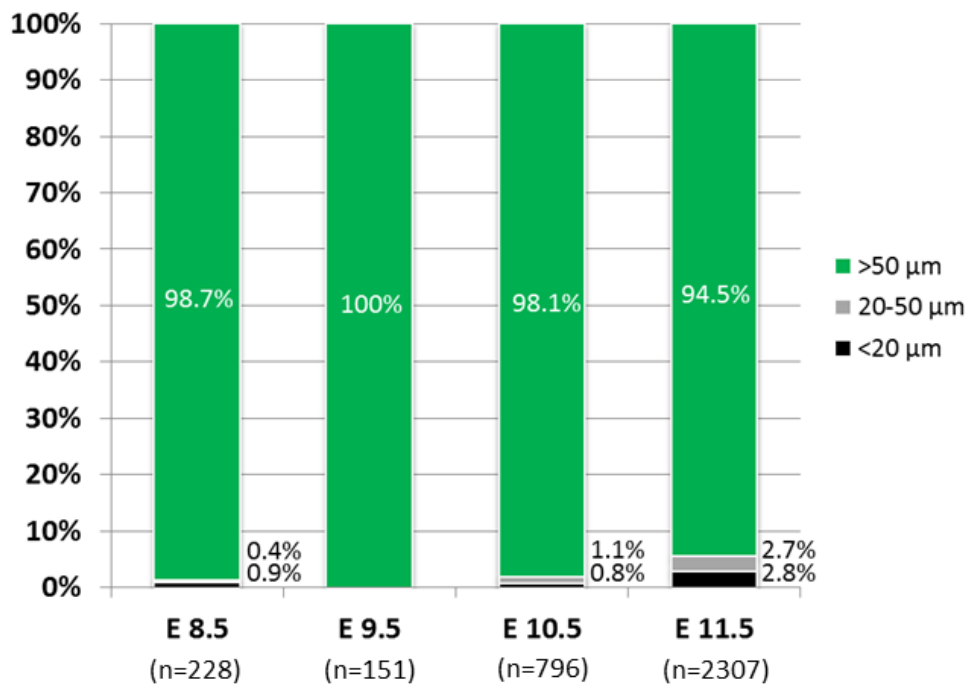
Figure 8 | Graphical representation of PGC-neuron distance in the mouse embryo. The distance between the observed PGCs and the respectively closest detectable neuron, separately analysed for each embryonic day, n = number of cells available for analysis.

2.1.1.3 Comparing neuronal development between mouse and marmoset embryos

Figure 9 A-C exemplarily shows an E 10.5 mouse embryo double stained for TUBB3 and OCT4 as well as single stainings of the two markers. While OCT4-positive PGCs were clearly detectable in the gonad, no TUBB3 signal was visible in neither the gonad nor the adjacent tissue. **Figure 10 A-D** shows the neuronal development observed in mouse embryos by TUBB3 staining: On E 8.5, neurons were clearly visible in the developing brain and started to appear in the neural tube (**Figure 10 A**). The intensity of these signals increased on the E 9.5 embryos (**Figure 10 B**). Interestingly, a clear gradient of TUBB3-positive neurons in the neural tube from cranial to caudal was observed between those two embryonic days (shown in **Figure 9 D**). On E 9.5, first ganglia started to appear in the mesenchyme around the gut, which did not show any histological signs of smooth muscle differentiation at this stage. While the signals in the aforementioned tissues became more pronounced on E 10.5, neurons also started to appear in the region around the aorta (**Figure 10 C**). This was best recognisable on the transversal embryo sections. Presence of neurons in the mesentery was not observed but cannot be excluded. Most important for this study was the finding that by E 11.5 there was still no innervation of the gonad detectable (**Figure 10 D**), although 90 % of all PGCs were present in the gonad (**Figure 6**). A summary of the observed TUBB3 signal intensity in different tissues at different developmental stages in the mouse embryo is given in **Table 3**.

These findings regarding the spatio-temporal development of the peripheral nervous system in the mouse are different from the marmoset embryos, where at the earliest investigated stage (GD 65) the neuronal development had already progressed further than that in the latest mouse embryo as judged from TUBB3 staining. In the GD 65 marmoset embryos, TUBB3 staining gave a clear signal in the brain, neural tube, ganglia, ganglia of the gut, the gut epithelium and the gut mesenchyme (**Figure 1 A**). There was also a strong signal in the epithelia of the mesonephros. However, importantly, also in the marmoset embryos, there was no signal detectable in the gonads of even the oldest investigated embryo (GD 90, **Figure 1 D**), confirming the mouse data that PGCs are present in the developing gonad before any nerve fibres can be detected in the vicinity of the embryonic gonad.
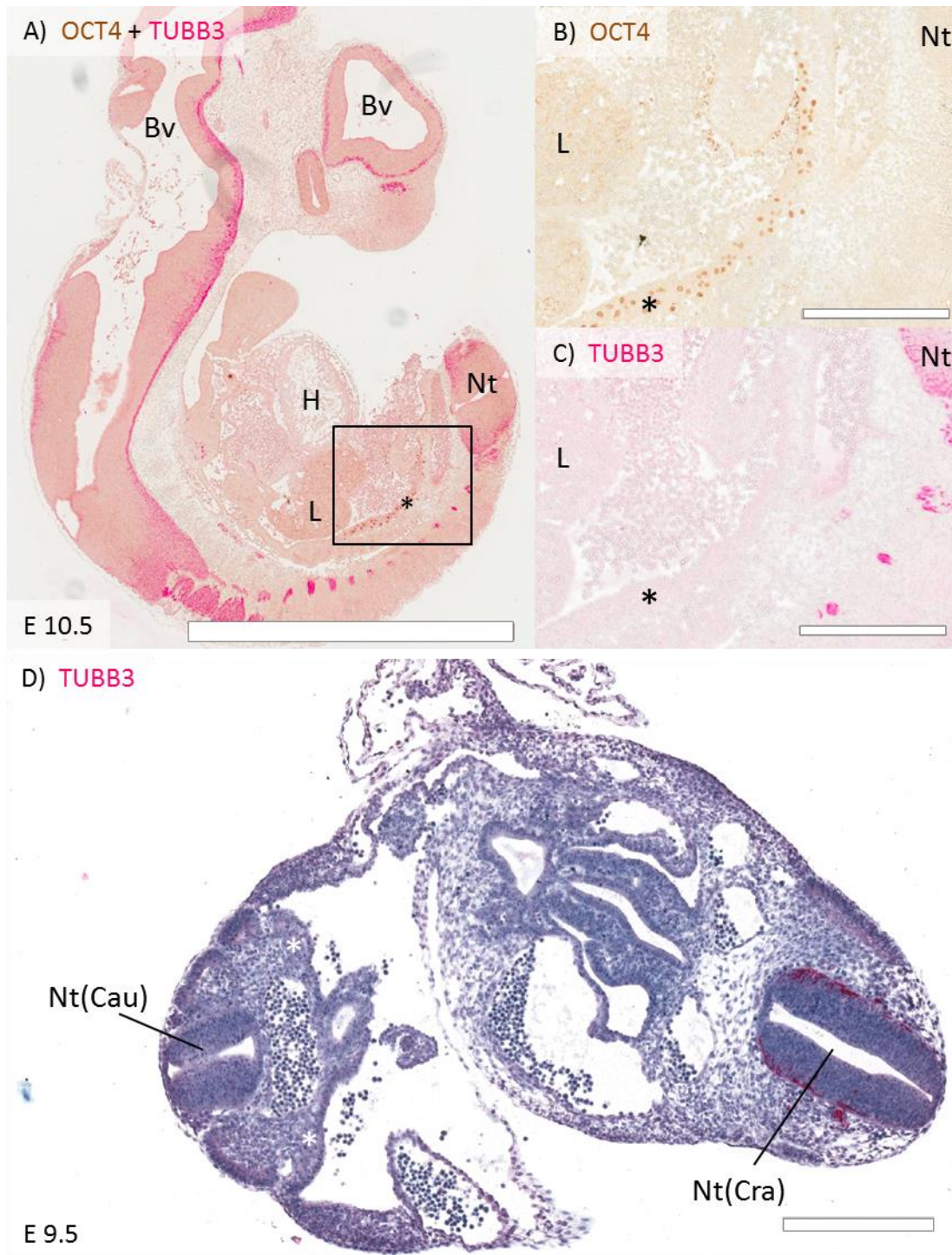
Figure 9 | Neuronal development observed in the mouse embryo I. A) Representative sagittal overview section of an E 10.5 embryo immunohistochemically double stained for OCT4 (brown) and TUBB3 (pink). Scale bar ≙ 2 mm. **B+C)** Higher magnification of the area highlighted in A), immunohistochemically stained for OCT4 (B) or TUBB3 (C). Scale bar ≙ 300 µm. **D)** Representative transversal section of an E 9.5 embryo immunohistochemically stained for TUBB3. Bv: Brain vesicle, H: Heart, L: Liver, Nt: Neural tube, Nt(cau): Neural tube in the caudal region of the embryo, Nt(cra): Neural tube in the cranial direction of the embryo. The asterisks mark the developing genital ridge. Scale bar ≙ 300 µm.
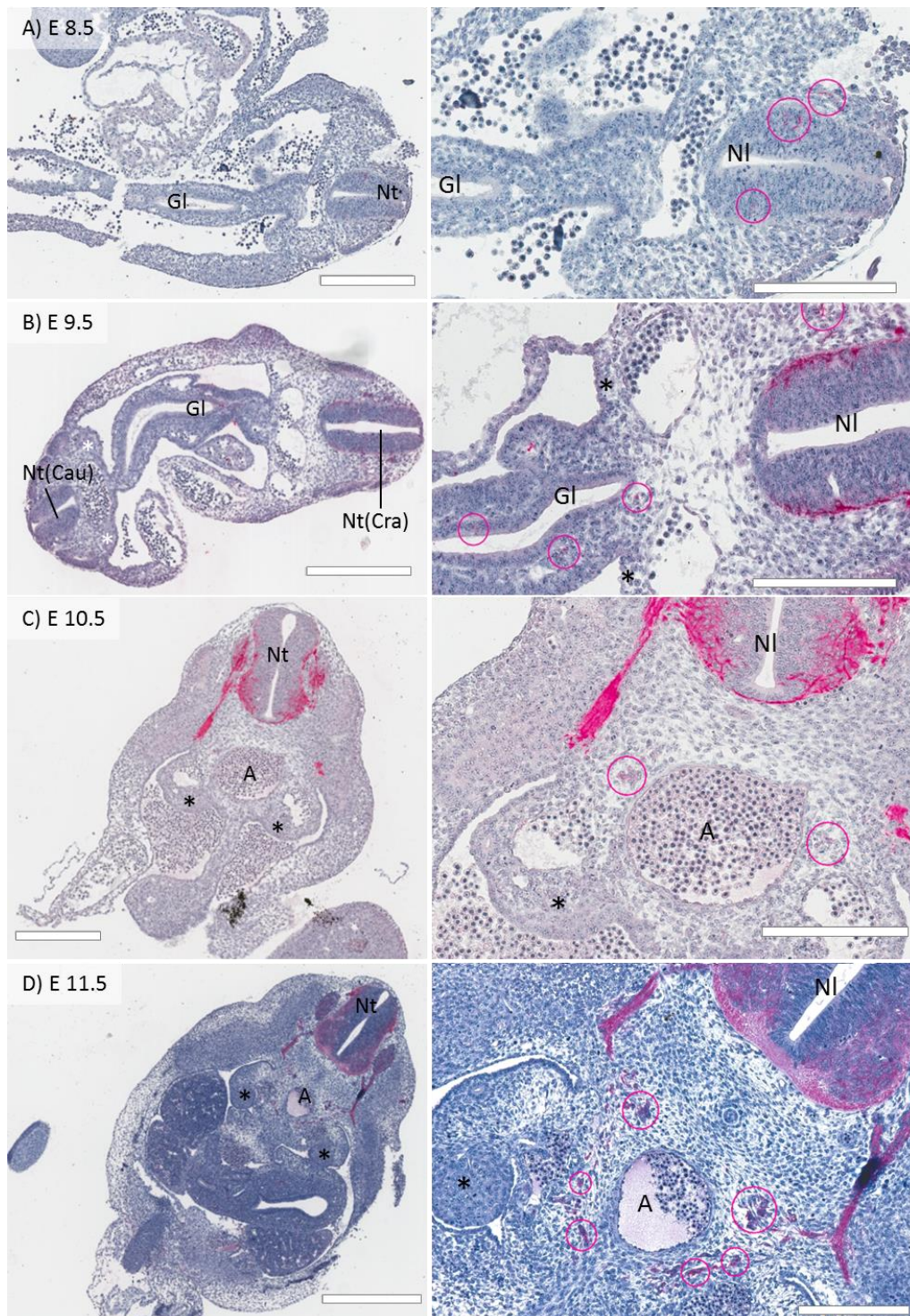
Figure 10 | Neuronal development observed in the mouse embryo II. Sections of different embryonic stages immunohistochemically stained for TUBB3. Left panel: Overview of the respective stage in lower magnification. Right panel: Higher magnification of the left image. **A)** Representative transversal section of an E 8.5 embryo. **B)** Representative transversal section of an E 9.5 embryo. **C)** Representative transversal section of an E 10.5 embryo. **D)** Representative transversal section of an E 11.5 embryo. A: Dorsal aorta, Gl: Gut lumen, Nl: Neural lumen, Nt: Neural tube. The asterisks mark the developing genital ridges. Pink circles highlight appearing neurons. Scale bar ≙ 600 μm (D left panel), 400 μm (B left panel), 300 μm (A+C left panel), 200 μm (all images in right panel).

Table 3 | The observed TUBB3 signal intensity in different tissues at different developmental stages in the mouse embryo.

	Brain	Neural tube	Ganglia	Gut mesenchyme	Peri-aortic region	Mesentery	Gonad
E 8.5	++	+	-	-	-	-	-
E 9.5	++	++	+	+	-	-	-
E 10.5	+++	+++	+++	++	+	?	-
E 11.5	+++	+++	+++	++	++	?	-

-    = No signal visible
+   = Neurons start to appear, sometimes still weak signal, few cells
++   = Neurons clearly recognisable
+++ = Strong staining signal, high cell numbers

In order to confirm that TUBB3 staining reveals all present neurons, marmoset embryos were also stained for microtubule-associated protein 2 (MAP2), which is another protein specifically expressed in neurons (Source: The Human Protein Atlas; https://www.proteinatlas.org/ENSG00000078018-MAP2/tissue). **Figures 11 and 12** show that both TUBB3 and MAP2 are expressed by almost the same cells, with the difference that TUBB3 seems to be additionally expressed in epithelial cells of the gut and kidney (**Figure 12 A**).

45
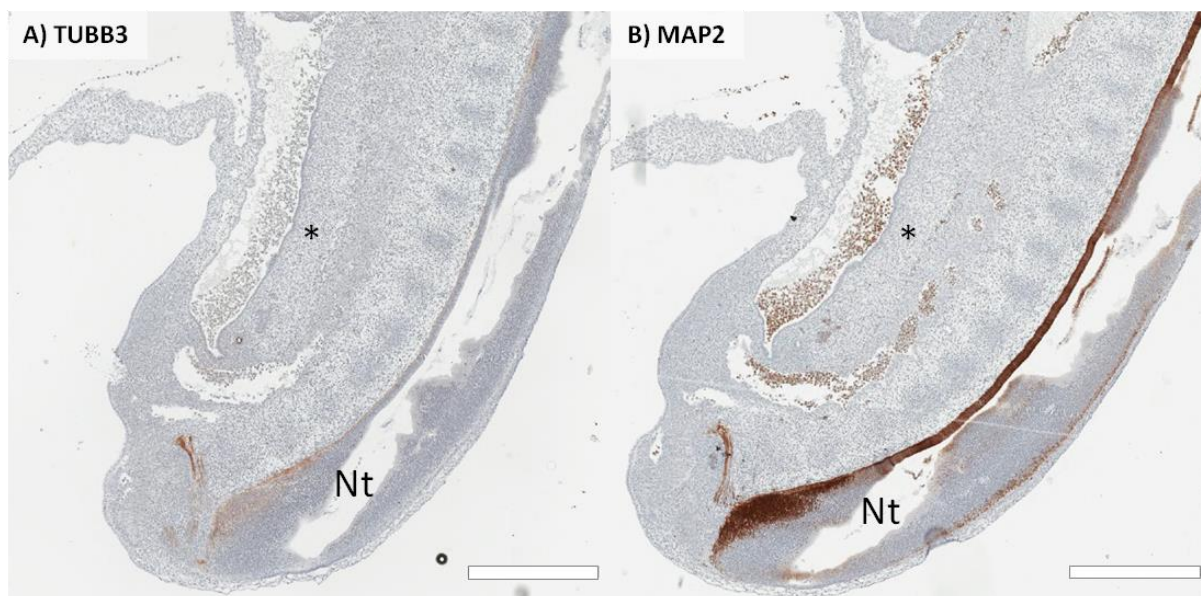
Figure 11 | MAP2 and TUBB3 staining pattern is comparable in the marmoset monkey embryo I. Immunohistochemical staining of tissue sections in a marmoset GD 71 embryo for TUBB3 **(A)** and MAP2 **(B)**. Nt: Neural tube. Asterisks mark the developing urogenital ridge. Scale bar ≙ 600 µm.
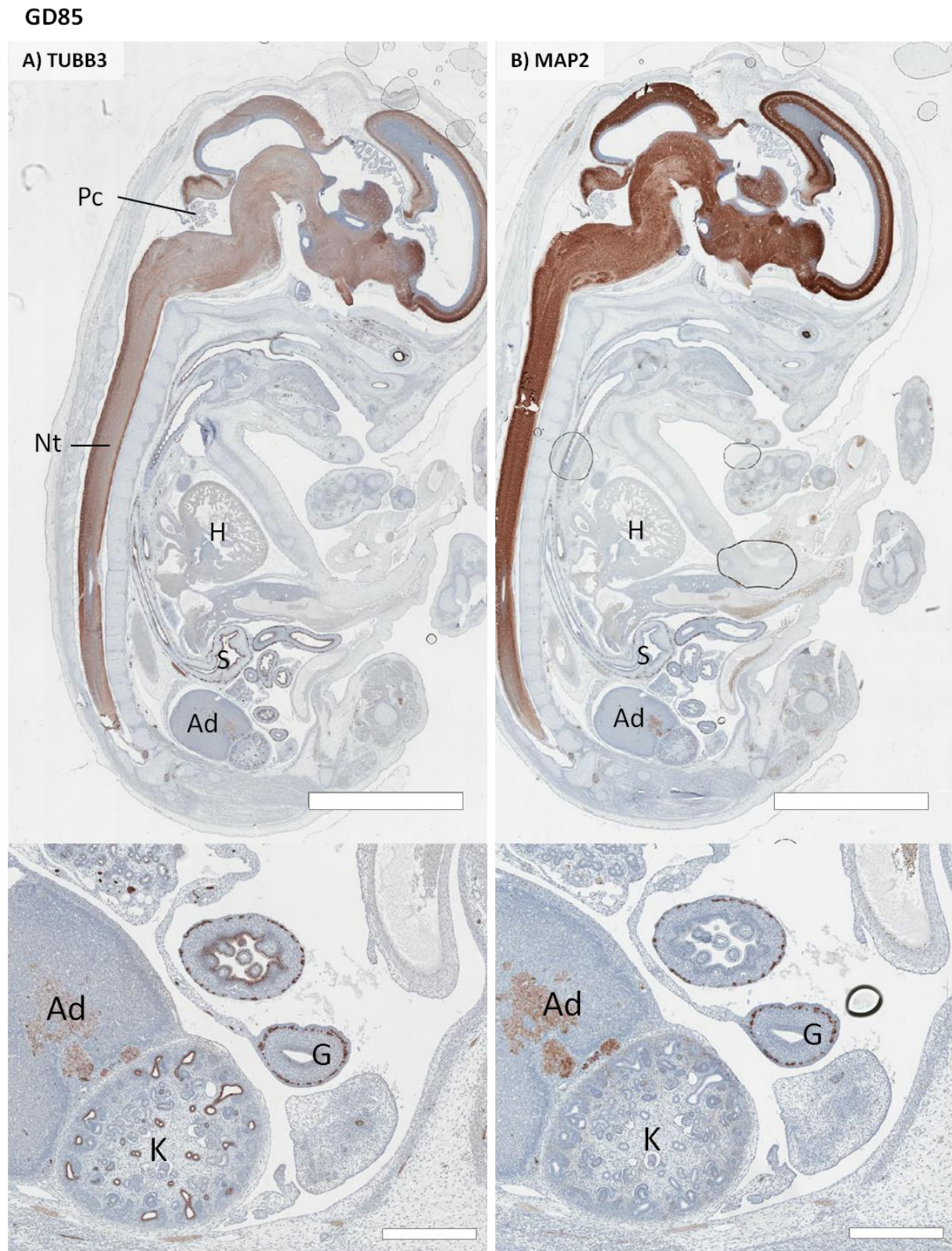
GD85

Figure 12 | MAP2 and TUBB3 staining pattern is comparable in the marmoset monkey embryo II.
Immunohistochemical staining of tissue sections in a marmoset GD 85 embryo for TUBB3 **(A)** and MAP2 **(B)**.
Ad: Adrenal gland, G: Gut, H: Heart, K: Kidney, Nt: Neural tube, Pc: Plexus choroideus, S: Stomach.
Scale bar ≙ 4mm (top images), 500 µm (bottom images).
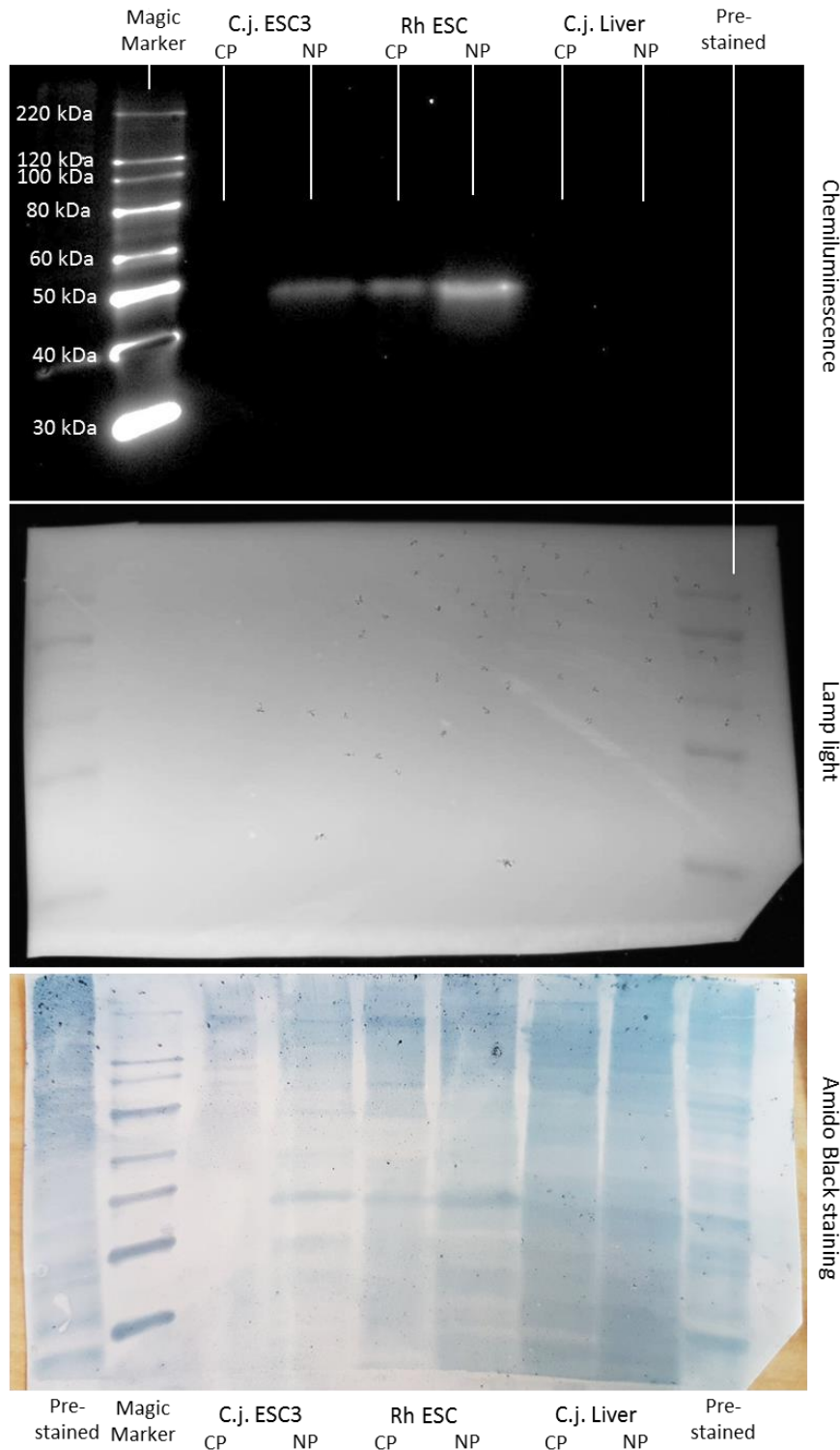
Figure 13 | Characterisation of OCT4A antibody via Western Blot. Top image shows chemiluminescence antibody signal, middle image shows the blot membrane under normal light for size comparison, bottom image shows the blot membrane stained with Amido Black as control for the presence of protein in the sample. CP: Cytosolic protein fraction, NP: nuclear protein fraction. A single, distinct band of the expected size is detected in the nuclear protein samples of marmoset and rhesus monkey embryonic stem cells as well as the cytosolic protein sample of the rhesus ESCs. No band is visible in the liver sample which was used as negative control.
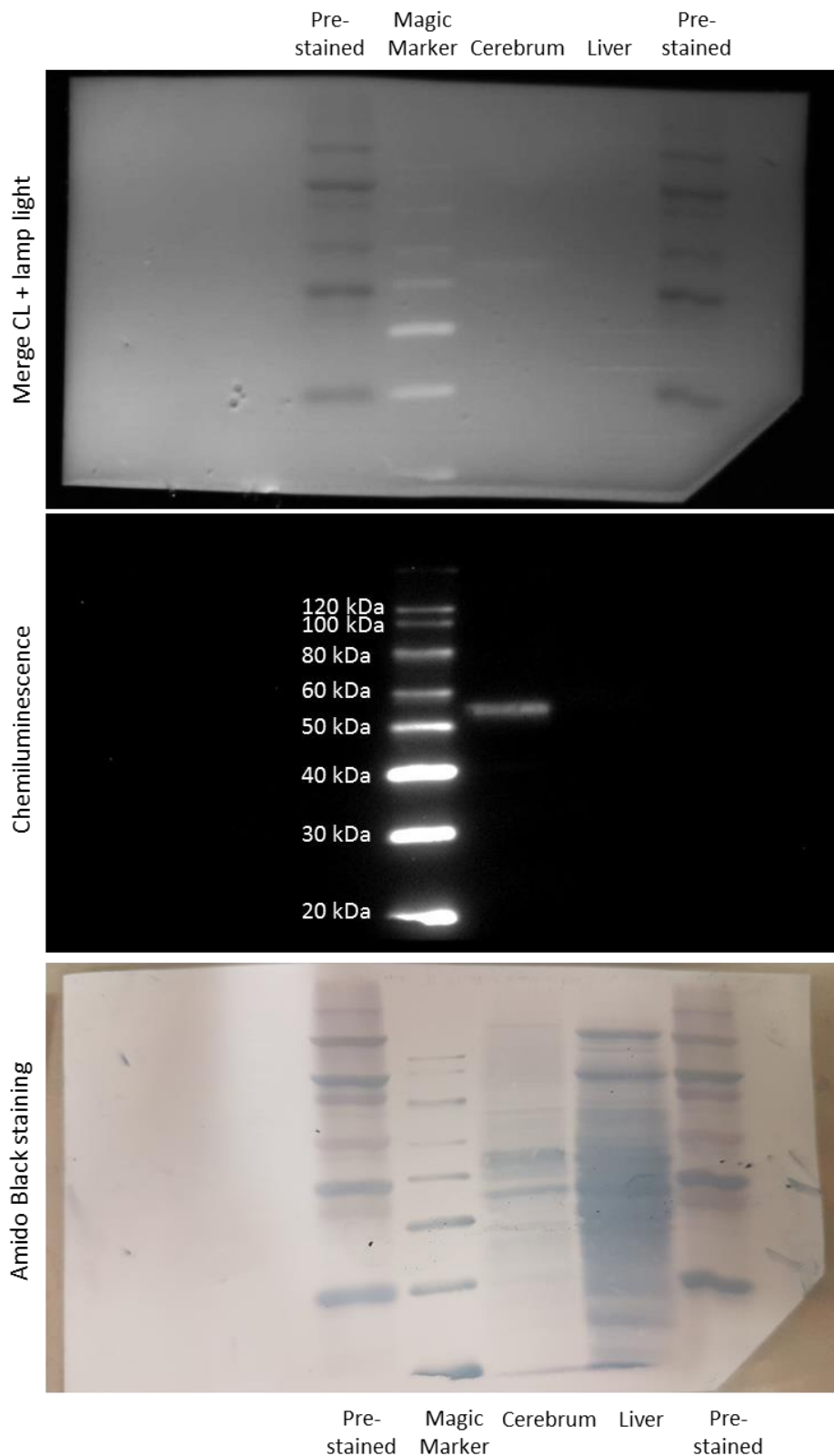
Figure 14 | Characterisation of TUBB3 antibody via Western Blot. Middle image shows chemiluminescence antibody signal, top image shows the blot membrane under normal light for size comparison. A single, distinct band is detected in the marmoset monkey brain protein sample. No band is visible in the marmoset liver sample, which was used as negative control. Bottom image shows blot membrane stained with Amido Black as control for the presence of protein in the samples.

To further corroborate the specificity of the chosen antibodies, they were analysed via Western Blot (WB). OCT4A as a pluripotency factor is supposed to be highly expressed in embryonic stem cells (ESCs) of marmoset and rhesus monkey, and not expressed in the liver, which was chosen as negative control. The WB revealed one distinct band in the ESC protein samples and no signal in the liver sample (**Figure 13**) at the apparent molecular weight of ~50 kDa. The calculated molecular weight of OCT4A is 38.6 kDa. For the TUBB3 WB, protein samples of marmoset brain and liver were used. Also in this blot, one distinct band around the calculated weight of 50.4 kDa was revealed in the positive control and no signal was detectable in the negative control (**Figure 14**), confirming the specificity of the antibodies.

2.1.2 SOX17 expression in the germ line of non-human primates

2.1.2.1 SOX17 in early marmoset monkey (*Callithrix jacchus*) PGCs

SOX17 is a transcription factor that has been shown to be the key regulator of germ cell fate in the human, where it is the first gene to be expressed in PGCs and induces the germ cell specification process[76]. I therefore wanted to investigate whether it is also detectable in early marmoset PGCs. Sequential sections of GD 49 and GD 53 marmoset embryos were stained alternatingly for OCT4A to identify the PGCs, and SOX17. As shown in **Figure 15**, corresponding SOX17 and OCT4A signal could be observed in two different sets of neighbouring tissue sections. It is however difficult to ultimately determine via IHC whether the signal is detected in the same cell. In the GD 53 embryo, SOX17 staining produced a lot of background, which is why many slides were not available for analysis. **Figure 16** shows a slide of this embryo, but no SOX17 signal was detected in the area with OCT4A-positive cells. Staining marmoset embryo sections of GD 65 and GD 75 shows that there was clearly no SOX17 signal detectable in OCT4A-positive PGCs at these stages (**Figure 17**).
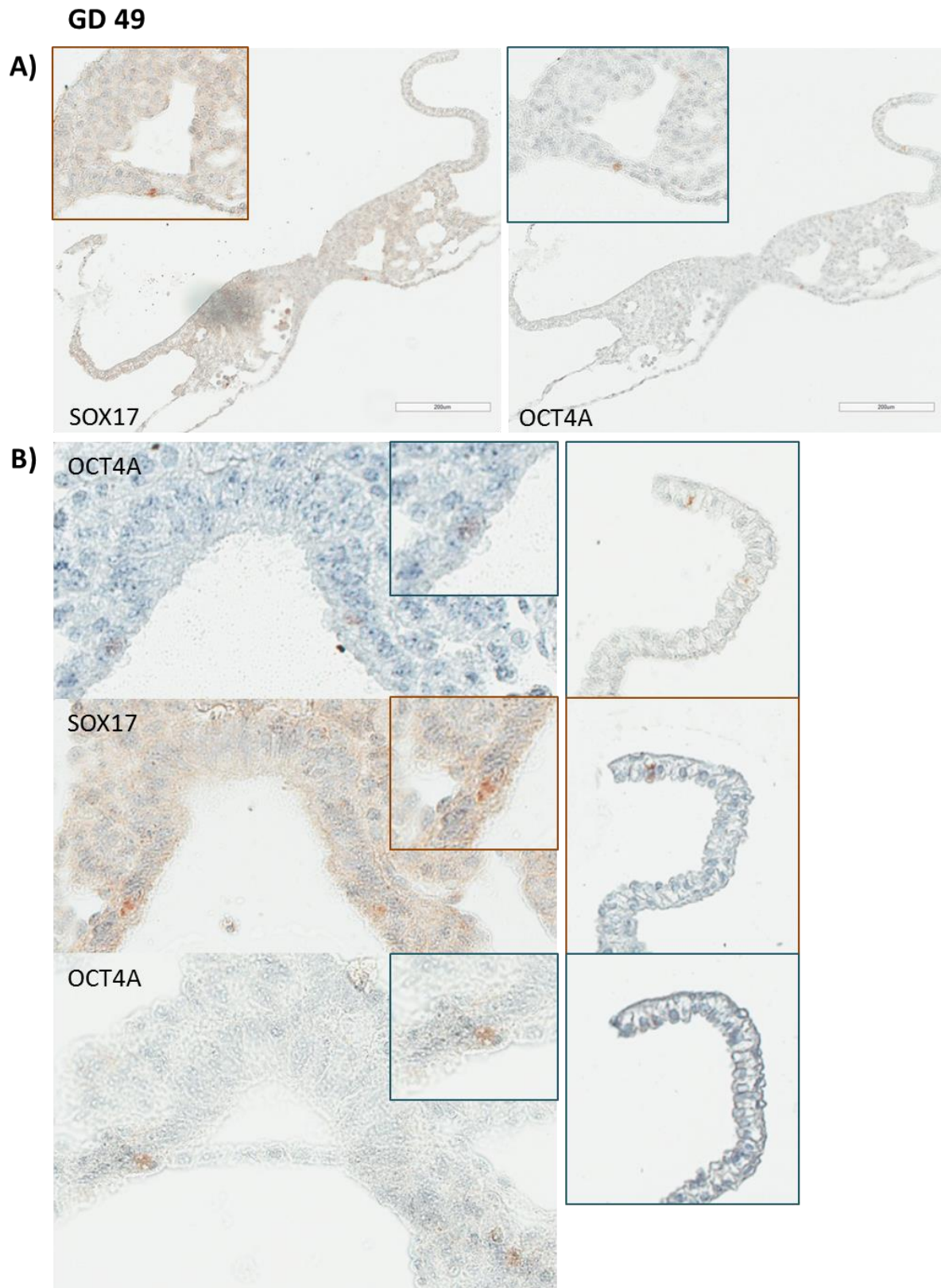
Figure 15 | SOX17 expression in the GD 49 marmoset embryo. Immunohistochemistry of sequential tissue sections of a GD 49 marmoset embryo alternatingly stained for SOX17 and OCT4A as a marker for PGCs. **A)** Two sequential sections with corresponding SOX17 and OCT4A-positive cells. **B)** Three sequential sections with corresponding SOX17 and OCT4A-positive cells. The right panel of B) shows a different area on the same sections with two corresponding SOX17 and OCT4A-positive cells. Scale bar ≙ 200 µm.

50
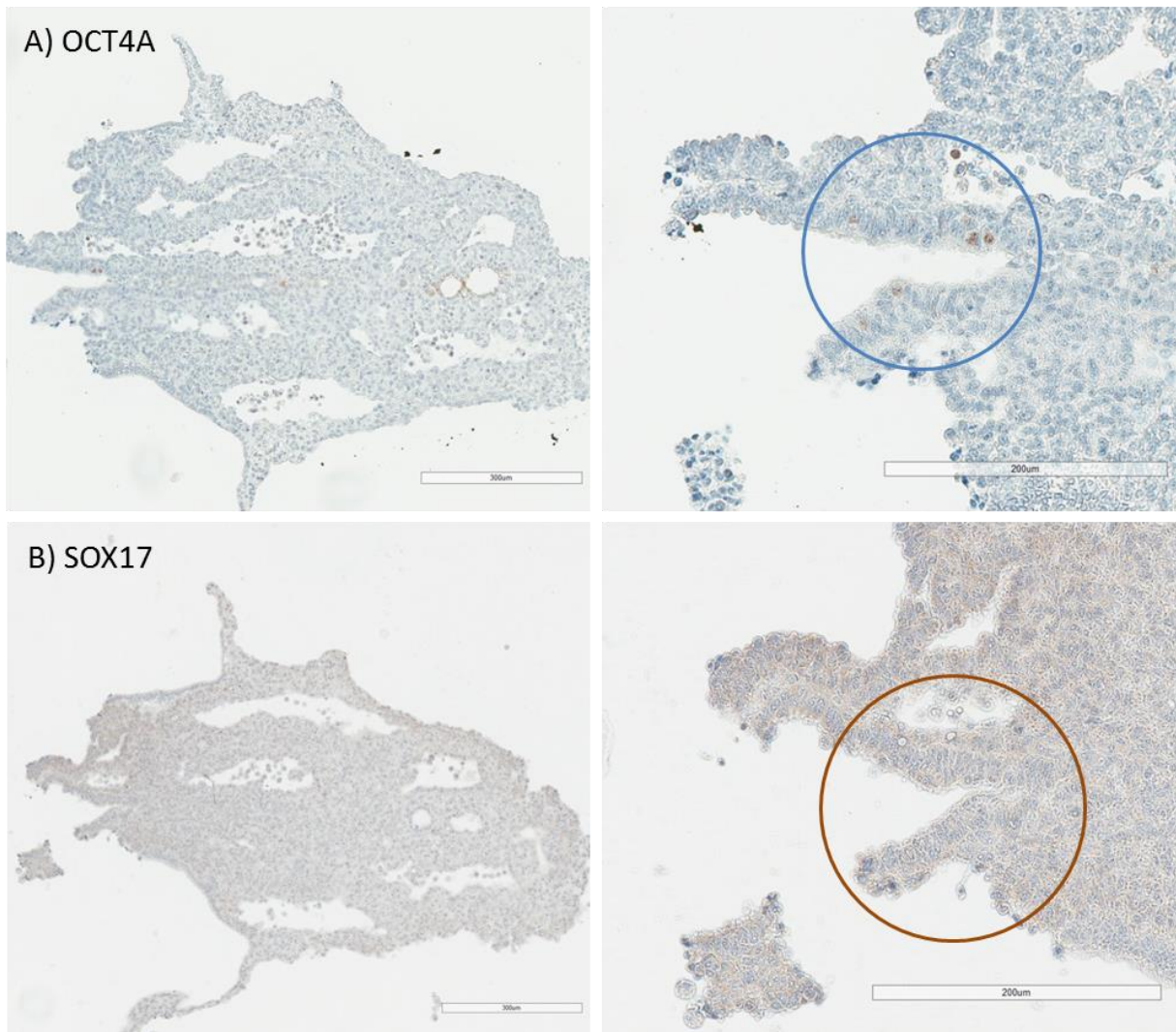
GD 53

A) OCT4A

B) SOX17

Figure 16 | SOX17 expression in the GD 53 marmoset embryo. Immunohistochemistry of transversal sequential tissue sections of a GD 53 marmoset embryo alternatingly stained for OCT4A as a marker for PGCs **(A)** and SOX17 **(B)**. The blue circle highlights an area with 6 OCT4A-positive PGCs. The red circle highlights the same area on the SOX17-stained slide, where no SOX17-positive cells are detectable. Scale bar ≙ 300 µm (left panel), 200 µm (right panel).
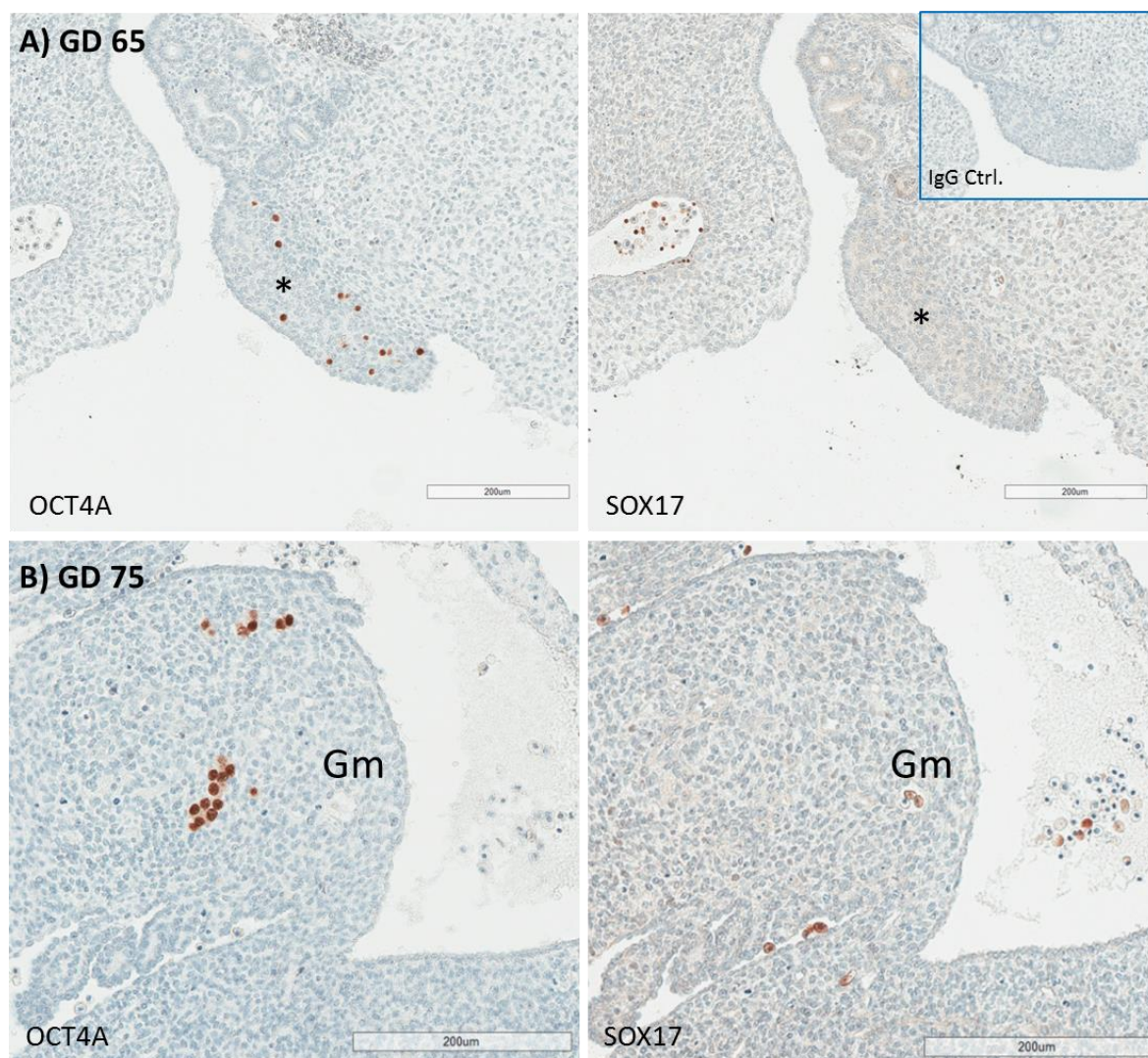
Figure 17 | SOX17 expression in the GD 65 and GD 75 marmoset embryo. Immunohistochemistry of tissue sections of a GD 65 **(A)** and a GD 75 **(B)** marmoset embryo stained for OCT4A as a marker for PGCs (left panel) and SOX17 (right panel). Inlay in A) shows IgG isotype control. Gm: Gut mesenchyme. Asterisks mark developing genital ridges. Scale bar ≙ 200 µm.

2.1.2.2 Differential SOX17 expression in NHP gonads

Figure 18 shows SOX17 staining in the marmoset neonatal and adult ovary, respectively. It includes staining of SALL4, which is a pluripotency associated transcription factor in the early embryo and later on detected in germ cells and haematopoietic stem cells, and SSEA-5, which is also a marker of pluripotent stem cells[112] but whose role in germ cells is not yet determined. While SALL4 was still expressed in the neonatal ovary and not expressed in adult oocytes anymore, it was the other way around with SOX17, which was not detectable in the neonatal ovary but specifically expressed in adult oocytes. SSEA-5 could also be detected in adult oocytes, and was also expressed on germ cells in the neonatal ovary.
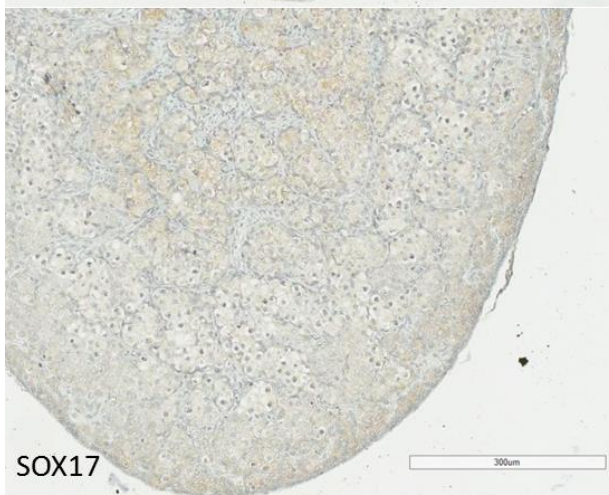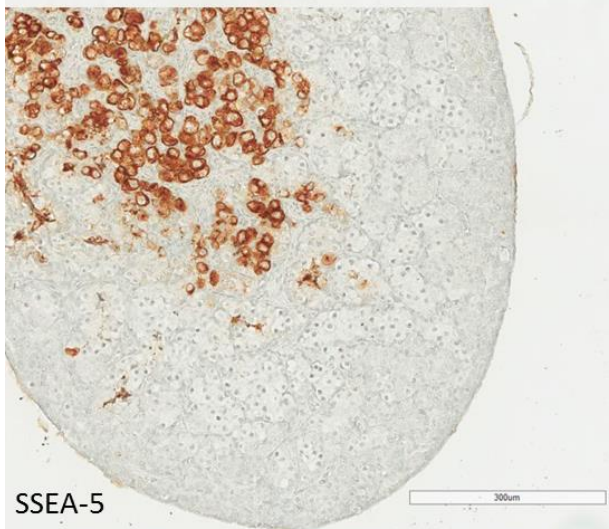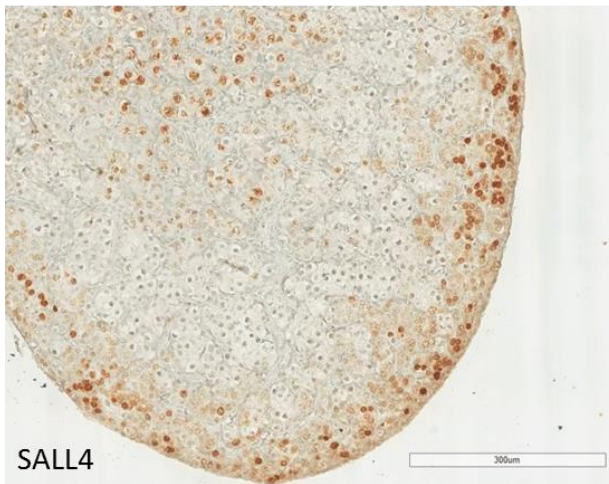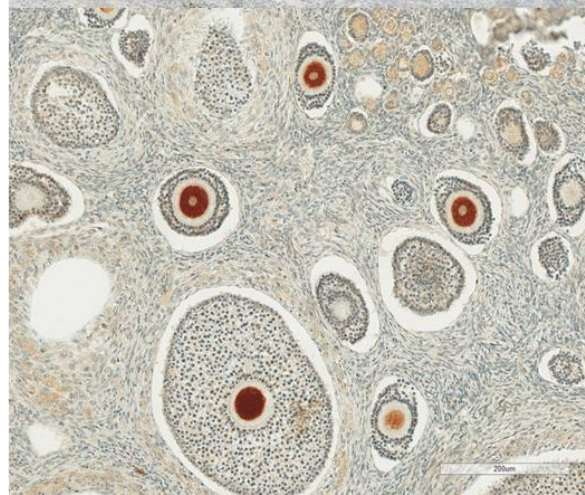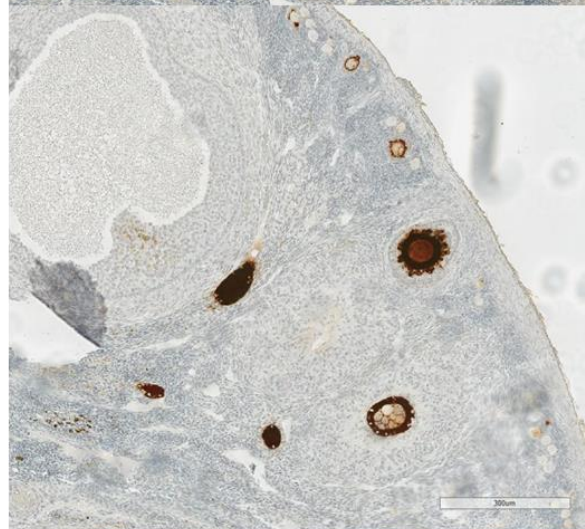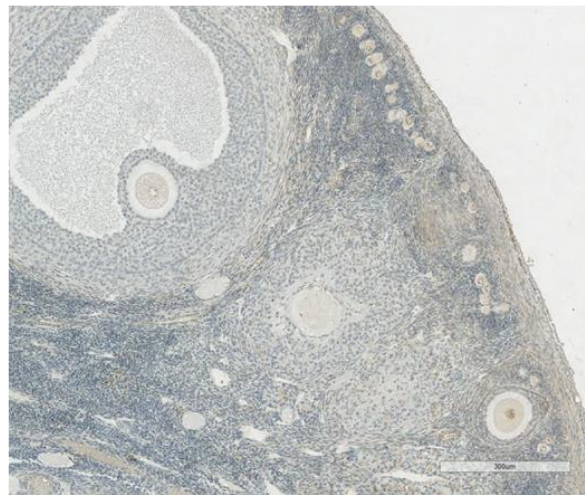
Figure 18 | SOX17 expression in the marmoset monkey ovary. Immunohistochemical staining of a marmoset (*Callithrix jacchus*) neonatal ovary **(A)** and adult ovary **(B)** for SALL4 (top panel), SSEA-5 (middle panel) and SOX17 (bottom panel). Scale bar ≙ 300 µm (all except bottom panel of B), 200 µm (bottom panel of B).
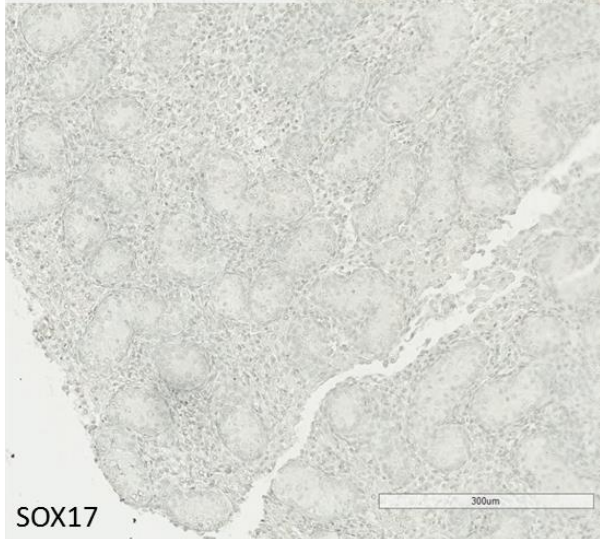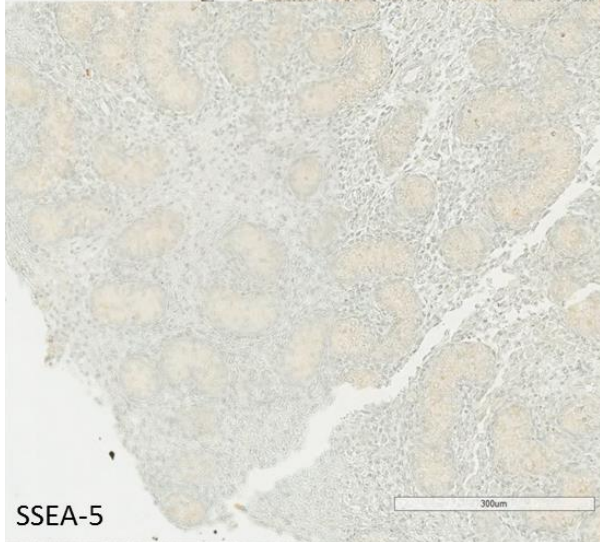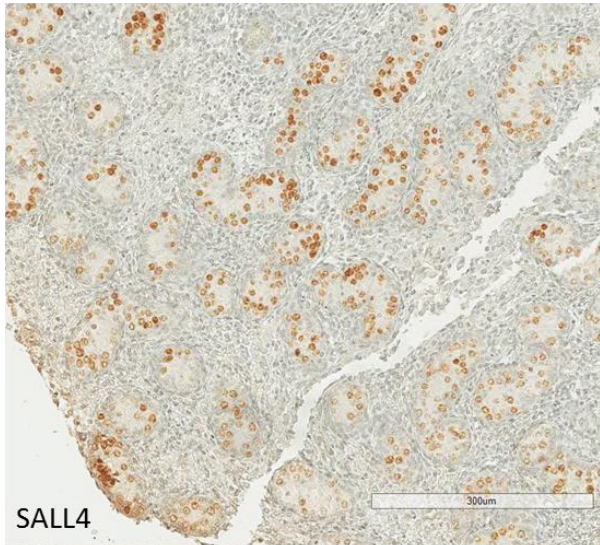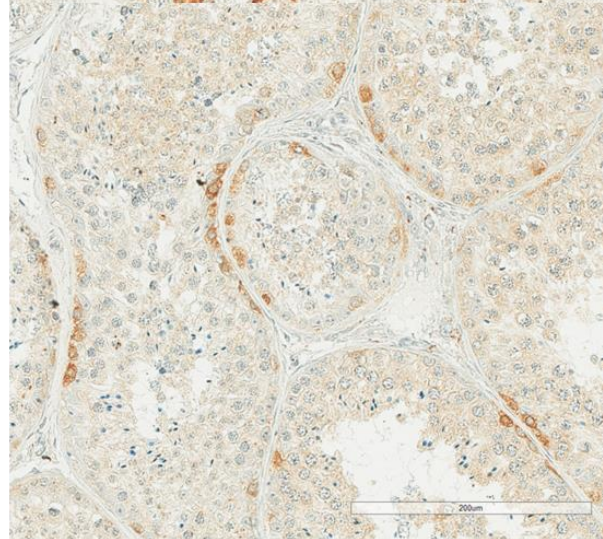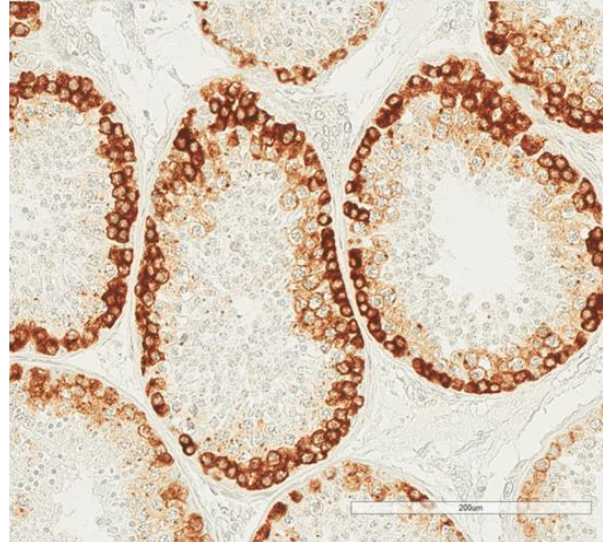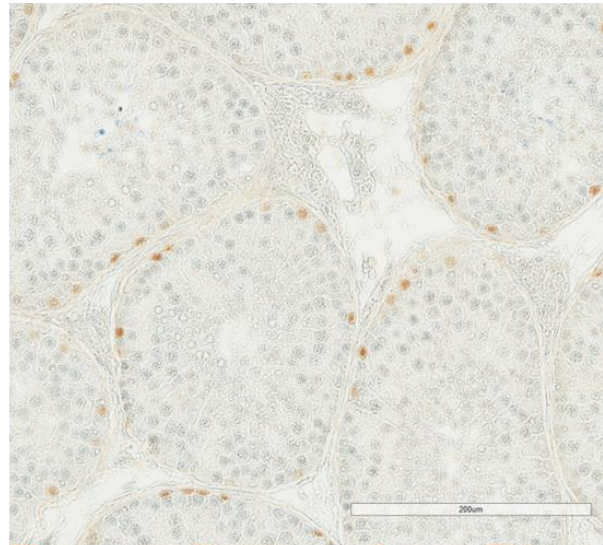
Figure 19 | SOX17 expression in the marmoset monkey testis. Immunohistochemical staining of a marmoset (*Callithrix jacchus*) neonatal testis **(A)** and adult testis **(B)** for SALL4 (top panel), SSEA-5 (middle panel) and SOX17 (bottom panel). Scale bar ≙ 300 µm (A), 200 µm (B).

54

Figure 19 shows the same staining approach as in Figure 18 but in the marmoset neonatal and adult testis. SOX17 and SSEA-5 were not detectable in the neonatal testis, while SALL4 was expressed in the spermatogonia in the seminiferous tubules. In the adult testis, SALL4 expression was restricted to some spermatogonia, possibly the spermatogonial stem cells, while SSEA-5 was expressed in the spermatogonia (pre-meiotic germ cells) and the primary spermatocytes (early meiotic germ cells). Interestingly, SOX17 IHC resulted in a staining pattern similar to that observed with SALL4 in regard to the cell type, where a fraction of the spermatogonia exhibited SOX17 expression. However, SALL4 was detected in the nucleus whereas SOX17 signal was detected in the cytoplasm.
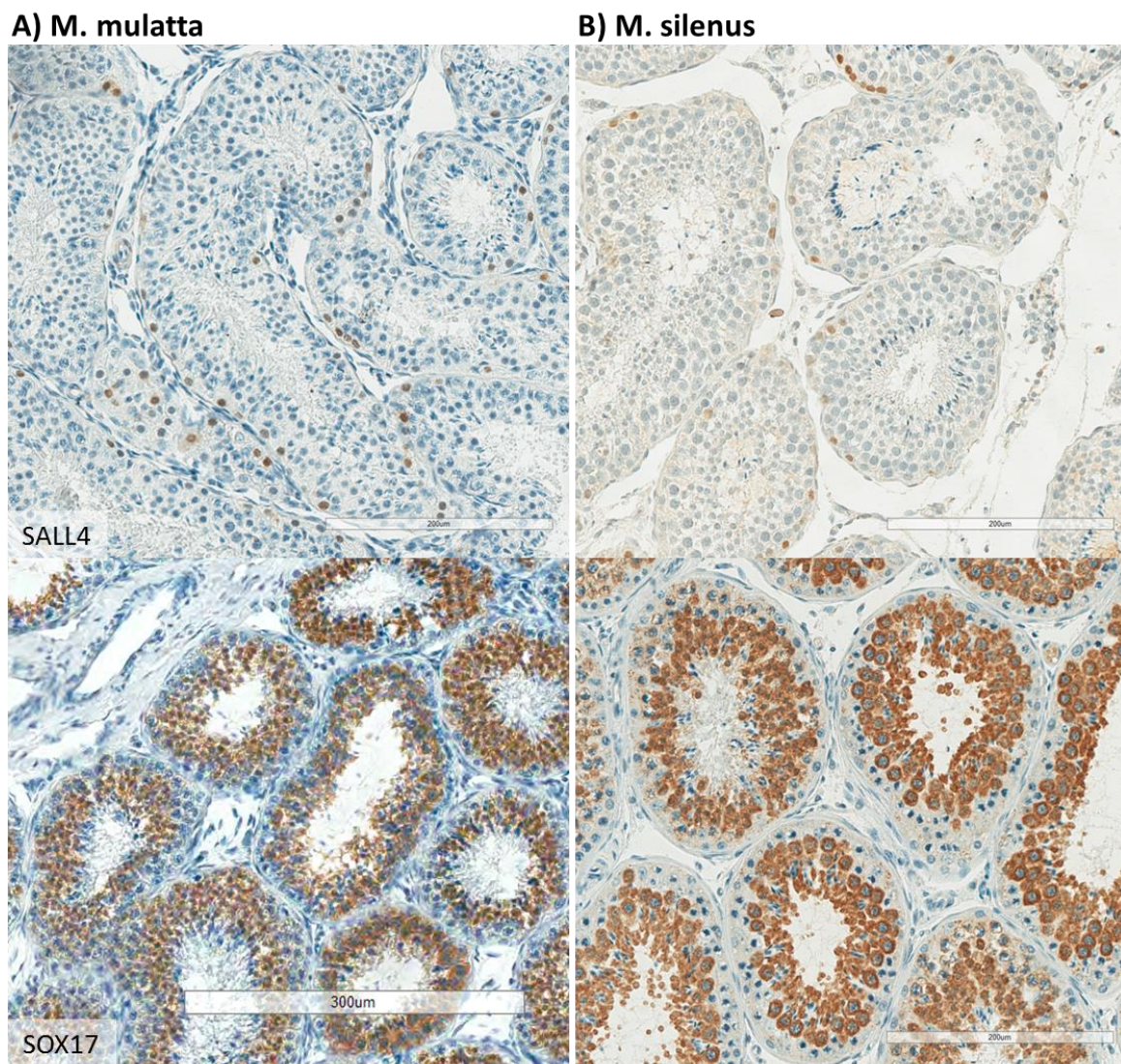
Figure 20 | SOX17 expression in the macaque testis. Immunohistochemical staining of a rhesus monkey (*Macaca mulatta*) adult testis **(A)** and lion-tailed macaque (*Macaca silenus*) adult testis **(B)** for SALL4 (top panel) and SOX17 (bottom panel). Scale bar ≙ 200 μm (top panel + bottom panel of B), 300 μm (bottom panel of A).

Finally, adult testes of rhesus macaque (*M. mulatta*) and lion-tailed macaque (*M. Silenus*) were stained for SALL4 and SOX17 (**Figure 20**). SALL4 was reliably detected in the spermatogonia of both species. In contrast to the marmoset testis, SOX17 was expressed in the macaque testis in most meiotic and post-meiotic germ cells (secondary spermatocytes, round and elongated spermatids). To better appreciate and compare this finding, higher magnifications of adult germ cells of the investigated species are shown in **Figure 21**, with cross sections of the seminiferous tubules from the basement membrane to the lumen (**Figure 21 B-D**).
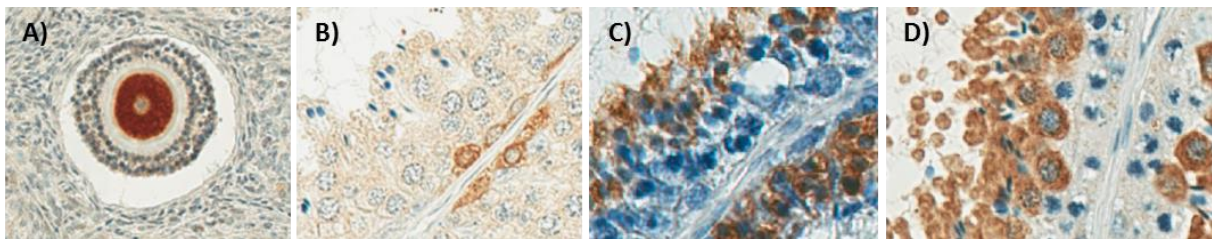
Figure 21 | SOX17 expression in NHP germ cells. Immunohistochemical staining for SOX17 in a marmoset monkey oocyte **(A)** and seminiferous tubules of the marmoset monkey **(B)**, the rhesus monkey **(C)** and the lion-tailed macaque **(D)**. All images higher magnification of images in Figures 15-17.

2.1.3 Searching for PGC selection and characterisation markers

2.1.3.1 ANPEP/CD13 is a novel surface marker on marmoset PGCs

Primordial germ cells can be identified by their expression of pluripotency factors. This was confirmed for the embryos isolated in this study as shown in **Figure 22**. While the available NANOG antibody always led to some amount of background staining (**Figure 22 B**), LIN28 and SALL4 were still expressed in many tissues of the younger embryos (**Figure 22 C+D**) and were therefore not suitable to identify PGCs in all embryo stages. Previous attempts in our lab have shown that marmoset PGCs do not seem to express any of the known surface proteins of human and mouse PGCs or ESCs (SSEA-1,-3,-4,-5; TRA-1-60, Tra-1-81). As tested before, SSEA-5 was not expressed on marmoset PGCs (**Figure 22 E**). Only OCT4A was specifically and robustly expressed in PGCs of all investigated stages (**Figure 22 A**) and therefore chosen to identify PGCs in all parts of this study.
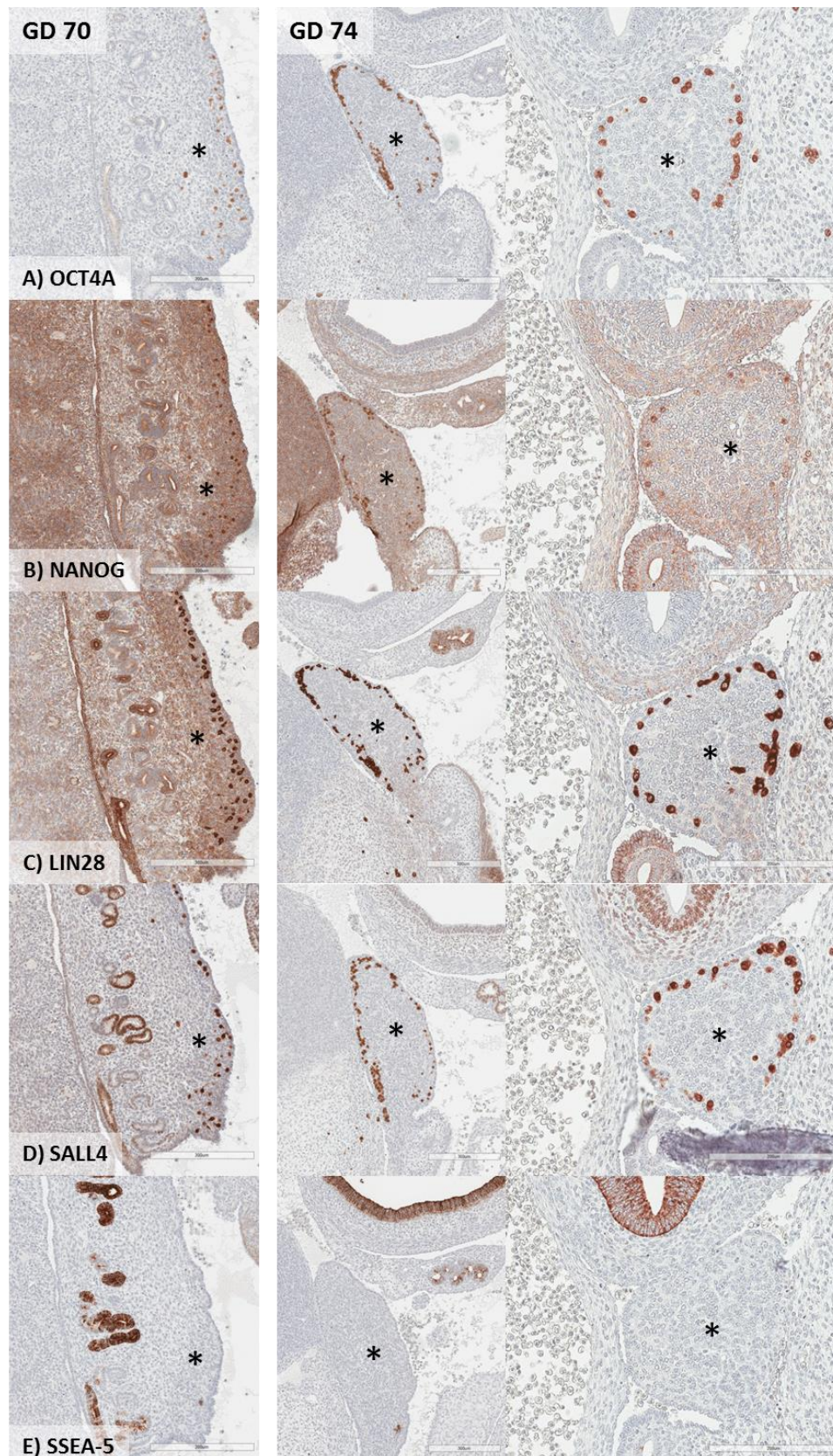
Figure 22 | Pluripotency factor expression in marmoset embryonic gonads. Immunohistochemical staining for OCT4A **(A)**, NANOG **(B)**, LIN28 **(C)**, SALL4 **(D)** and SSEA-5 **(E)** on tissue sections of a marmoset GD 70 embryo (left panel) and a GD 74 embryo (middle and right panel). Asterisks mark the genital ridge. Scale bar ≙ 300 µm (left and middle panel), 200 µm (right panel).

57
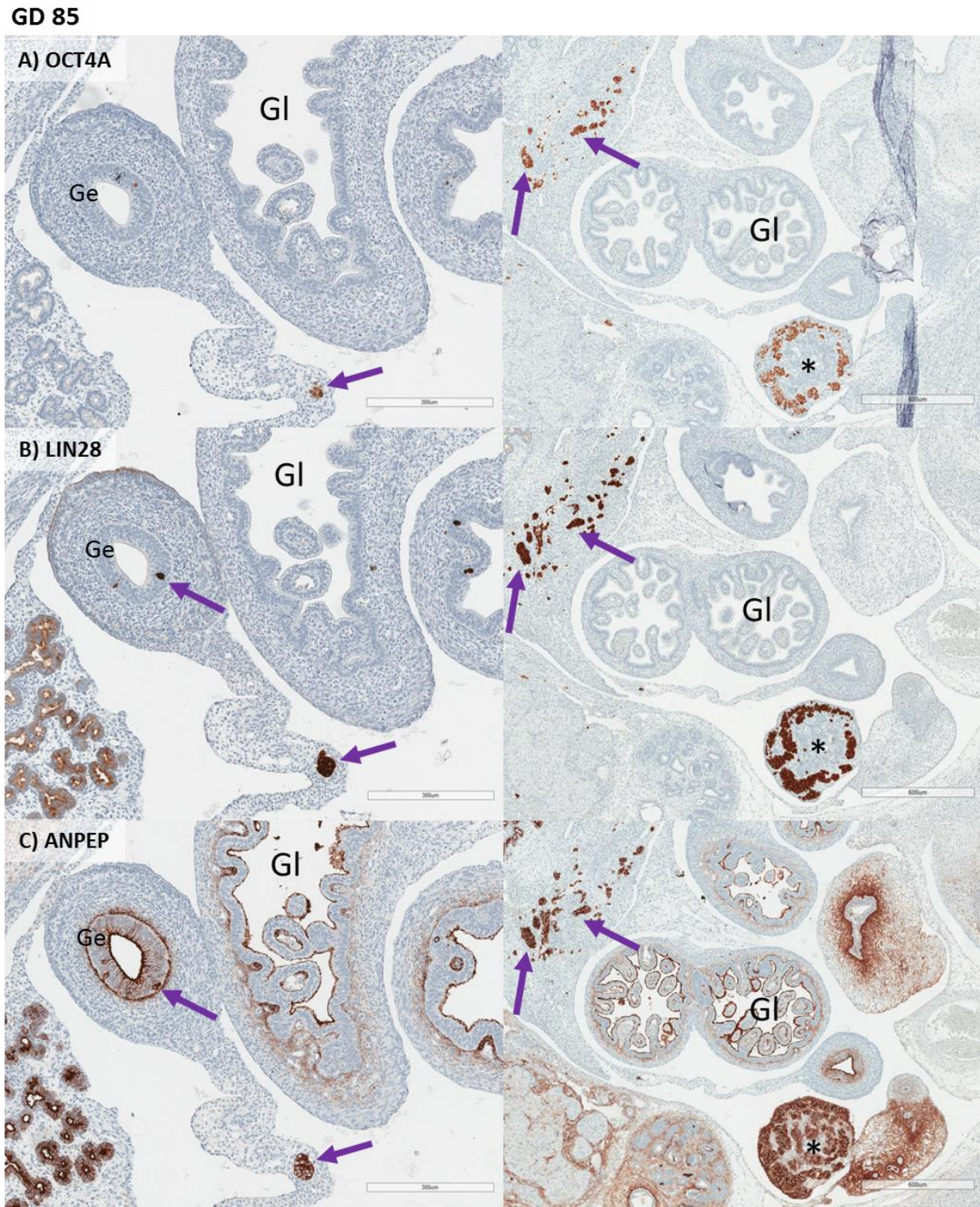
Figure 23 | Pluripotency factor and ANPEP expression on marmoset PGCs. Immunohistochemical staining for OCT4A **(A)**, LIN28 **(B)**, and ANPEP **(C)** on tissue sections of a marmoset GD 85 embryo. Gl: Gut lumen. Ge: Gut epithelium. Asterisks mark the embryonic gonad. Purple arrows highlight clusters of migrating PGCs that can be recognised in all three tissue sections. Scale bar ≙ 300 μm (left panel), 600 μm (right panel).
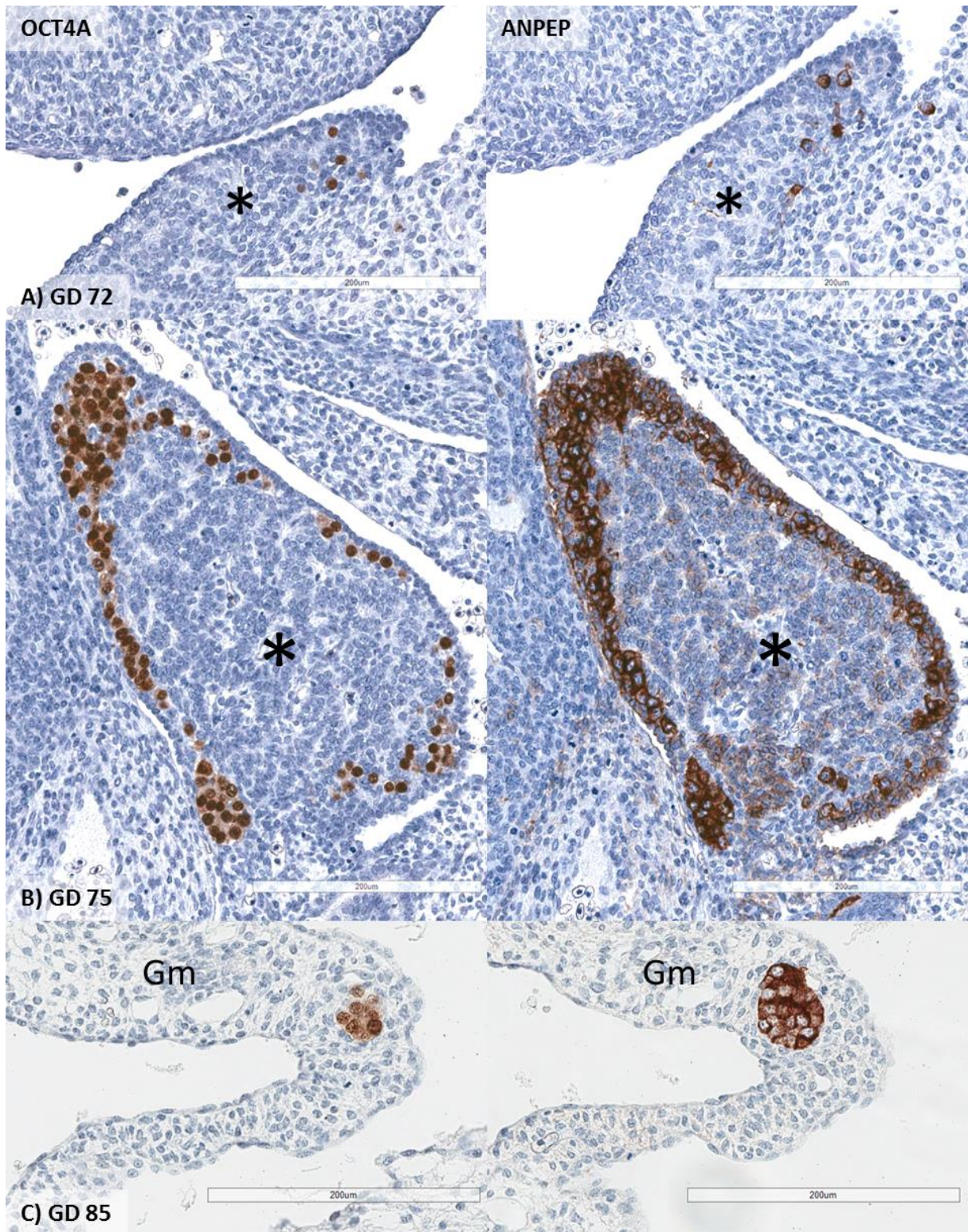
Figure 24 | ANPEP expression on marmoset PGCs. Immunohistochemical staining for OCT4A (left panel) and ANPEP (right panel) on tissue sections of marmoset embryos at GD 72 **(A)**, GD 75 **(B)** and GD 85 **(C)**. Gm: Gut mesenchyme. Asterisks mark the genital ridge. Scale bar ≙ 200 μm.

The work of a colleague suggested Aminopeptidase N (ANPEP, or CD13) to be expressed on human germ cell tumours (seminoma). Since seminoma share the expression of several genes with PGCs and spermatogonia[113], marmoset germ cells were stained for CD13 (unpublished data). Staining of marmoset PGCs revealed ANPEP expression on the PGC surface. **Figure 23** shows sections of a GD 85 embryo stained for OCT4A, LIN28 and ANPEP, where individual clusters of PGCs can be nicely identified in consecutive tissue sections (purple arrows). By comparison of these markers, the different subcellular localisations of the proteins are clearly distinguishable, with OCT4A being in the nucleus, LIN28 in the cytoplasm and ANPEP on the cell surface. However, although ANPEP/CD13 was strongly expressed on the PGC surface, it is not a specific marker as visible in **Figure 23 C**. In **Figure 24**, higher magnifications of ANPEP-positive marmoset PGCs are shown, confirming that ANPEP can be found on gonadal PGCs (**Figure 24 A+B**) as well as migratory PGCs (**Figure 24 C**).

2.1.3.2 CD31 is expressed on the surface of marmoset PGCs

Platelet endothelial cell adhesion molecule-1 (PECAM-1), or CD31, is usually found on endothelial or haematopoietic cells. Since it was also shown to be expressed on migratory and gonadal mouse PGCs[114], I wanted to test marmoset PGCs for expression of CD31. As **Figure 25** shows, the PGCs in the embryonic gonad of GD 74 and GD 85, revealed by OCT4A expression, actually also showed CD31 signal on their surface, making this a new potential candidate for PGC selection. Additionally, CD31 was expressed on the endothelia of blood vessels in the gonad and other parts of the embryo. In the GD 70 embryo, the genital ridge is still less condensed and single PGCs spread over a wider area. This together with CD31 expression in more tissues/more background staining however made it impossible to identify the PGCs via CD31 expression in the GD 70 embryo (data not shown).

60

A) GD74

B) GD85
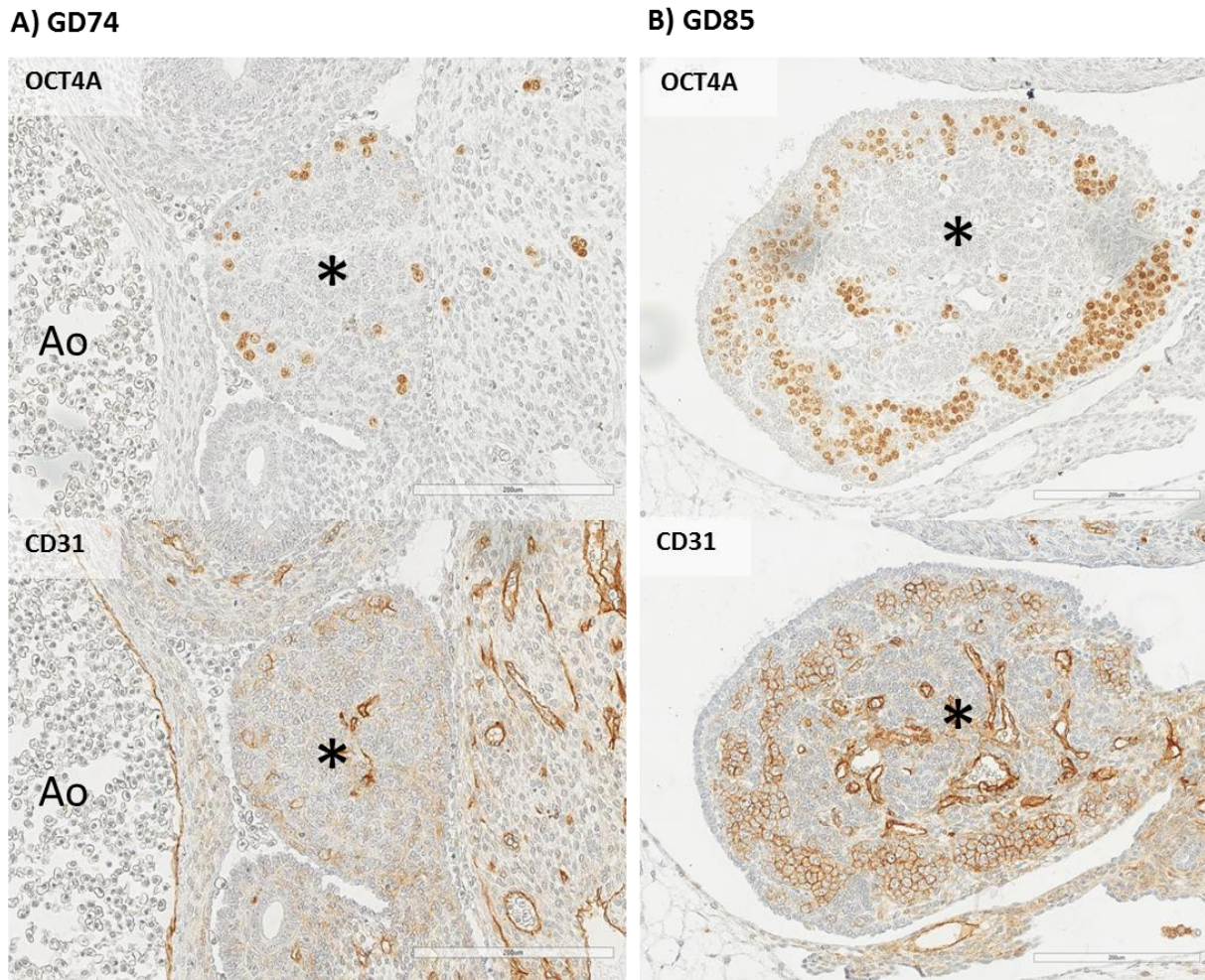
Figure 25 | CD31 expression in the marmoset monkey embryonic gonad. Immunohistochemical staining of tissue sections for OCT4A (top panel) and CD31 (bottom panel) in marmoset embryos at GD 74 **(A)** and GD 85 **(B)**. Ao: Aorta. Asterisks mark the embryonic gonad. Scale bar ≙ 200 μm.

2.1.3.3 Transcription factor PAX5 is not expressed in marmoset PGCs

Paired box protein 5 (PAX5) is considered to be a master regulator of B-cell development and can be found on naive B-cells in the bone marrow and lymphatic organs. Unpublished data shown during a conference talk (Dr. Renee Reijo-Pera; XVIth International Workshop on the Development and Function of the Reproductive Organs; Münster, Germany, 2015) indicated that OCT4 might form a heterodimer in early mouse PGCs with PAX5 instead of SOX2 as in pluripotent stem cells. I wanted to test whether PAX5 could also be detected in early marmoset PGCs. For this purpose, sequential sections of GD 50 and GD 72 marmoset embryos were stained alternatingly for OCT4A to identify the PGCs, and PAX5. The results are shown in **Figure 26**. PAX5 antibody stained cells in marmoset and rhesus bone marrow and spleen (**Figure 26 C** and not shown), confirming that the used antibody is suitable for the

detection of the marmoset PAX5 protein. However, no PAX5 was detectable in PGCs of both investigated embryonic stages (**Figure 26 A+B**).
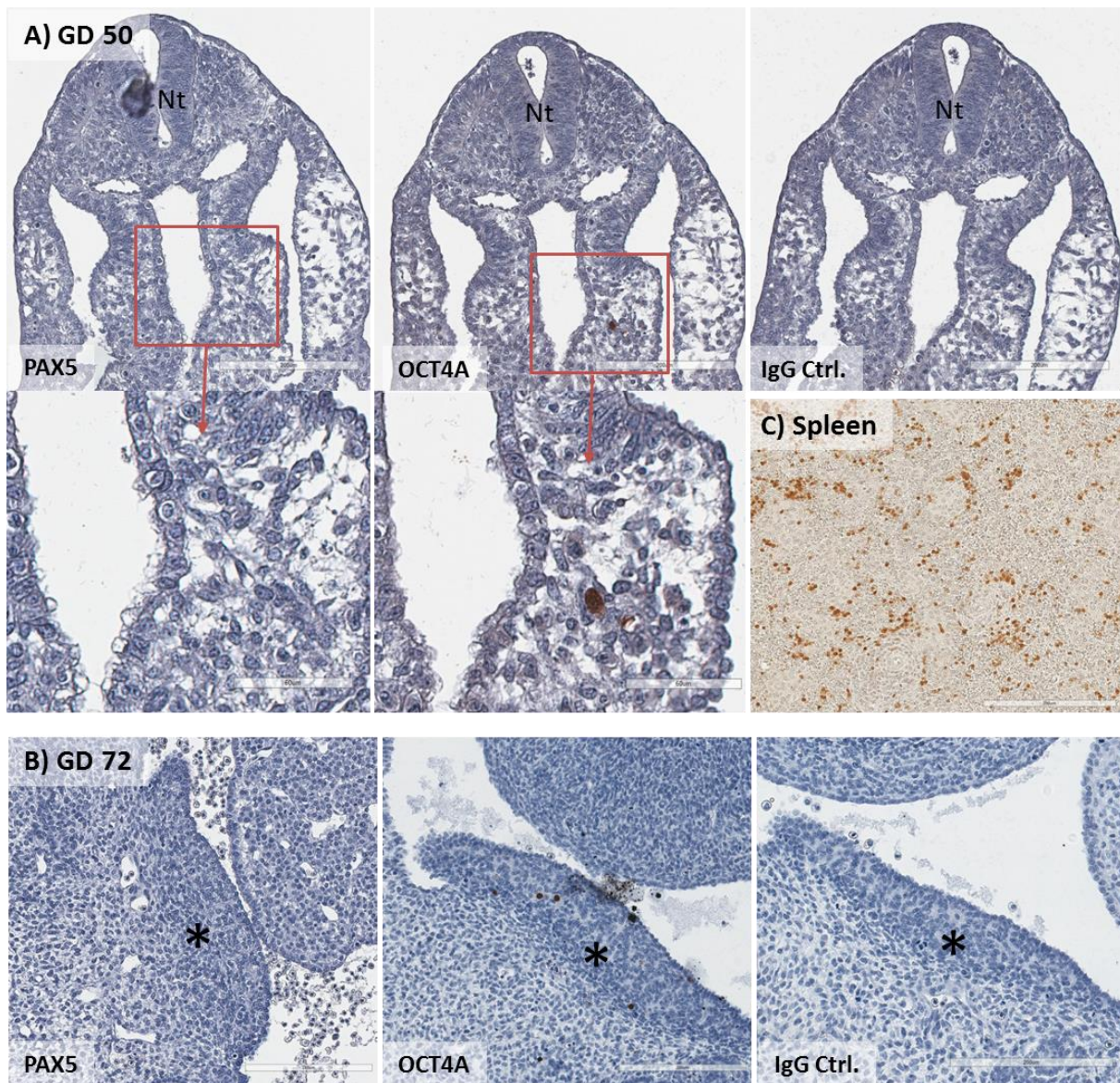
Figure 26 | PAX5 expression in the marmoset monkey embryo. Immunohistochemical staining of tissue sections in a marmoset GD 50 embryo **(A)** and a GD 72 embryo **(B)**. Sequential sections stained for PAX5 (left panel), OCT4A (middle panel) and IgG isotype control (right panel). The red boxed areas are shown in higher magnification (bottom panel of A). **C)** PAX5 staining of a marmoset monkey neonatal spleen used as positive control for PAX5 expression. Nt: Neural tube. Asterisks mark the developing genital ridge. Scale bar ≙ 200 µm (A+B), 60 µm (A bottom panel).

2.1.3.4 Expression of NLRP7 in oocytes begins around birth

The cytoplasmic NACHT, LRR and PYD domains-containing protein 7 (NLRP7) is highly expressed in the marmoset pre-implantation embryo[115] and marmoset ESCs[14], both of

which are part of the germline or germline-derived. As mentioned, many factors expressed in the pre-implantation embryo and in ESCs are also expressed in pre-meiotic germ cells. I therefore wanted to test the hypothesis that NLRP7 might be a marker of pre-meiotic germ cells.
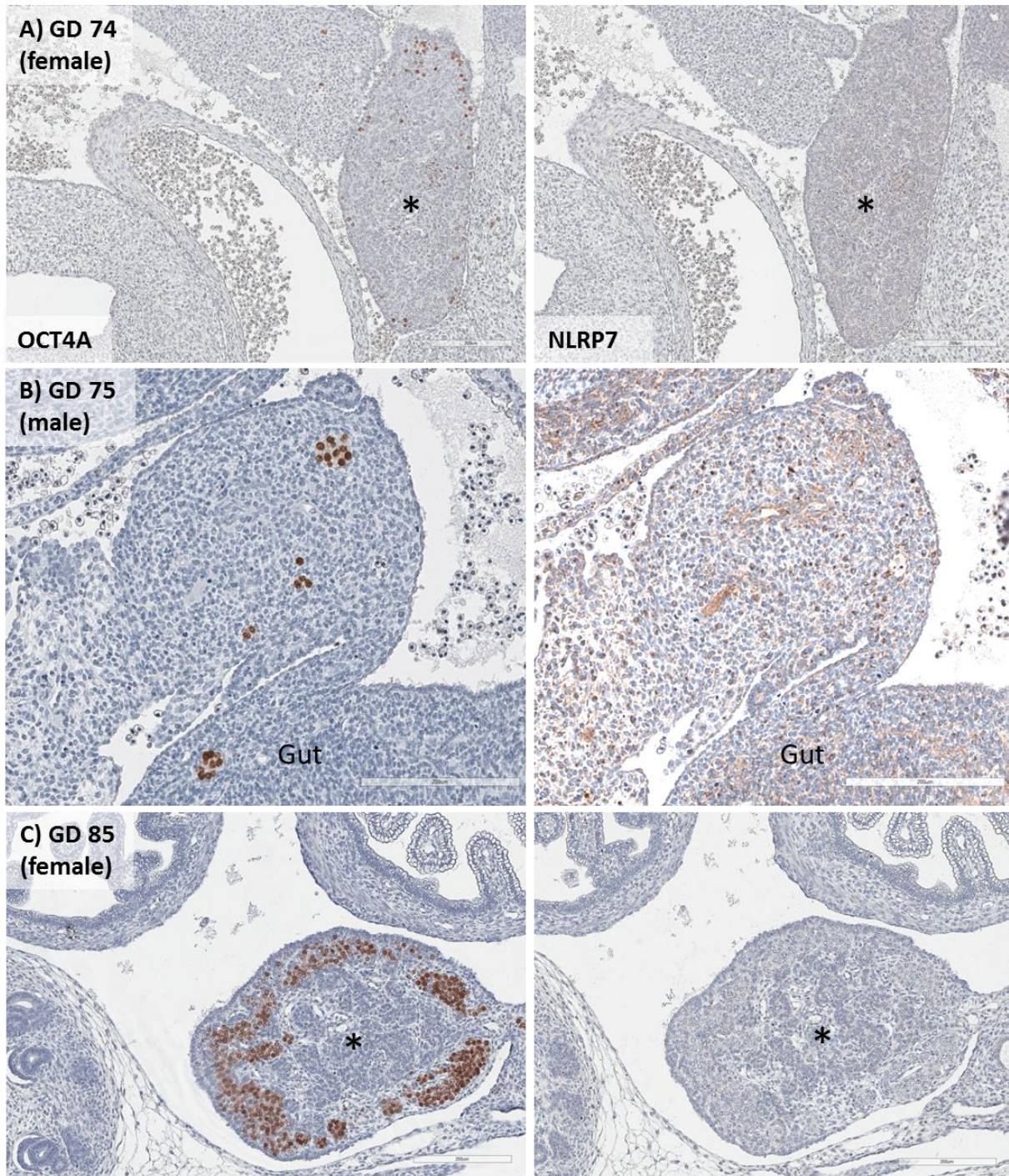
Figure 27 | NLRP7 expression in the marmoset monkey embryo. Immunohistochemical staining for OCT4A (left panel) and NLRP7 (right panel) on tissue sections of marmoset embryos at GD 74 **(A)**, GD 75 **(B)** and GD 85 **(C)**. Asterisks indicate genital ridges. Scale bar ≙ 200 µm
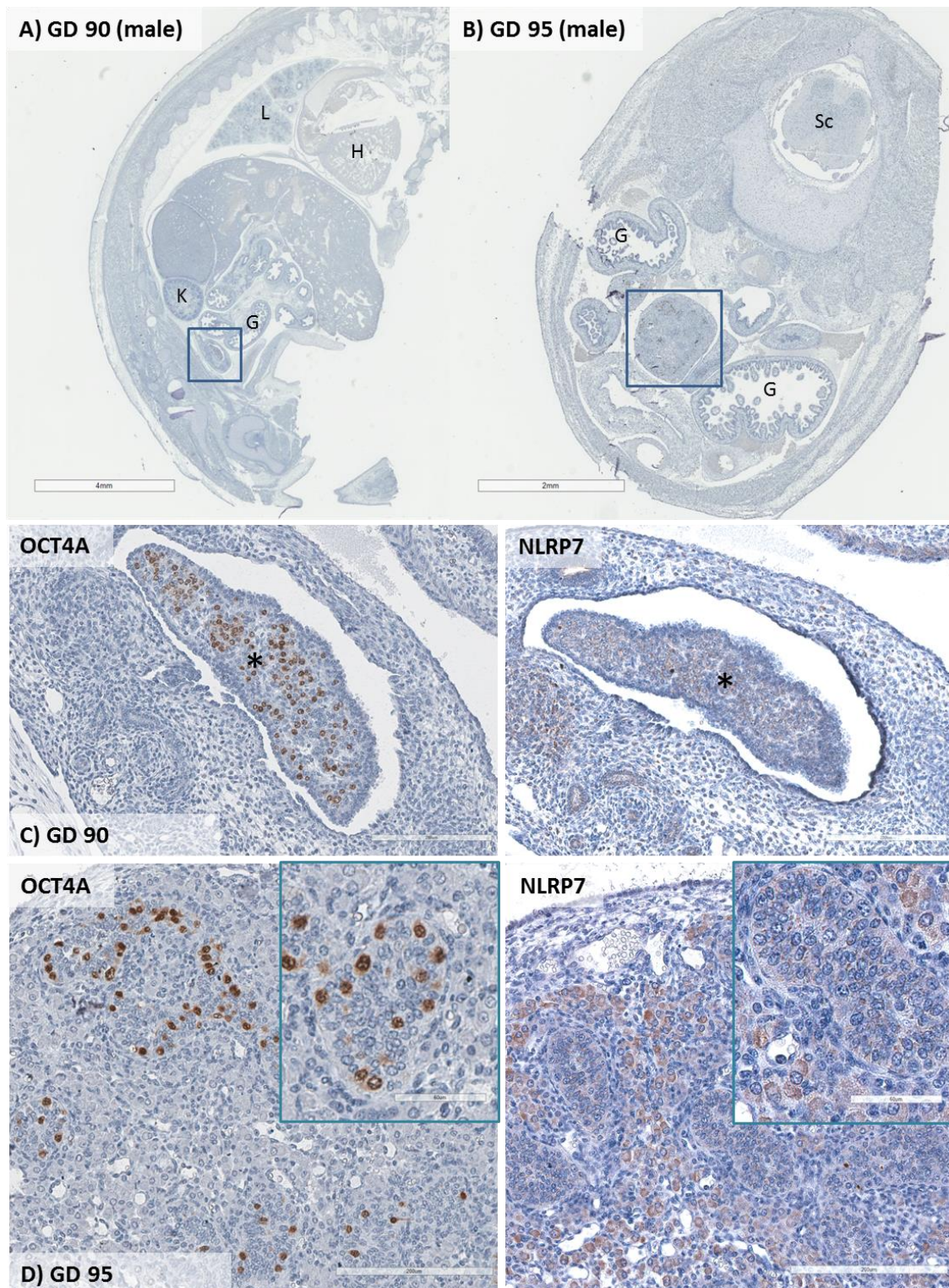
Figure 28 | NLRP7 expression in the marmoset monkey foetal gonad. A) + B) Histological overview sections of a GD 90 ((A), sagittal) and GD 95 ((B), transversal) marmoset foetus. G: Gut, H: Heart, K: Kidney, L: Lung, Sc: Spinal cord. Boxed area shows foetal gonad. Scale bar ≙ 4mm (A), 2 mm (B). **C) + D)** Immunohistochemical staining for OCT4A (left panel) and NLRP7 (right panel) on tissue sections of a marmoset GD 90 foetus (C, higher magnification of foetus in A) and a GD 95 foetal gonad (D, higher magnification of foetus in B). Inlays in D) show higher magnification of a developing seminiferous tubule. Asterisks indicate foetal gonad. Scale bar ≙ 200 μm (C, D), 60 μm (inlays in D).

Figure 27 shows marmoset embryos of both sexes at different gestational days with PGCs marked by OCT4A. No NLRP7 signal could be detected in any of the PGCs. **Figure 28** gives a histological overview of two male marmoset foetuses cut in the transversal and sagittal plane, with the foetal gonad tissues indicated in the blue-boxed areas. A higher magnification of the foetal gonads stained for OCT4A and NLRP7 again revealed no NLRP7 signal in the germ cells but rather in interstitial cells of the foetal testis. **Figure 29** shows neonatal and adult marmoset gonads stained for NLRP7. VASA and LIN28 stainings are included in the neonatal gonads to mark the germ cells. Neither in the neonatal nor the adult testis, any signal for NLRP7 was detectable in the germ cells. In the adult ovary, oocytes showed strong NLRP7 expression, while in the neonatal ovary already moderate signal for NLRP7 could be detected in the cytoplasm of the germ cells.
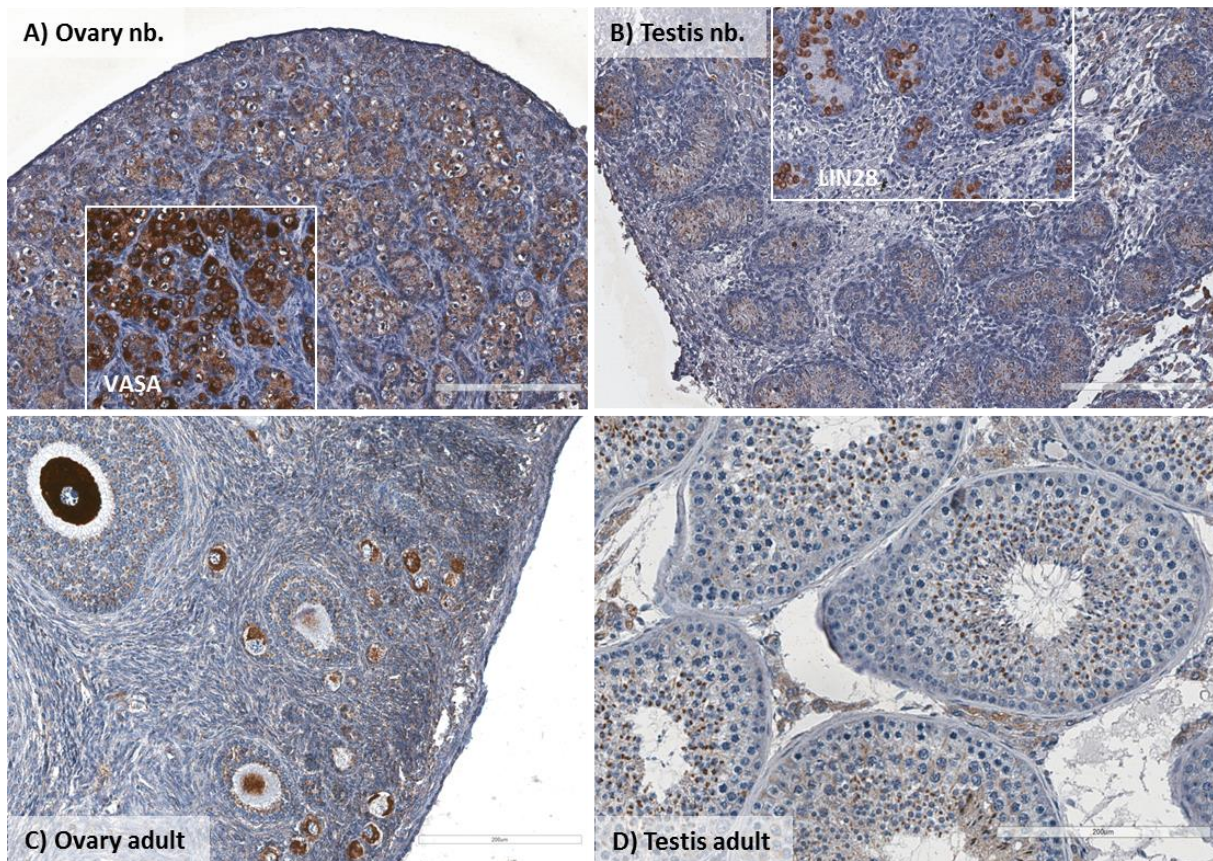
Figure 29 | NLRP7 expression in adult marmoset monkey gonads. Immunohistochemical staining for NLRP7 on tissue sections of a marmoset neonatal ovary **(A)**, neonatal testis **(B)**, adult ovary **(C)** and adult testis **(D)**. Inlay in A) shows VASA staining in the same ovary, inlay in B) shows LIN28 staining in the same testis. Scale bar ≙ 200 μm.

65

2.2 Part II – Cell culture studies

2.2.1 Mouse (*Mus musculus*) PGC culture

Mouse embryonic germ cell (EGC)-derivation was attempted to establish the protocol and practice before using the very limited marmoset monkey embryo material. Mouse embryonic stem cells were cultured in parallel as control (**Figure 30**). An overview of all performed mouse PGC culture approaches during this project is given in **Table 4**.
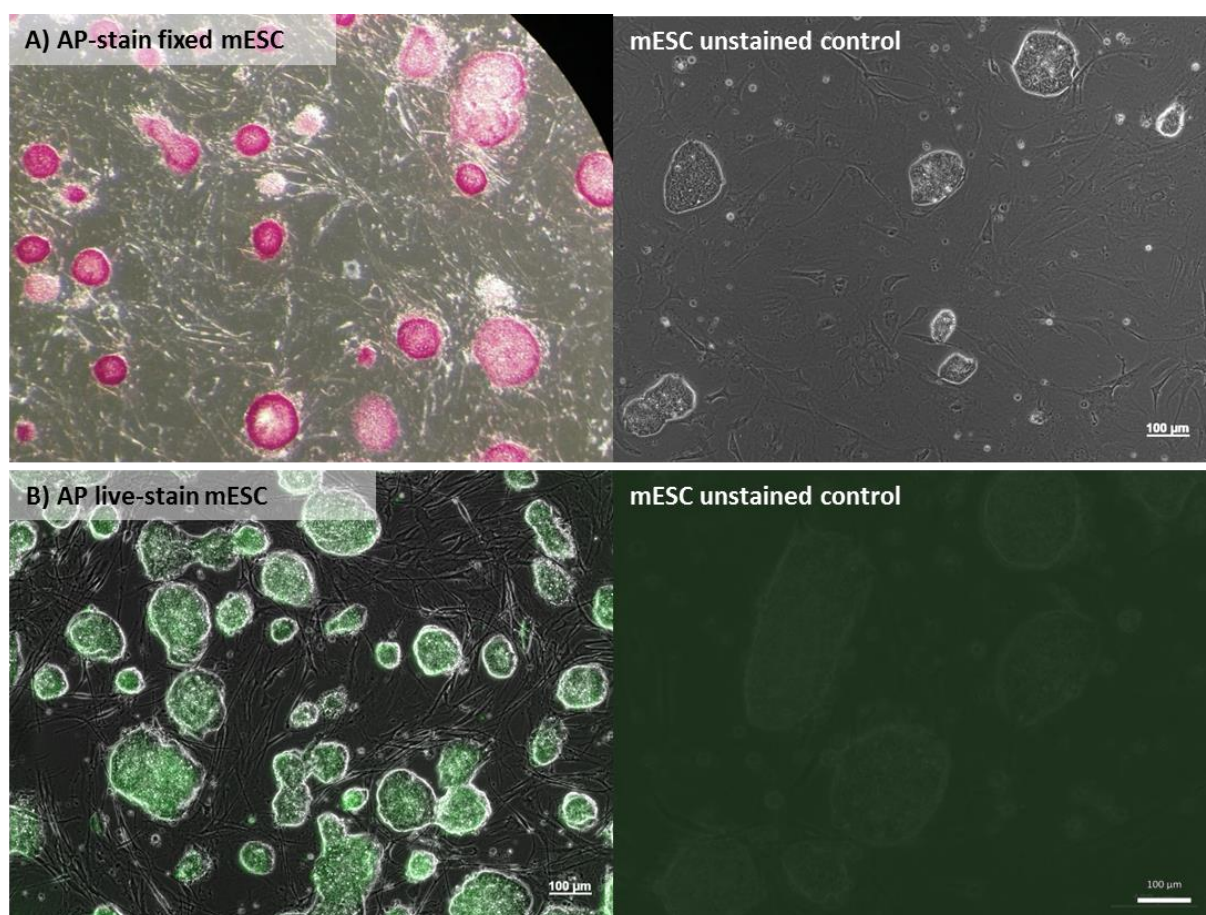
Figure 30 | Different AP-staining methods on mouse ESC. A) Mouse C57BL/6 embryonic stem cell colonies fixed and stained for expression of Alkaline Phosphatase (purple colour) and unstained control. **B)** Mouse C57BL/6 embryonic stem cell colonies after AP-live stain (green fluorescence) and unstained control. Scale bar ≙ 100 µm.

The initial protocol was based on publications by Durcova-Hills (2008)[101] and De Miguel (2011)[68]. Briefly, embryonic genital ridges (GR) and mesonephroi (MN) containing the PGCs were dissected from embryos of embryonic day (E) 10.5 to E 13.5. It was also attempted to culture a cell suspension of E 8.5 embryo fragments.

66

Table 4 | Overview of all mouse embryo retrieval and culture approaches for EGC derivation.

Strain	Embryonic day	Method	Feeder	Medium	Embryos/Cell number/Plating?	Result Cell Culture
CD1	E8.5	Embryo fragment digestion, plating	SNLP (1.5 Cryos/Plate)	ESM + gf	0.5 of one embryo/well; 24-well plate	Wells overgrown; AP live st. after 8d negative
CD1	E10.5	"	"	"	"	After 5d wells totally overgrown, feeder detach --> discarded
CD1	E12.5	GR digestion, plating	SNLP (2 Cryos/Plate)	"	0.25 of one embryo/well; 24-well plate	Picking of "colonies" difficult (manually and Accutase), nothing grew out after, AP-negative
CD1	E7.5	Embryo fragment digestion, MACS purification	SNLP (1.5 Cryos/Plate)	"	After MACS: 1/12 of total cells/well; 12-well plate	After 7d feeder bad; AP st. negative --> **Pellet for IHC** negative for LIN28 + OCT4
CD1	E8.5	"	"	"	"	"
CD1	E12.5	**GR digestion**, MACS purification	SNLP (2.5 Cryos/Plate)	"	Before MACS: 525 000 cells total; After MACS: 110 000 cells total, **2300 cells/well** on 2x 24-well plates with **removable foil bottom**	After 4d feeder detached --> discarded. Foil bottom wells for IF are useless.
CD1	E13.5	Digestion/FACS analysis	-	-	After digestion: 1.1x10^6 cells total	**10-12 %** of genital ridge cells SSEA-1 positive = PGCs
BL/6	**E11.5**	MACS purification	SNLP (3.5 Cryos/Plate)	ESM + gf	After MACS: 20 000 cells total from 12 Embryos; **1600 cells/well** on 12 well-plate	Feeder not too bad! After 9d AP-positive colonies! After 11d minimum 1 colony/well! However not visible by eye without staining.
CD1	E12.5	MACS and FACS	-	-	Before MACS: 3.3x10^6 cells total	Unstained: 2% SSEA-1 positive (Background); Before MACS: 34% SSEA-1 positive; After MACS: 94% SSEA-1 positive! **Purification works**
CD1	E11.5	MACS purification	SNLP (4 Cryos/Plate)	ESM + gf	After MACS: 120 000 cells total, **5000 cells/well** on 2x12 well-plates	AP live st. after 10d negative, subsequent AP fixed staining also negative.
BL/6	E11.5	"	"	"	After MACS: 30 000 cells total, **5000 cells/well** in 5 wells of 6 well-plate	After 7d 1 colony visible without staining! Manually picked --> no further outgrowth. No other colonies visible after AP staining
"	"	"	SNLP Mitomycin C-treated	"	5000 cells on 10 cm-dish with Mitomycin-inactivated SNLP feeders	AP st. after 8d negative
BL/6	E11.5	"	**MEFs**	"	After MACS: 17 500 cells total, **5800 cells/well** in 3 wells of 6 well-plate	No colonies visible; AP st. after 10d negative
BL/6	E12.5	"	SNLP (4 Cryos/Plate)	**M-10 + gf**	After MACS: 40 000 cells total, **13000 cells/well** in 3 wells of 6 well-plate	No colonies visible; AP st. after 8d negative
BL/6	E11.5/12.5	**FACS sorted**	**SNLP/MEF Mix**	ESM + gf	After Sort: 17 000 cells total of 12 Embryos (2.1% SSEA-1 positive cells of total cell suspension); **5600 cells/well** in 3 wells	AP live stain after 8d (old and new Kit) + AP stain on fixed cells --> negative
BL/6	E11.5	Digestion of GR, 48hr plating	SNLP (1.5 Cryos/Plate)	**mPGC medium (ESM + 10% FCS)**	2 GR (=1 embryo)/well; 6-well	AP st. after 48h in: 82/89/92 AP-positive cells per well (= per embryo)
BL/6	E11.5 (12.5?)	Digestion of GR, 8d plating	SNLP (1.5 Cryos/Plate)	mPGC Medium	2 GR (=1 embryo)/well; 6-well	AP live and fixed stain --> no colonies, quantification failed
BL/6	E11.5	MACS purification	SNLP (1.5 Cryos/Plate)	mPGC Medium	Density gradient: 10'000, 5'000, 3'000, 2'000, 1'000, 500 cells/well; 6-well plate	No colonies visible bye eye, AP stain revealed purple colonies of single cell layer; Nr. per well corresponds with starting cell number (15, 8, 4, 2, 0, 0)
"	"	"	"	"	Rest-well (remaining PGCs plated)	1 colony visible bye eye (in feeder gap), manually picked --> no further outgrowth
BL/6	**E10.5**	**Bonn protocol**	Sl4-m220	**N2B27 PGC medium**	2 GR (=1 embryo)/well; 6-well	After 14d: swimming cell clumps. Most potential colonies already overgrown/grainy. --> pick earlier!
BL/6	E10.5	Bonn protocol	Sl4-m220	N2B27 PGC medium	2 GR (=1 embryo)/well; 6-well	After 8d: some colonies with nice morphology, but floating/detach during medium change. AP-st. positive on some colonies, but with granular morphology/floating. After 12d: almost nothing left on plate --> initial cell density too high?
BL/6	E10.5	Bonn protocol	Sl4-m220	N2B27 PGC medium	2 GR (=1 embryo)/well; 6-well	After 7d: AP-st. on some wells --> very few purple colonies, detached --> PGCs in suspension? Few remaining attached colonies --> AP-negative. Still trouble with feeder cells. Pick of 12 attached and 12 floating colonies and subculture as EGCs/2i --> after 11 days of subculture large colonies in 3/24 wells detectable (=12.5%) from originally attached and floating colonies --> AP-negative.

Exemplary images of mouse embryo dissections are given in **Figure 31 A+B**. GR and MN had to be enzymatically digested and cells had to be cultured on special feeder cells that express a membrane-bound form of stem cell factor (SCF), which according to literature is essential for EGC derivation[97, 98]. If the culture of the PGCs and their conversion into EGCs was successful, colonies would appear after 7-12 culture days that express the protein Alkaline Phosphatase (AP), which is considered a hallmark of pluripotency. **Figure 30** shows pictures of mouse ESCs stained for AP-expression with two different methods. Both staining methods showed clear AP-signal of undifferentiated ESC colonies. **Figure 31 C+D** shows a representative image of a PGC culture 5 days after cell isolation. Small round structures (indicated by arrows) could be observed in the culture plates that were thought to be potential colonies. However they did not express AP and did not lead to further colony formation when sub-cultured on fresh culture plates.
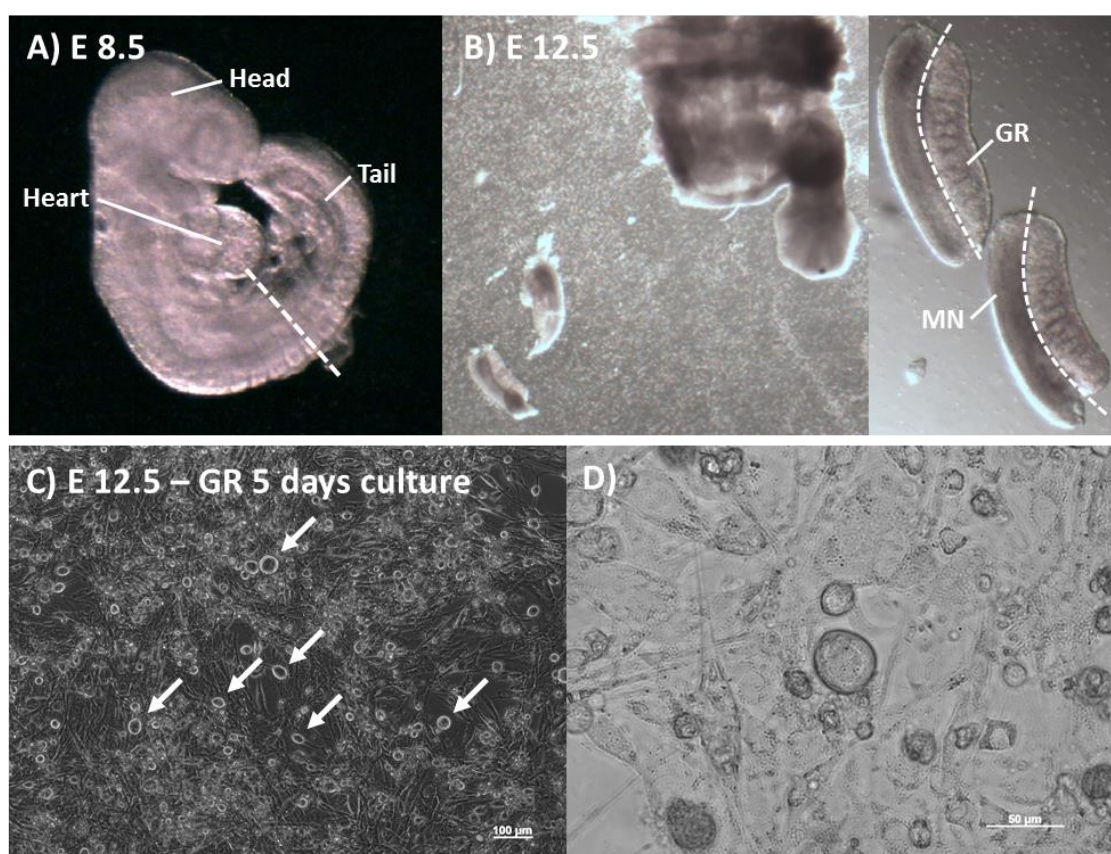
Figure 31 | Mouse GR isolation and PGC culture initiation. A) Representative mouse E 8.5 embryo. Dotted line marks posterior third of embryo which contains PGCs. **B)** Representative mouse E 12.5 embryo after preparation of the urogenital ridges and higher magnification of isolated UGR (right panel). Dotted line indicates border between genital ridge and mesonephros. **C)** Exemplary picture of culture dish 5 days after GR culture initiation. Arrows indicate potential cell colonies. Scale bar ≙ 100 μm. **D)** Higher magnification of potential colony in C). Scale bar ≙ 50 μm.

To enrich the proportion of PGCs in the starting cell population for the culture, MACS purification was performed. The mouse PGCs were labelled using α-SSEA-1 antibody and isolated from the GR cell suspension over a magnetic column. The efficiency of the enrichment protocol was tested via flow cytometry analysis of the cell suspension before and after MACS. **Figure 32** shows that the proportion of SSEA-1-positive PGCs of the total E 12.5 GR cells was 33.8 %, after MACS a purity of 93.6 % was achieved. Despite the high percentage of SSEA-1-positive cells, most likely PGCs, no colonies appeared in the culture. Additionally, the quality of the feeder cells was low, with the cells detaching from the plate and forming web-like structures instead of an evenly-spread surface for the PGCs to grow on. Despite several changes of cell density and the culture medium, the problem with the feeder cells could not be overcome.
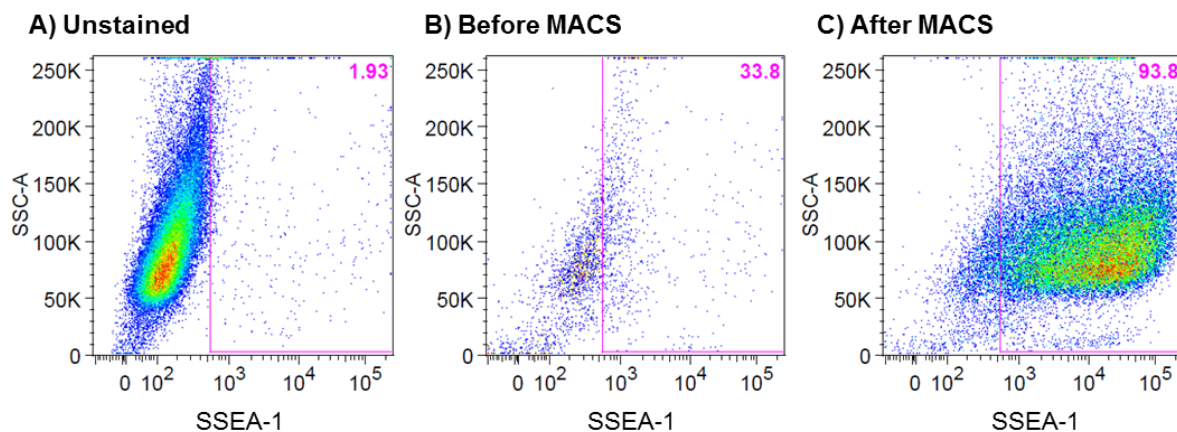
Figure 32 | FACS analysis of purification efficiency of mouse E 12.5 GR cells. MACS was performed on mouse E 12.5 genital ridge cell suspension using α-SSEA-1 antibody to select PGCs. Cells were collected before and after the purification process and analysed via flow cytometry. Plots show singlet cells gated for SSEA-1, pink number indicates percentage of SSEA-1-positive cells. **A)** Unstained control. **B)** Cells before MACS purification. **C)** Cells after MACS purification.

After switching from mouse embryos of CD1 genetic background to mice of C57BL/6-background, AP-positive cell colonies could be detected in one culture approach (**Figure 33**, no colour image available). However, these colonies were not detectable by eye and only revealed by their purple colour after AP-staining due to them being formed by a monolayer of cells that was hardly distinguishable from the feeder cell layer below. In another experiment, one potential EGC colony appeared that could be detected by eye. This colony was sub-cultured, but did not lead to the formation of further EGC colonies.
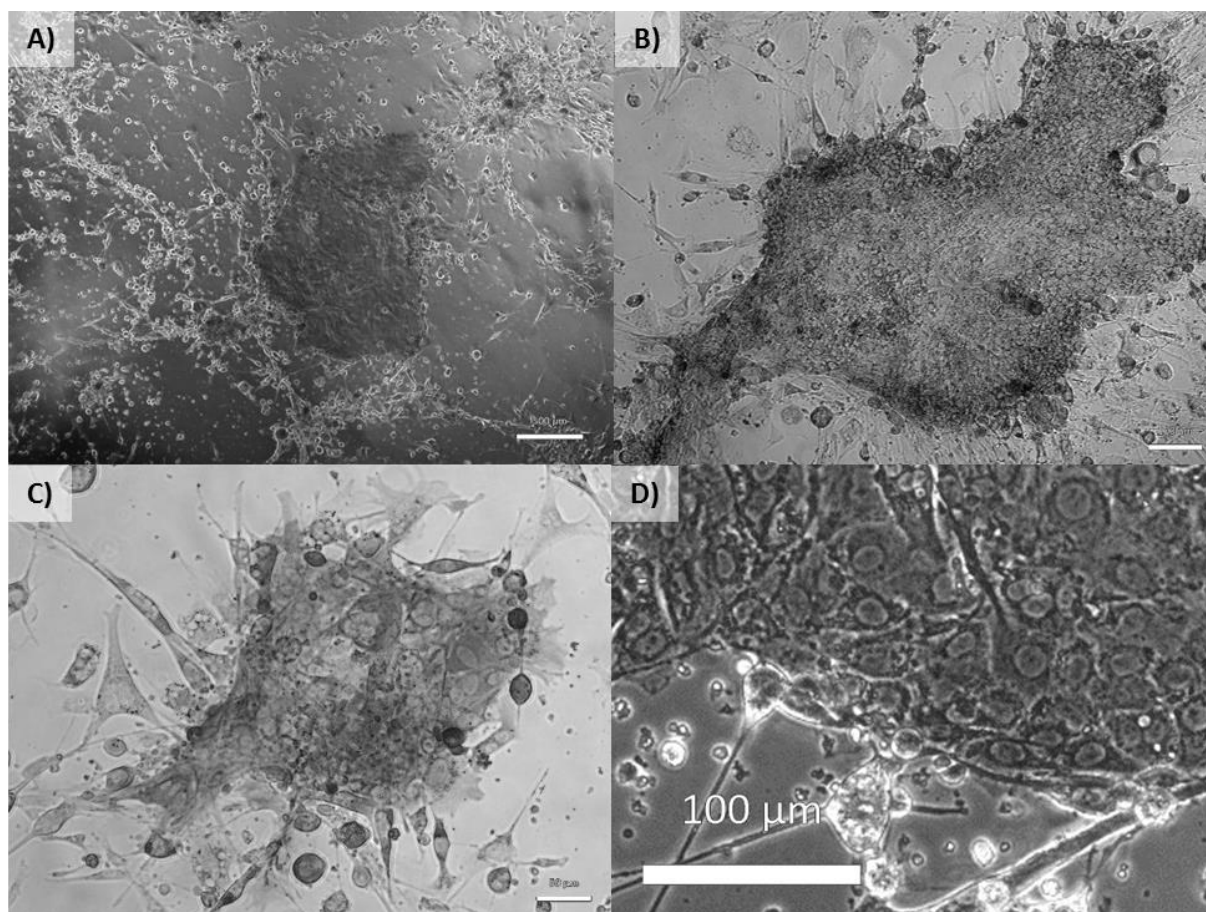
Figure 33 | Mouse E 11.5 GR cells 11 days in culture stained for Alkaline Phosphatase. AP-stain revealed several AP-positive colonies after C57BL/6 PGCs were purified via MACS and cultured for 11 days. **A-D)** Examples of AP-positive colonies shown in different magnifications. Scale bar ≙ 500 μm (A), 100 μm (B+D), 50 μm (C).

After this, the formation of primary EGC colonies could not be satisfyingly reproduced. Therefore, I implemented a more sophisticated culture protocol that I obtained from and learned in the group of Prof Hubert Schorle (Department of Developmental Pathology and Department of Molecular Diagnostics, Institute of Pathology, Bonn Medical School), where they successfully derive mouse EGCs. The protocol is based on a publication by Leitch *et al.*[102]. I also obtained a different line of feeder cells (SI^4-m220) from Prof Schorle's group in an attempt to overcome the feeder quality issues. With the new protocol, primary EGC colonies were expected to form after 12-14 culture days. **Figure 34** shows an exemplary image of a PGC culture dish after 14 days. While colonies seemed to form, they never showed the expected morphology with clear colony borders and a smooth surface. Instead they seemed to consist of cell clumps with a grainy surface. They also detached easily from the feeder cells and there were also many floating structures detectable.
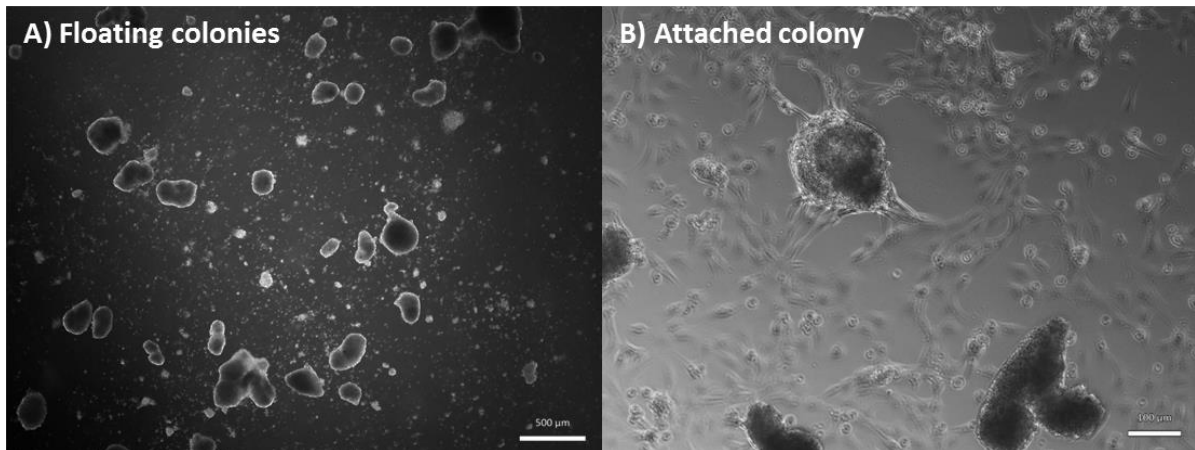
Figure 34 | Mouse E 10.5 GR cells 14 days in culture. Exemplary pictures of mouse GR culture plates after 14 days of culture using the protocol acquired in Bonn. **A)** Floating structures of unknown identity, possibly detached colonies. **B)** Potential EGC colony still attached to the culture dish. Scale bar ≙ 500 µm (A), 100 µm (B).
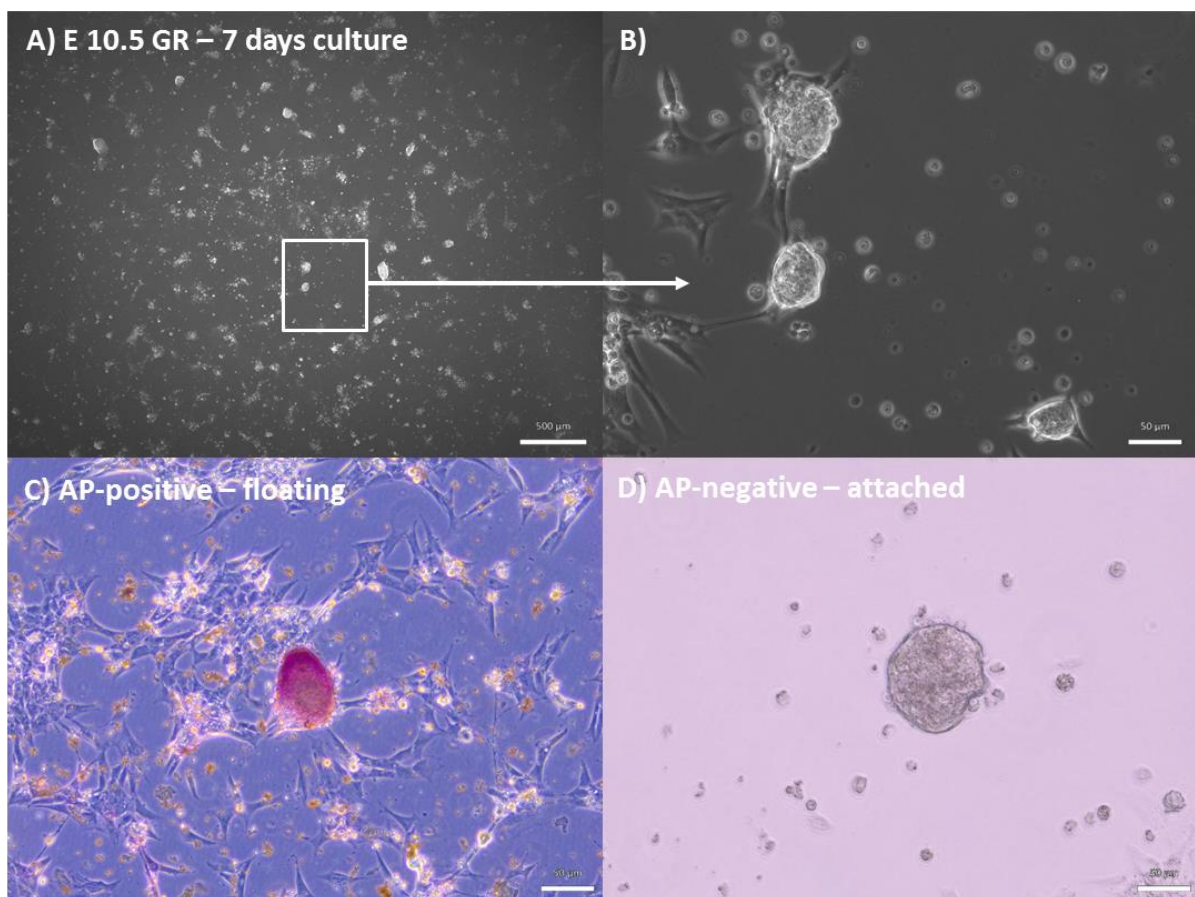
Figure 35 | Mouse E 10.5 GR cells 7 days in culture stained for Alkaline Phosphatase. Mouse GR culture plates after 7 days of culture using the protocol acquired in Bonn stained for expression of AP. **A)** Representative picture of mouse GR culture dish. **B)** Higher magnification of boxed area in A), showing potential colonies detach rapidly from the plate surface. **C)** AP-positive floating EGC colony. **D)** AP-negative attached colony of unknown identity. Scale bar ≙ 500 µm (A), 50 µm (B-D).

This problem was already observed after 8 days of culture. AP-stain of such a culture after 7 days revealed few AP-positive colonies that had detached (**Figure 35 C**). However, it remains unclear whether this happened during the staining progress or already before. Colonies remaining attached to the plate showed no AP-signal (**Figure 35 D**). An attempt to pick and sub-culture these primary colonies, both attached and floating, actually led to the formation of secondary colonies in 1/8 (12.5 %) of the culture wells. However, also in these colonies no clear AP-activity could be detected and their identity as EGCs could not be confirmed (**Figure 36**).

EGC colonies 11 days after picking
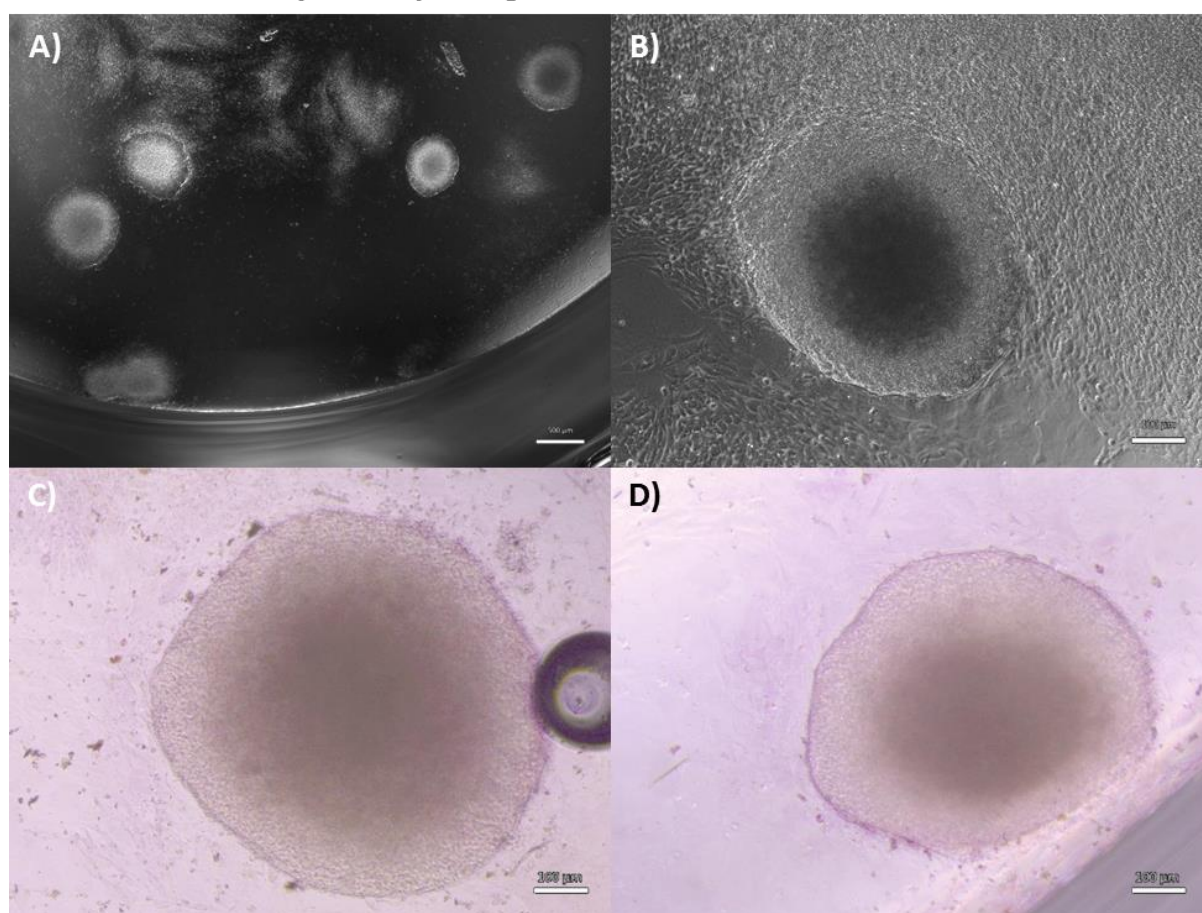
Figure 36 | Potential mouse EGCs 11 days sub-cultured stained for Alkaline Phosphatase. Primary mouse EGC colonies from Figure 35 were manually picked and sub-cultured. Appearing secondary EGC colonies were stained for AP-expression after 11 days. **A)** Representative picture of mouse EGC culture dish. **B)** Higher magnification of colony in A). **C) + D)** AP-stain revealed no clear AP-activity in the potential EGC colonies. Scale bar ≙ 500 µm (A), 100 µm (B-D).

2.2.2 Common marmoset monkey (*Callithrix jacchus*) PGC culture

2.2.2.1 Retrieval of staged marmoset monkey embryos and GR preparation

In order to obtain marmoset monkey embryos of defined developmental stages, the timepoint of ovulation in the female marmosets had to be determined. This was done by monitoring the reproductive cycle via blood progesterone levels. The progesterone cycle of a representative female common marmoset is illustrated in **Figure 37**, with progesterone levels given on the y-axis and the twice-weekly dates of blood sampling on the x-axis. In the natural cycle, blood progesterone levels lie distinctly below 10 ng/ml during the follicular phase, and increase significantly to values > 20 ng/ml after ovulation. The day when progesterone levels exceed the 10 ng/ml-threshold is defined as the day of ovulation or gestational day (GD) 0. This allowed to calculate the exact age of the embryos. Since the female marmosets are housed together with a male mating partner, pregnancy usually occurs, in which case progesterone levels will remain high throughout pregnancy even after the luteal phase. When the females are not pregnant, progesterone levels will decrease again after completion of the luteal phase until they reach the baseline levels. It is possible to manipulate the reproductive cycle by giving intramuscular doses of the hormone Prostaglandin $F_{2\alpha}$ (PGF) as indicated in the graph. This will induce the lysis of the corpus luteum, which is the major source of progesterone and essential for the maintenance of pregnancy. Hence, luteolysis will terminate the early pregnancy and induce the maturation of a new cohort of ovarian follicles. After set-up of a new mating pair, the female reproductive behaviour including the initiation of pre-implantation pregnancy was first monitored over a period of 2-3 cycles to ensure that both animals were fertile (occurrence of pregnancy) and that external regulation of the cycle via PGF was possible. If this was the case for a given breeding pair, the day of ovulation was determined and the pregnancy continued until retrieval of the embryos at the intended gestational day. It is important to note that the GD and the developmental stage do not necessarily correspond exactly, which is in contrast to the highly regularly proceeding pre-natal development in mice. Looking at the Carnegie stages 10-16, it was observed that at a given GD in the marmoset a variation of ± 2 stages can occur[116]. The intra-litter variation that was observed at the developmental stages isolated in this study was however rather small, which has also been described before[116].

73
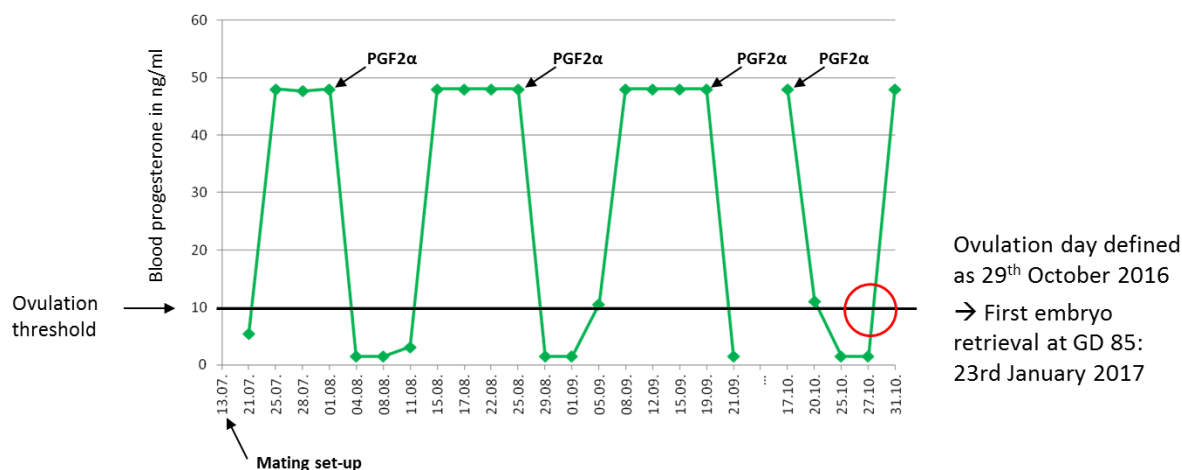
Figure 37 | Progesterone values along the reproductive cycle of a representative female common marmoset.
After set-up of a marmoset monkey mating pair, blood progesterone levels in the female were measured twice per week to monitor the reproductive cycle. The black line indicates the ovulation threshold level of 10 ng/ml. Black arrows indicate days of external Prostaglandin F2α-administration, which resets the cycle and induces a new follicle maturation. The red circle indicates the day of ovulation after which pregnancy prevailed and embryos of defined age could be retrieved.

Figures 38 and 39 give an anatomical overview of the embryos used for this project. The Embryo in **Figure 38** represents the earliest developmental stages that were used (approx. corresponding to Carnegie stages 14-15). **Figure 39** shows a GD 85 embryo, which was classified as Carnegie stage 20 and was the oldest retrieved stage. Most retrieved embryos were measured and weighed and the results are depicted in **Figure 40**, confirming the inter-litter developmental variation.

After obtaining the embryos via caesarean section, they were isolated from the placenta and the PGC-containing tissues dissected. Representative images of the dissection process and the target tissues are shown in **Figures 41 and 42**. In **Figure 41 A** a very small embryo is shown, where the urogenital ridges (UGR) cannot yet be separated into GR and MN and were therefore treated as one tissue.

74

GD 71

HE-staining

Bv

Pc

Nt

Ao

Pe

He

Gut

UGR

3 mm
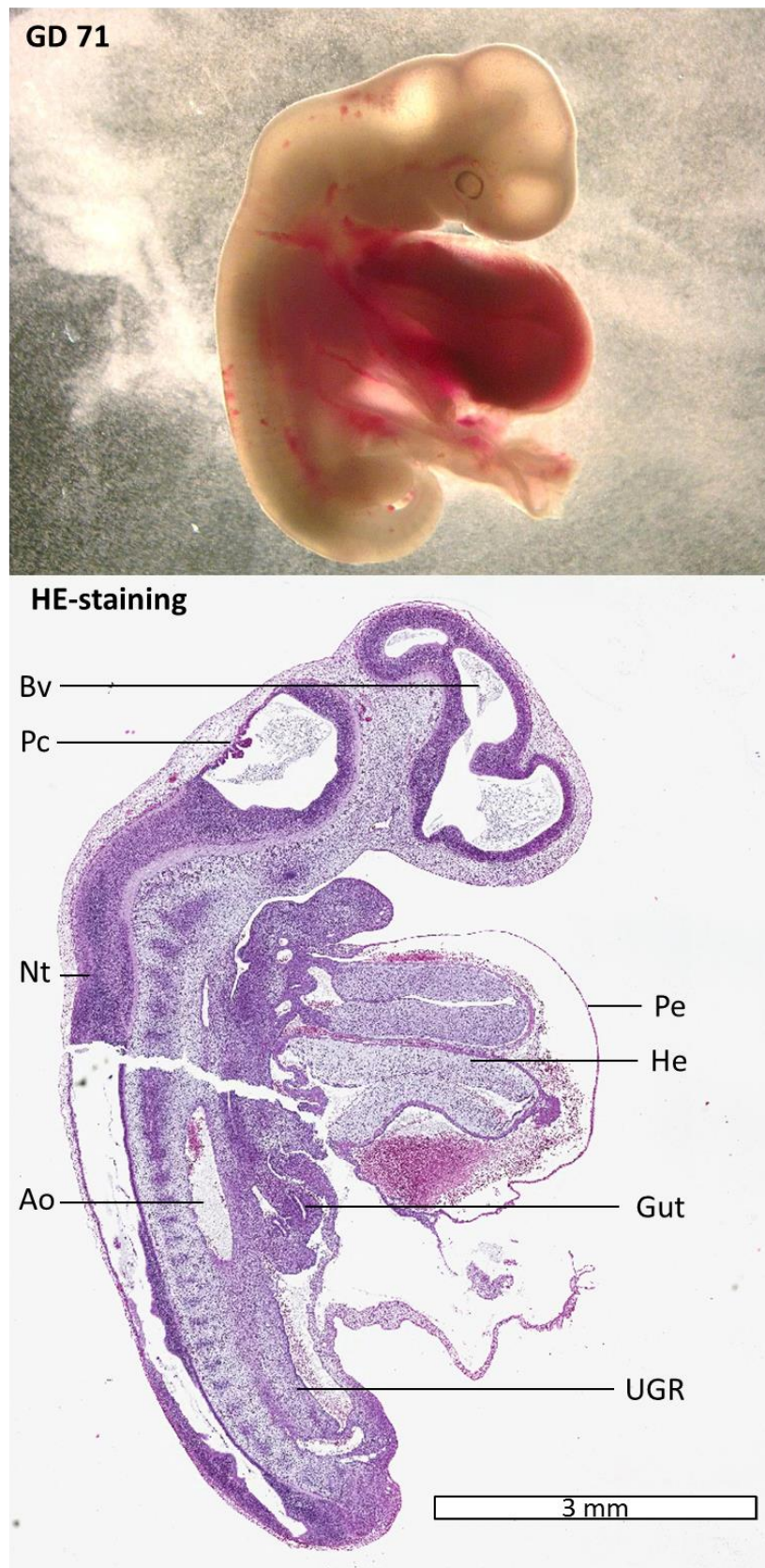
Figure 38 | Overview of a GD 71 marmoset monkey embryo. Top picture shows a representative GD 71 marmoset embryo after dissection from the placenta. Bottom image shows a representative histological section of the embryo shown in the top picture. Ao: Aorta, Bv: Brain vesicle, He: Heart, Nt: Neural tube, Pc: Plexus choroideus, Pe: Pericardium, UGR: Urogenital ridge.

GD 85

HE-staining

Bv

Pc

Nt

Tr

He

Oe

Lu

Ad

K

E

T

St

Gut

Go

5 mm
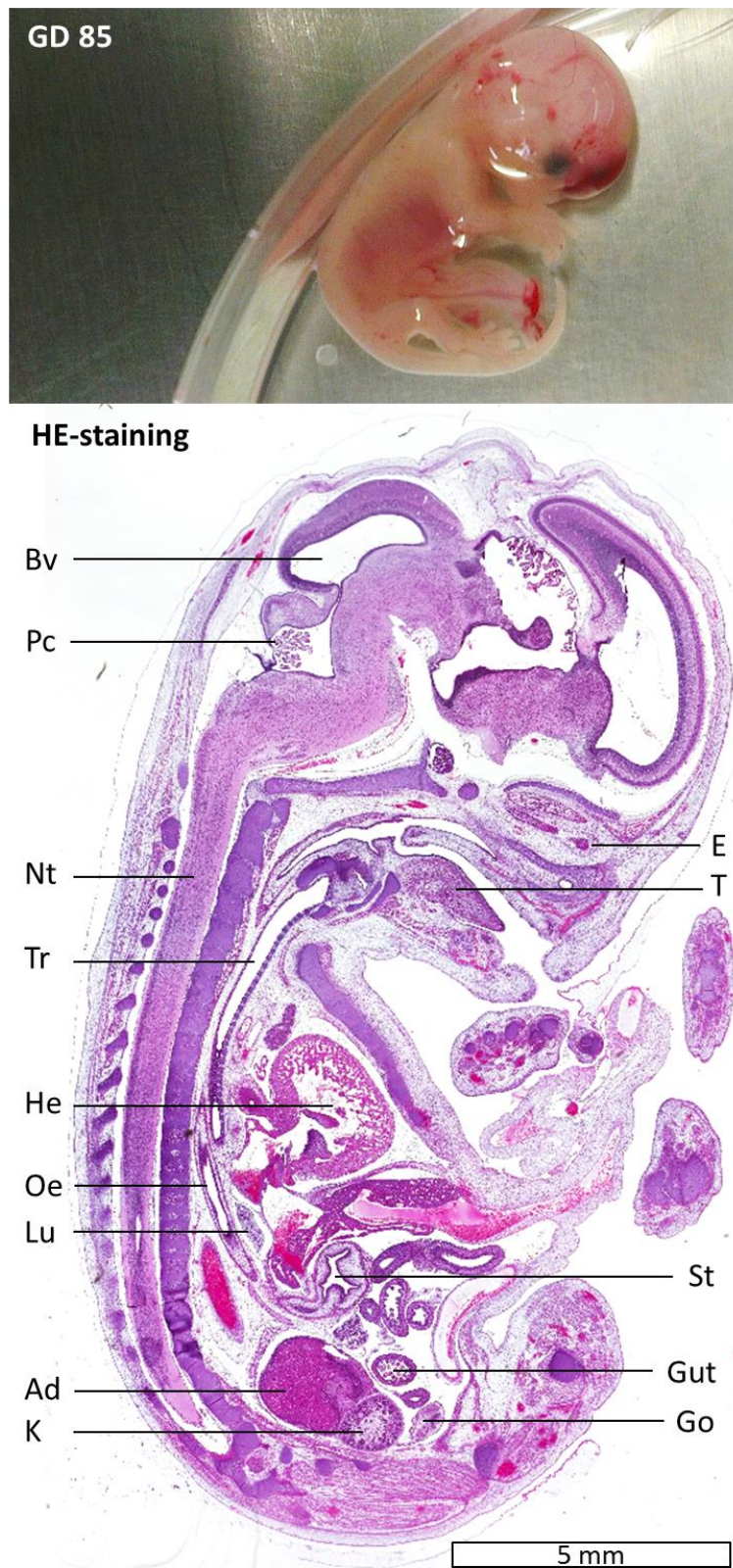
Figure 39 | Overview of a GD 85 marmoset monkey embryo. Top picture shows a GD 85 marmoset embryo after dissection from the placenta. Bottom image shows a representative histological section of the embryo shown in the top picture. Ad: Adrenal gland, Ao: Aorta, Bv: Brain vesicle, E: Eye, Go: Gonad, He: Heart, K: Kidney, Lu: Lung, Nt: Neural tube, Oe: Oesophagus, Pc: Plexus choroideus, Pe: Pericardium, St: Stomach, T: Tongue, Tr: Trachea.
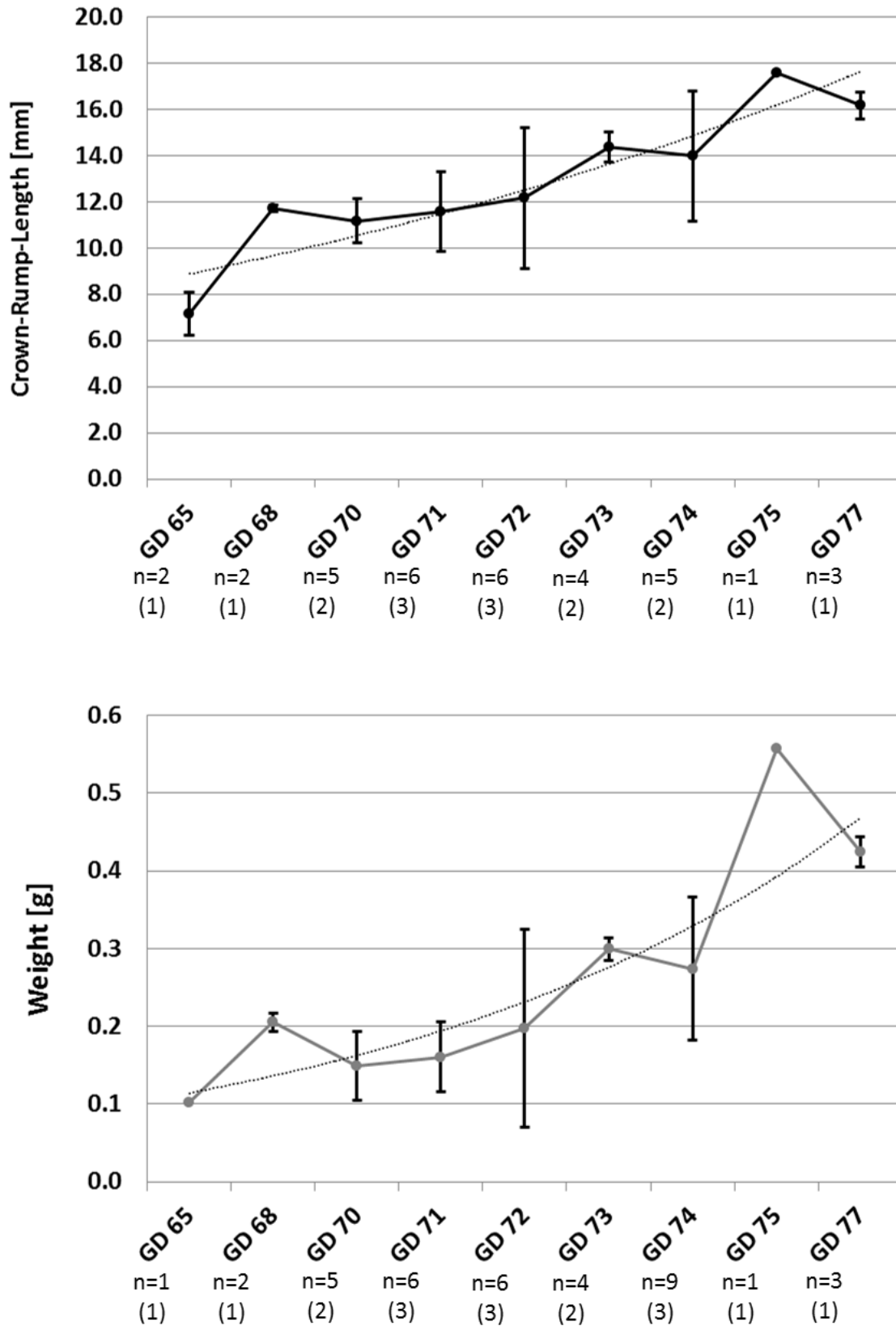
Figure 40 | Graphical representation of the size and weight of the retrieved marmoset monkey embryos.
Data points represent mean of one gestational day, error bars indicate standard deviation. n = number of available embryos per GD with number in brackets indicating the number of litters the embryos came from.
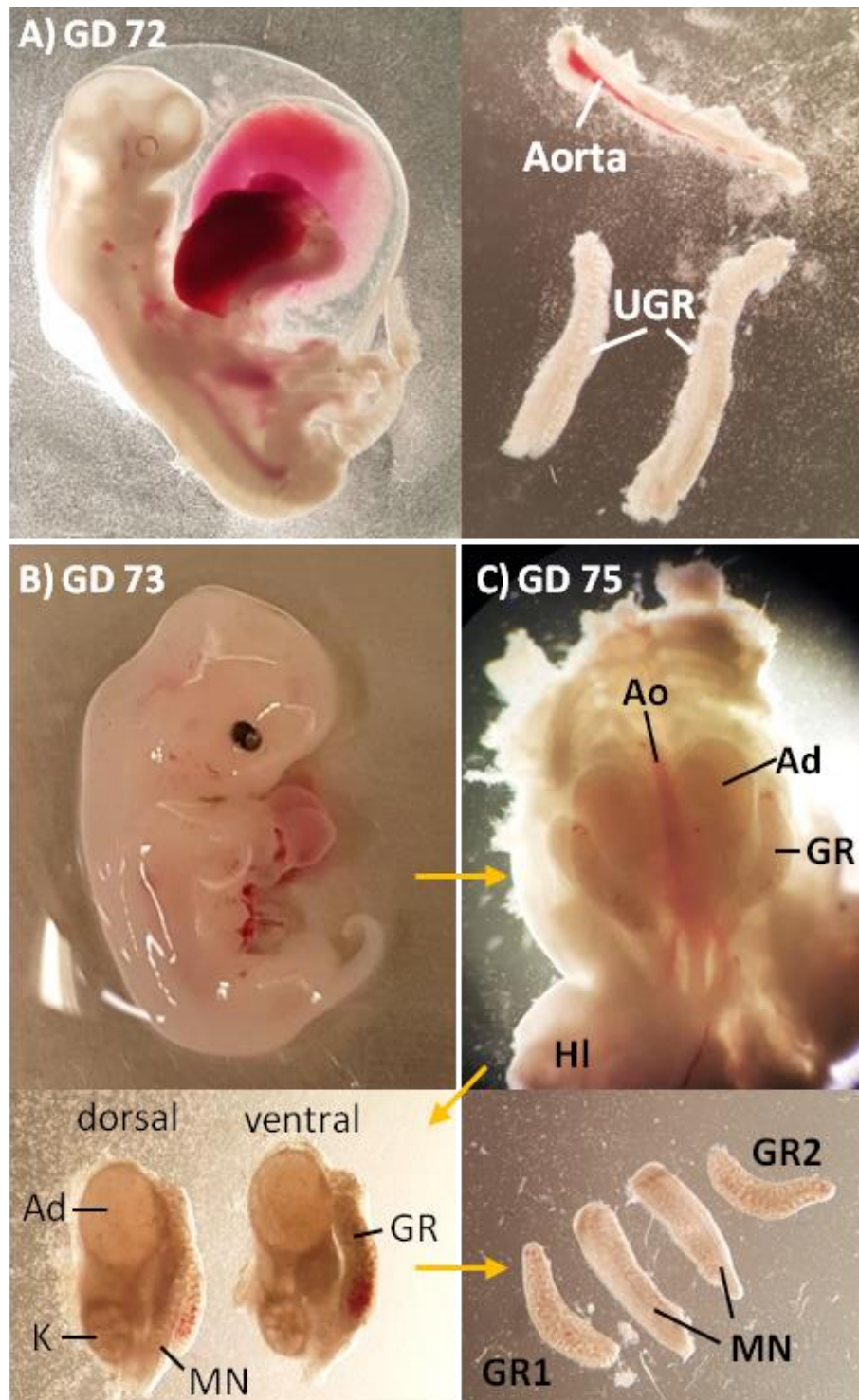
Figure 41 | Dissection strategy of marmoset monkey genital ridges and mesonephroi I. A) Picture of a (rather small) GD 72 embryo still in the amnion after isolation from the placenta. Right panel shows the urogenital ridges after dissection as well as a piece of aorta. **B)** Picture of an intact representative GD 73 embryo after isolation from the placenta. Lower image shows two complexes consisting of kidney, adrenal gland, mesonephros and genital ridge after dissection out of the embryo. One is shown from the dorsal side, the other from the ventral side. **C)** Embryo fragment of a GD 75 embryo, lying on the back. Ventral view onto the aorta in the middle with the adrenal/kidney/MN/GR-complex on either side. Hl: Hind limb. Lower image shows the isolated and separated genital ridges and mesonephroi. Orange arrows show the GR-dissection step-by-step.
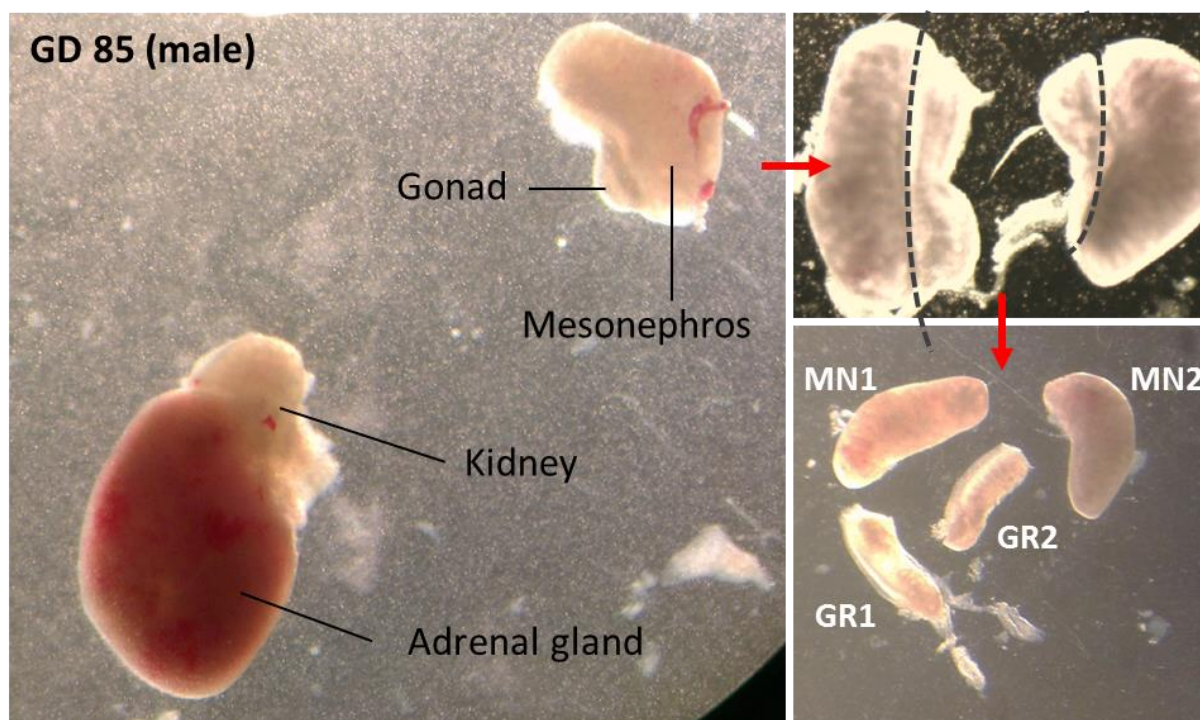
Figure 42 | Dissection strategy of marmoset monkey genital ridges and mesonephroi II. Isolated adrenal gland and kidney of a GD 85 embryo already separated from the mesonephros/genital ridge complex. The red arrows show the subsequent preparation steps, the dotted lines indicate the border between MN and GR. Note the advanced development of all organs compared to Figure 41.

An overview of all embryos retrieved for this project and the individual culture approaches is given in **Table 5**. As explained for the mouse PGCs, the culture protocol was based on a publication by Leitch, Surani, Smith *et al*. (2013). GR and MN were isolated, enzymatically digested and plated on SI⁴-m220 feeder cells until the appearance of primary EGC colonies. AP expression was considered necessary for the identification as pluripotent. Established marmoset ESCs[14] were cultured as control. **Figure 43** exemplarily shows a picture of marmoset ESC colonies. The colonies on the right are shown as an example of differentiation and were AP-negative. The colony on the lower left was stained positive for AP expression (no colour-image available) and shows the typical morphology of undifferentiated pluripotent marmoset monkey stem cell colonies: smooth surface and a distinct colony border, consisting of densely-packed small cells with a high nucleus-to-cytoplasm ratio and visible nucleoli.

Table 5 | Overview of all marmoset embryo retrieval and culture approaches for EGC derivation.

Gestational day (GD)	# of Embryos	Weight	Crown-Rump-Length	Sex	Digestion Method	Result Cell Culture
85	3	N.D. N.D. N.D.	N.D. N.D. N.D.	Male Male Female?	Trypsin 0.05 %	No colonies after 11 days, AP-stain negative, frozen for RNA-analysis (**Day 11**) Histology (gonad morphology indicates female)
74	3	N.D. N.D. N.D.	N.D. N.D. N.D.	Female Female Female	Trypsin 0.25 %	Culture failed (Trypsin in culture) Histology
70	3	0,159 g 0,148 g N.D.	10,8 mm 12,0 mm N.D.	Male Male Female	Trypsin 0.125 %	Culture failed (Trypsin in culture) Histology
71	1	N.D.	N.D.	N.D.	Trypsin 0.125 %	Histology
71	2	0,148 g 0,180 g	10,7 mm 10,95 mm	Male Female	Trypsin 0.25 %	Day 8: Appearence of quantifiable round structures (colonies? 13-16/well). Day 10: started to vanish (4-9/well). Day 11: Live and fixed AP-stain negative
77	3	0,402 g 0,436 g 0,436 g	16,8 mm 15,7 mm 16,0 mm	Female Male Male	Trypsin 0.25 %	No colonies, after 14 days, AP-stain negative Histology
73	2	0,289 g 0,294 g	14,5 mm 14,2 mm	Male Male	Collagenase/ Hyaluronidase	Cells stained for CD13 -> Sorter -> no CD13+ cells
71	1	0,085 g	9,0 mm	Female	Collagenase/ Hyaluronidase	No colonies after 10 days, AP-stain negative. Very bad feeder quality (detachment)
71	1	N.D.	N.D.	Female	Collagenase/ Hyaluronidase	No colonies after 14 days. Very bad feeder quality (detachment)
74	4	0,376 g 0,261 g 0,246 g 0,123 g	17,9 mm 12,4 mm 14,2 mm 10,4 mm	Female Female Female Female	-	Culture of all GR and MN as whole tissue explants. Cell-outgrowths. AP-stain after 7 days negative. Remaining tissues subcultured after 10 days. No resulting colonies.
72	2	0,180 g 0,168 g	13,1 mm 12,1 mm	Male Female	-	GR and MN manually fragmented to culture as tissue explants. Fragments attach well. Cell-outgrowths. Sub-cultured after 8 days. No resulting colonies after 7 days, frozen for RNA-analysis.
74	1	0,233 g	15,0 mm	Female	-	GR and MN frozen as control for culture-timeline RNA-analysis (**Day 0**)
72	2	0,2913 g 0,398 g	14,3 mm 16,0 mm	Female Female	-	GR and MN manually fragmented to culture for 4 days as tissue explants. Frozen for culture-timeline RNA-analysis (**Day 4**)
71	3	0,223 g 0,168 g 0,156 g	13,5 mm 12,0 mm 13,3 mm	Male Female Male	-	UGR frozen as control for culture-timeline RNA-analysis (**Day 0**)
75	1	0,557 g	17,6 mm	Male	-	GR and MN + other organs frozen for single-cell transcriptome analysis.
74	4	0,301 g 0,429 g 0,195 g 0,303 g	N.D. N.D. N.D. N.D.	Male Female Male Female	-	GR and MN + other organs frozen for single-cell transcriptome analysis.
65	2	0,101 g N.D.	7,8 mm 6,5 mm	Male Male	-	Histology
70	3	0,145 g 0,208 g 0,084 g	11,0 mm 12,2 mm 9,9 mm	Female Male Male	-	GR and MN manually fragmented to culture for 2 days as tissue explants. Frozen for culture-timeline RNA-analysis (**Day 2**)
72	2	0,053 g 0,094 g	7,5 mm 10,0 mm	Male Male	-	GR and MN manually fragmented to culture for 8 days as tissue explants. Frozen for culture-timeline RNA-analysis (**Day 8**)
68	2	0,214 g 0,197 g	11,8 mm 11,6 mm	Female Female	-	Histology
73	2	0,321 g 0,293 g	15,2 mm 13,6 mm	Male Male	-	GR and MN + other organs frozen for single-cell transcriptome analysis.

C.j. ESC AP-positive colony

100 µm
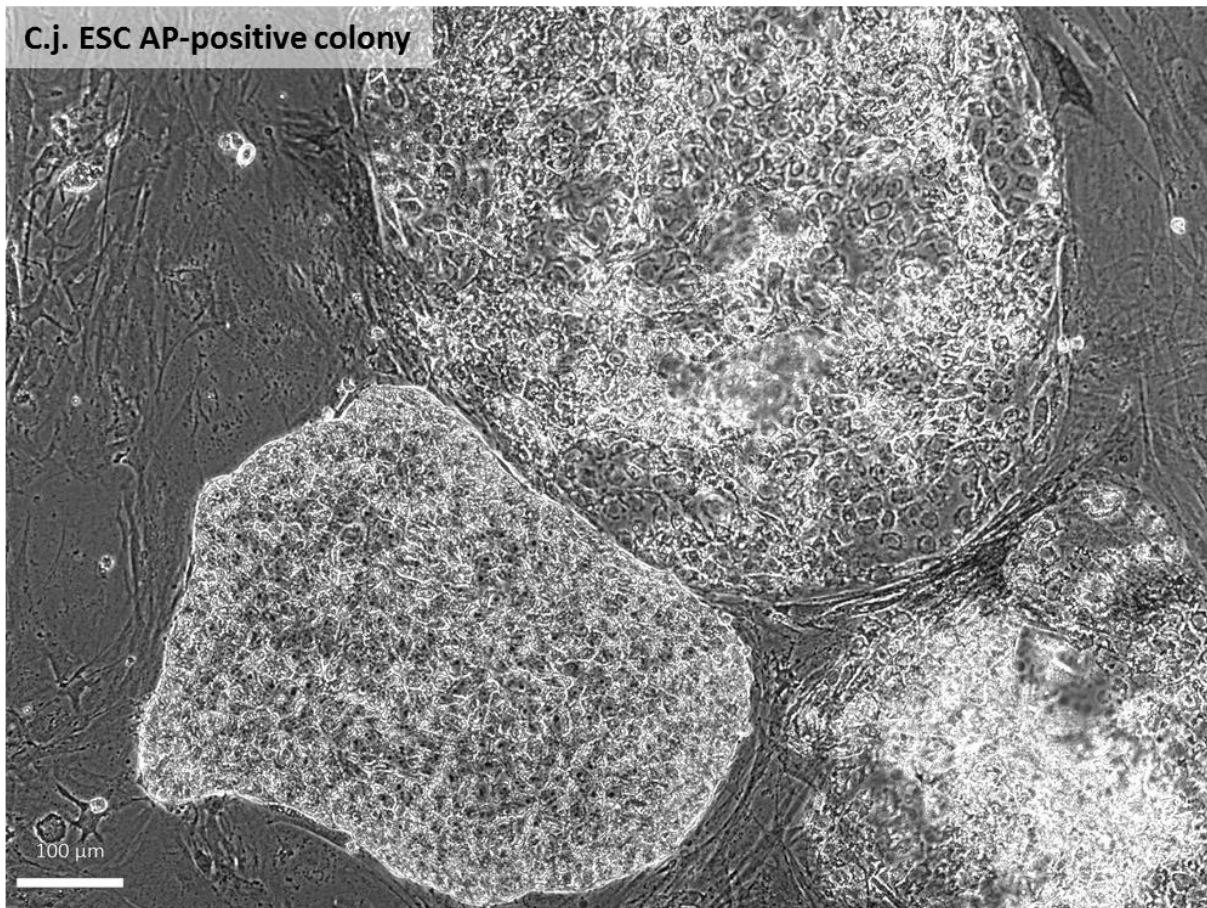
Figure 43 | AP-positive marmoset monkey ESC colony. Marmoset monkey embryonic stem cells were cultured as pluripotent cell control and stained for Alkaline Phosphatase (no colour image available). The colony in the lower left part of the image was AP-positive and exhibited the typical morphology of undifferentiated pluripotent stem cells. The colonies on the right were AP-negative. The lower right colony is already completely differentiated, the upper right colony shows morphological signs of differentiation and is in a borderline differentiation state.

Initially, the GR and MN were digested using varying concentrations of trypsin and then the whole cell suspension was plated. **Figures 44, 45 and 46** show exemplary microscopy images of respective culture plates. From time to time, the formation of roundish cell colonies on top of the mouse feeder cells could be observed. The colonies seemed to be a monolayer of cells with – morphologically – epithelial characteristics (**Figure 44 D+E**), as was observed sometimes in the mouse PGC culture (**Figure 33**). However, they never showed any signs of AP expression and vanished after several days. Additionally, round structures were also formed by the feeder cells (**Figure 44 C, 45 C+D**), making it difficult to confirm the presence of primary EGC colonies. Although trypsin digestion is the published method of choice, I suspected that the digestion with trypsin might be too stressful for the cells, or too

aggressive in the sense that relevant cell surface receptors might get impaired. Therefore, I switched to an enzyme solution consisting of hyaluronidase, collagenase and DNase to ensure that predominantly the tissue's extracellular matrix was digested and not the cells themselves. Additionally, DNase was used to digest sticky genomic DNA that was released from unintendedly destroyed cells. However, also this more gentle digestion did not lead to the formation of cell colonies. Additionally, the problem with the detaching feeder cells described for the mouse PGC culture also occurred (**Figure 45 A, Figure 46**).

GD 71
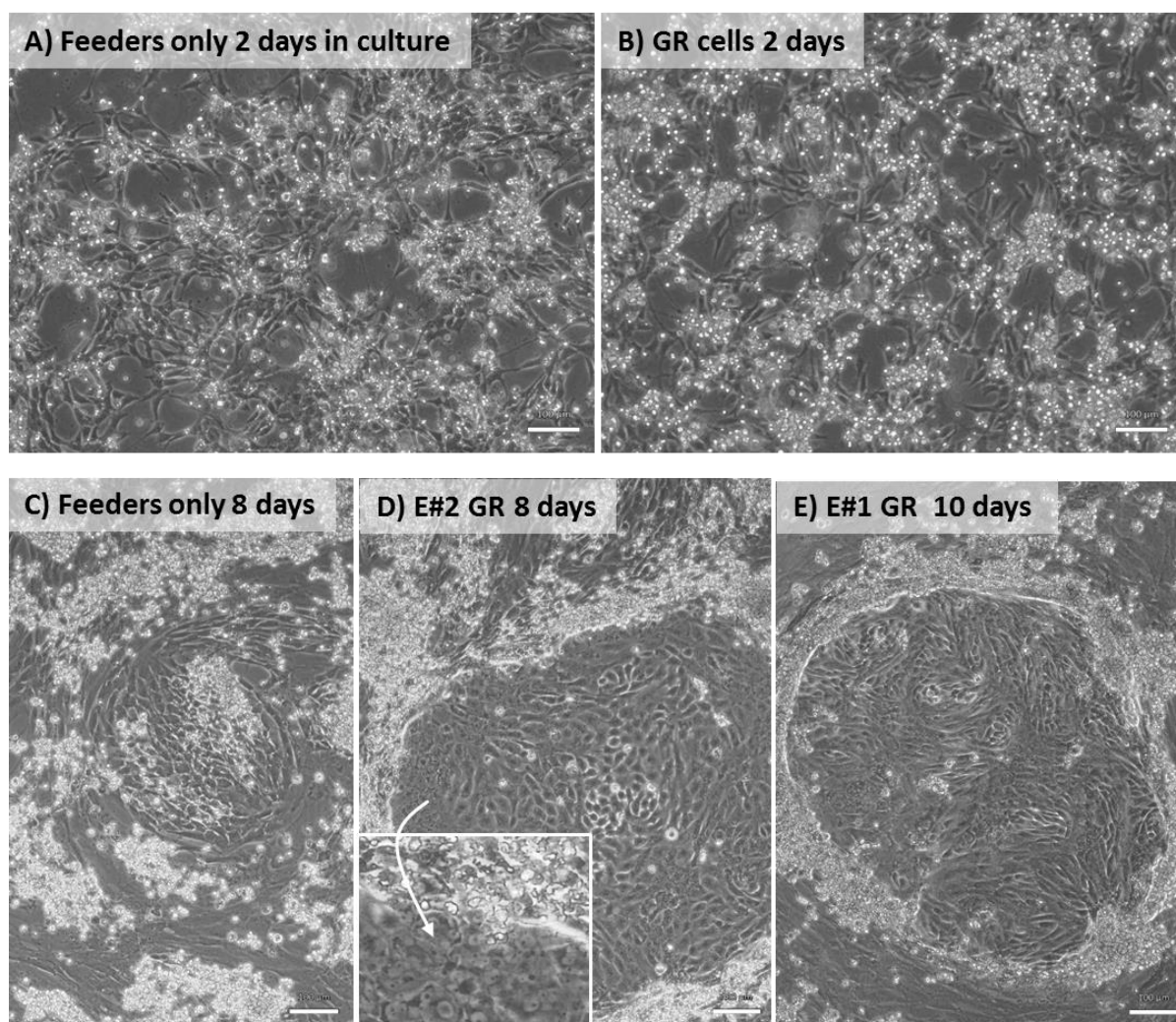
Figure 44 | Culture of marmoset GD 71 embryo GR cells. A) + B) Exemplary image of culture dish 2 days after culture initiation. No morphological difference can be observed between the feeders-only dish (A) and the well containing GR cells (B). **C)** Feeders-only control culture plate after 8 days of culture. Round structures formed by the feeder cells can be observed. **D)** Round structures/potential EGC colonies can be observed in the culture plates containing GR cells after 8 days. A monolayer of cells can be seen on top of the feeder cells (inlay, higher magnification of colony border). **E)** AP-stain after 10 days shows no AP-activity signal in potential colonies. Scale bar ≙ 100 μm.
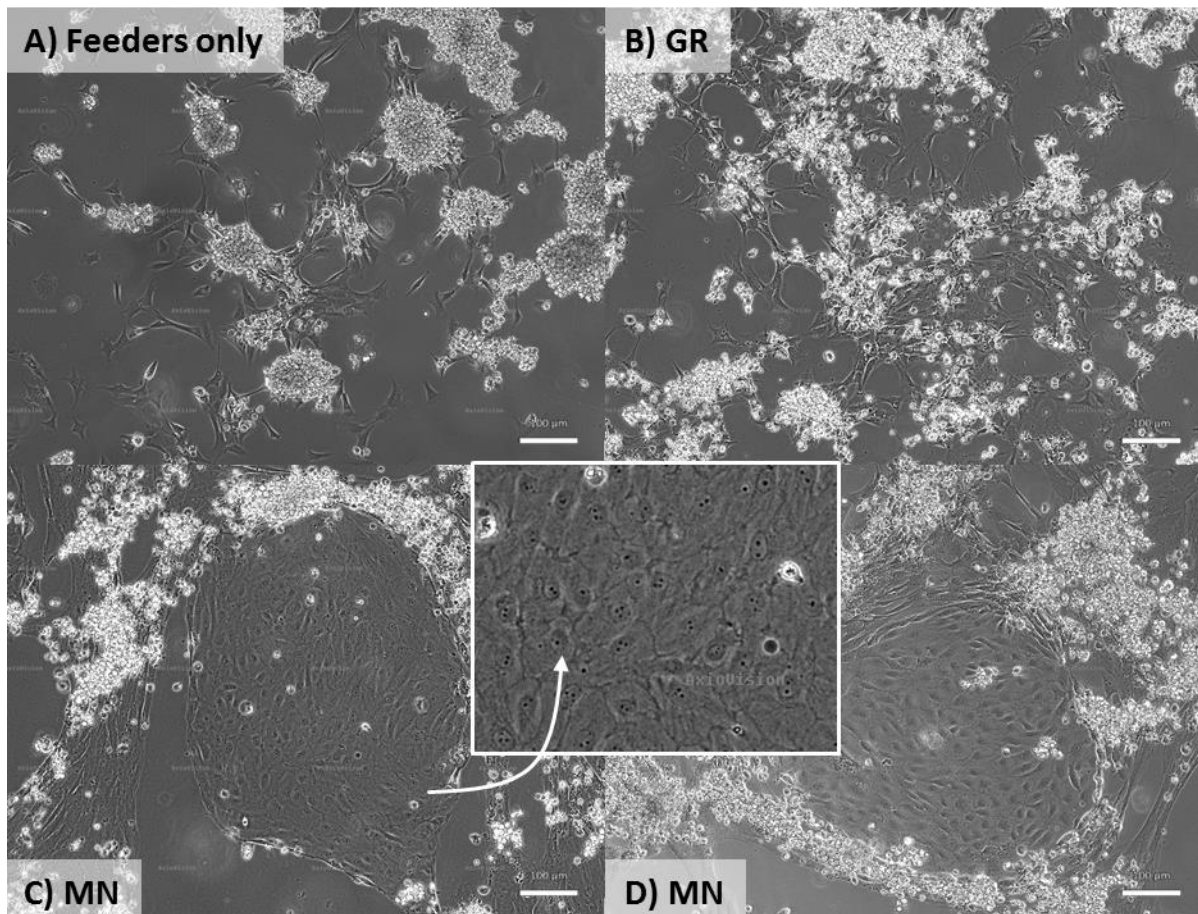
GD 77

Figure 45 | Culture of marmoset GD 77 embryo GR and MN cells. Exemplary image of culture dish 14 days after culture initiation. No morphological difference can be observed between the feeders-only dish **(A)** and the well containing GR cells **(B)**. In both cultures feeders are detaching and form floating cell clusters. **C) + D)** Culture wells containing mesonephros cells. Round structures can be observed (inlay: higher magnification of C). AP-stain after 14 days reveals no AP-activity signal in all wells. Scale bar ≙ 100 µm.
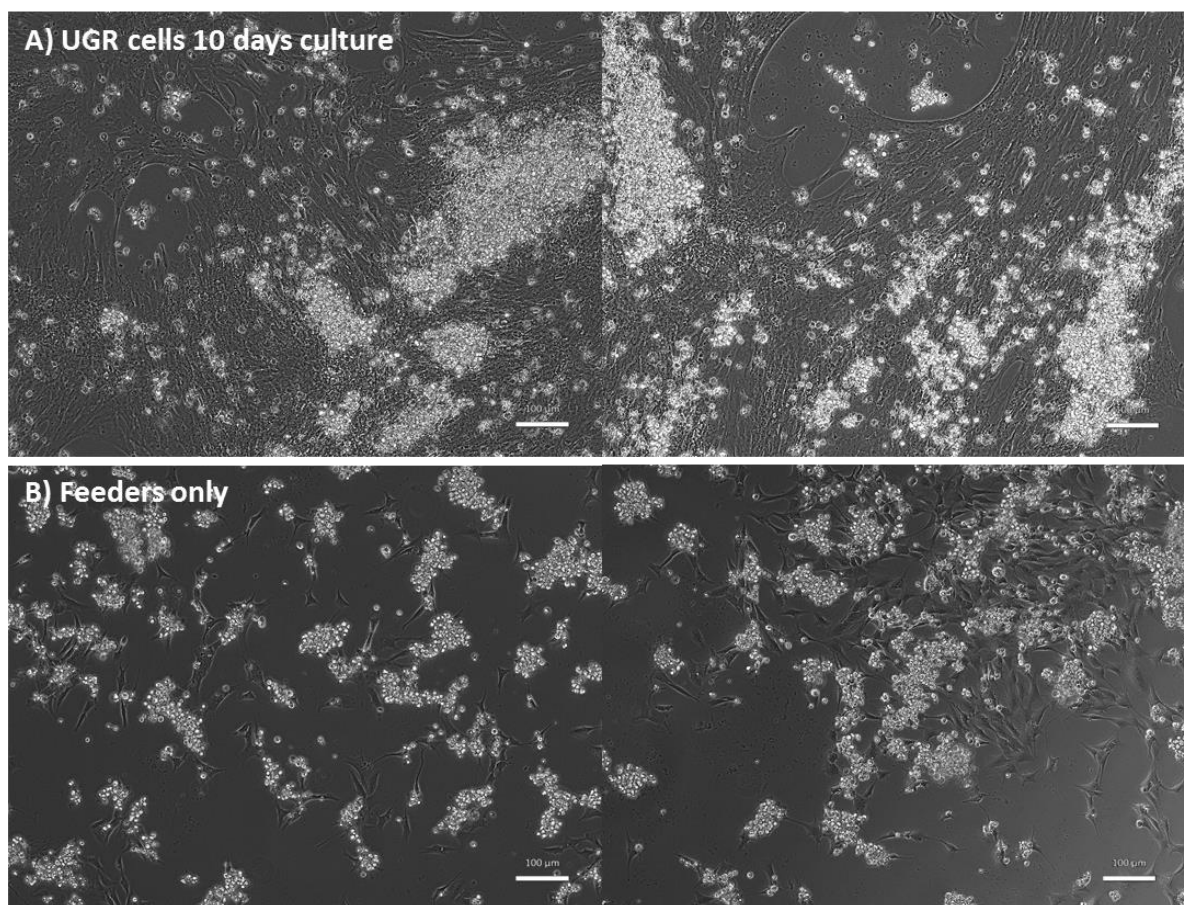
GD 71

Figure 46 | Culture of marmoset GD 71 embryo UGR cells. Exemplary pictures of plates cultured for 10 days, after implementation of a different enzyme digestion method. There seems to be a difference in feeder cell quality between the wells containing UGR cells **(A)** and feeder cells-only **(B)**, with more and better attached feeders in the UGR cell plates. Scale bar ≙ 100 µm.

2.2.2.2 Purification of live cells using ANPEP antibody fails

Based on the finding that no PGC-derived cell colonies could be established from the mixture of cells obtained from the whole GR (and MN), it was my goal to identify a PGC-specific cell surface protein to be able to purify or at least enrich the PGCs from the total cells of GR and MN, as has been done for mouse PGCs[101]. As shown in **Part I** by IHC, PGCs can be identified via pluripotency factor expression. However, since they are all intracellular transcription factors, they cannot be used to select the cells intact, which is a requirement if they are to be cultured further. As mentioned in chapter 2.1.3.1, marmoset PGCs do not express any of the known surface markers of human and mouse PGCs or ESCs like the SSEAs and the TRAs. When the PGC-specific cell surface expression of Aminopeptidase N (ANPEP, or CD13) was confirmed via IHC (**Figure 24**), an attempt was made to label the GR cell suspension with an

α-ANPEP-antibody and sort the cells in a FACS sorter. However, unexpectedly, during the sorting no ANPEP-positive cells could be detected (data not shown). Since ANPEP is also highly expressed on marmoset ESCs, I decided to use these cells as control to refine the FACS labelling and sorting protocol before proceeding with the embryo GR material. The results of the ESC-ANPEP flow cytometry test are shown in **Figure 47**. Compared to the unstained control, where a background-level of 0.4 % ANPEP$^+$-cells was measured, the staining of ESCs resulted in 3.5 - 3.9 % of total cells being measured as ANPEP-positive. The labelling efficiency was independent of the temperature used for antibody-incubation during the staining procedure (**Figure 47 C-E**). Based on IHC and immunofluorescence images (**Figure 48**), I expected > 90 % of the ESCs to be ANPEP$^+$. I first had no explanation for this unexpectedly low percentage of ANPEP-labelling, until the idea was brought to me that ANPEP as a peptidase might cut the antibody-peptide after it bound. This would mean that ANPEP in its intact form on live cells cannot be bound by this antibody. Only fixation in Bouin's solution, as occurs in the tissue preparation for IHC, leads to the inhibition of its enzymatic activity and therefore its detectability via antibody-binding. To test this hypothesis, marmoset ESCs were stained for ANPEP via immunofluorescence after Bouin-fixation of the cells as well as on un-fixed, live cells. As a control, an established ESC surface marker was used that should not interfere with the antibody even when the cells were still intact. For this purpose, the glycoprotein Tra-1-81 was chosen. DAPI-staining was performed as an indicator of cell viability, since dead cells are permeable for DAPI and intact cells are not[117]. As shown in **Figure 48**, after fixation Tra-1-81 as well as ANPEP could be detected on the cell surface of almost 100 % of ESCs. When the cells remained alive for the staining procedure, they suffered stress and the ESC colonies lost their typical morphology. However, most of them remained intact until the end of the staining procedure, which can be seen by the absence of a DAPI-signal in the cells (**Figure 49**). Tra-1-81 staining resulted in specific cell surface staining of live cells (**Figure 49 A**), whereas ANPEP was hardly detectable on any cell in the non-fixed sample (**Figure 49 B**). This strongly supports our hypothesis that this ANPEP-antibody cannot be used to select and enrich live cells.

85
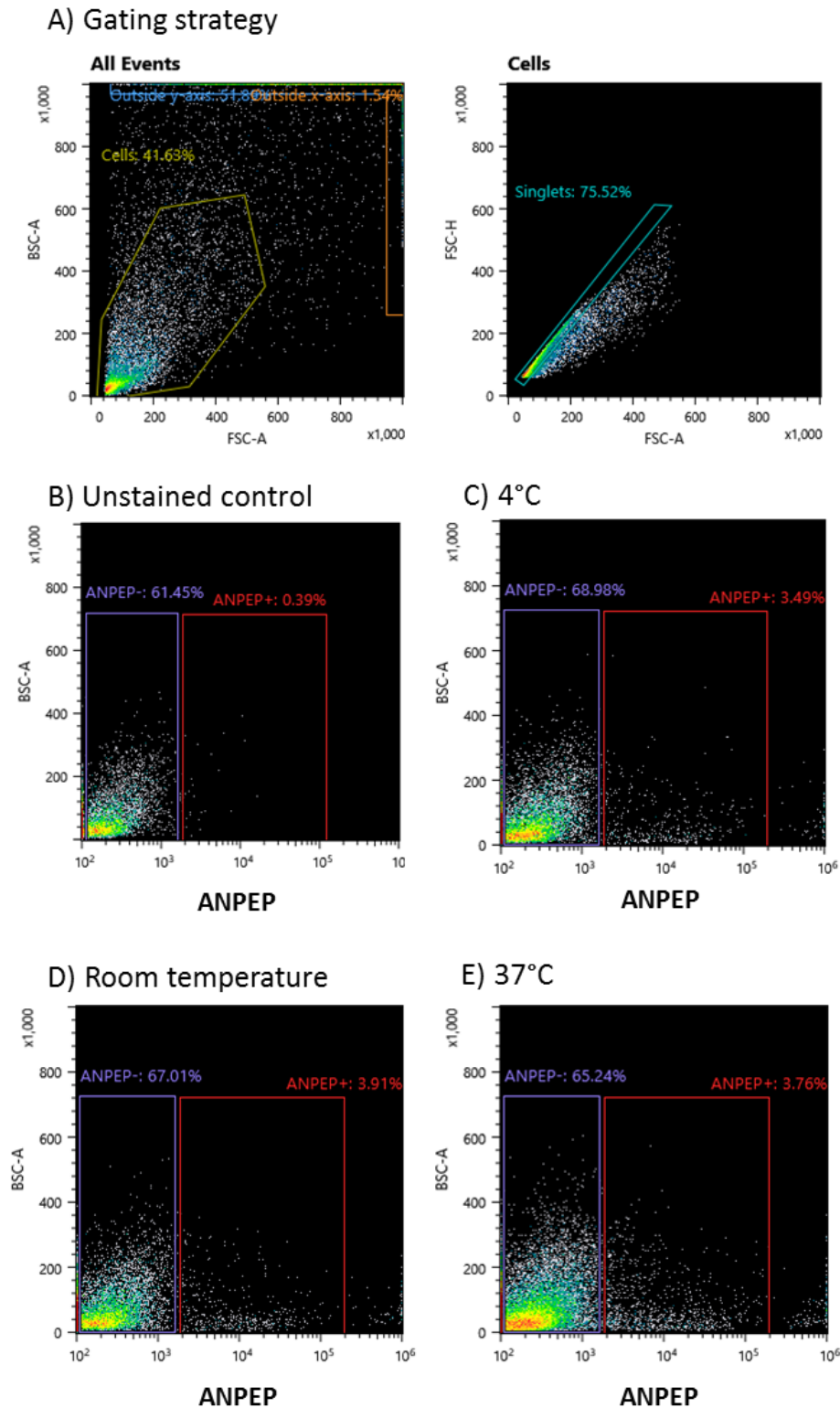
Figure 47 | FACS analysis of different staining approaches for ANPEP (CD13) on marmoset monkey ESCs.
Marmoset monkey embryonic stem cells were stained for FACS analysis using α-CD13 antibody and AlexaFluor488-coupled secondary antibody. Antibody incubations were performed at different temperatures as indicated above the plots. Plots in **(A)** depict the gating strategy to only analyse singlet cells. Plot **B)** shows unstained control cells to position gates for ANPEP-signal. Plots **C) – E)** show cells gated for ANPEP, purple and red numbers indicate percentage of cells per gate of total measured singlet cells.
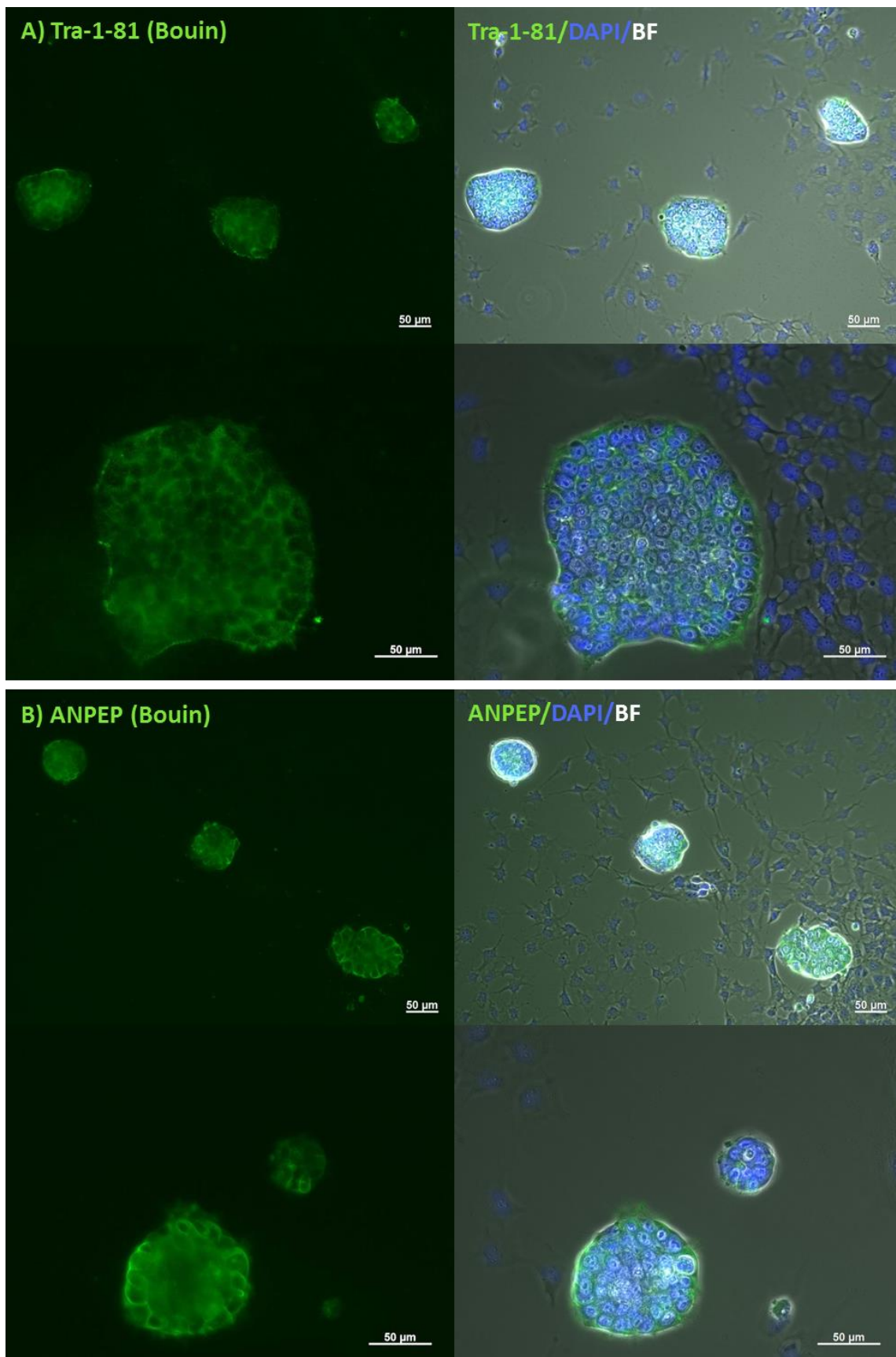
Figure 48 | IF staining of marmoset ESC surface proteins following fixation. Marmoset monkey embryonic stem cells were fixed in Bouin's solution and immunofluorescence staining performed for surface markers Tra-1-81 **(A)** and ANPEP **(B)**. DAPI control staining served as an indicator of cell viability. Scale bar ≙ 50 μm.
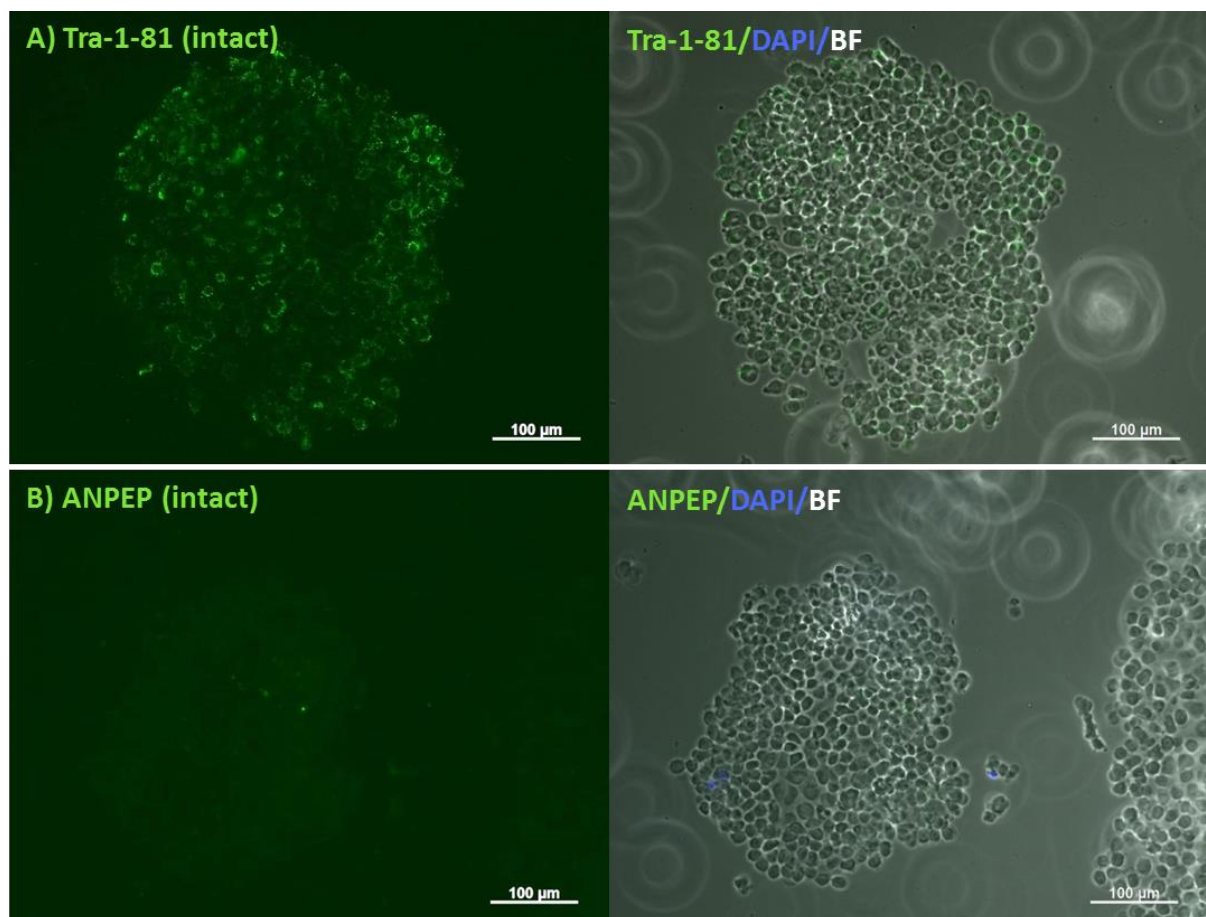
Figure 49 | IF staining of marmoset ESC surface proteins on intact cells. Marmoset monkey embryonic stem cells remained alive for immunofluorescence staining of surface markers Tra-1-81 **(A)** and ANPEP **(B)**. DAPI control staining served as an indicator of cell viability. Scale bar ≙ 100 µm.

2.2.2.3 Tissue explant culture and culture timeline

After the failed attempt to purify PGCs for culture, I decided to culture the GR and MN as whole-tissue-explants, as has been described for human genital ridges and EGC derivation[109]. As shown in **Figure 50**, the tissues attached nicely to the culture plate and an outgrowing (mono-)layer of cells could be observed after several days. However, the outgrowths did not exhibit AP-activity after 7 days and sub-culture after 10 days did not lead to colony formation. In an attempt to increase the surface for the cells to form monolayer outgrowths and potentially start growing as pluripotent cells, the GR and MN were manually plucked into smaller pieces and cultured as tissue fragments (**Figure 51**). However, this also did not result in AP-positive cells or colony formation after sub-culture.

GD 74
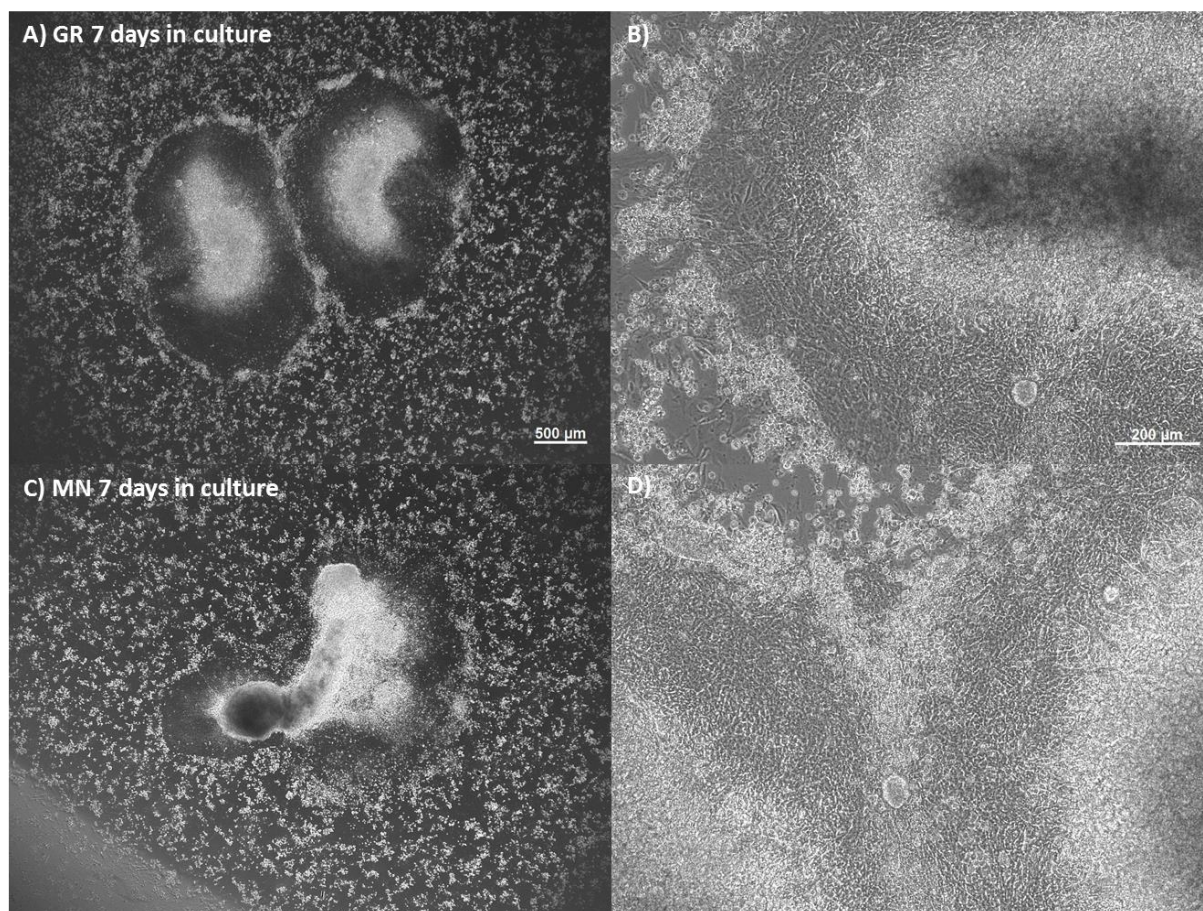
Figure 50 | Tissue explant culture of marmoset GD 74 embryo GR and MN. Marmoset monkey genital ridges **(A)** and mesonephroi **(C)** were plated as intact tissues, attached and microscopy images taken after 7 days of culture. Scale bar ≙ 500 μm. **B) + D)** Magnified view of tissue explant border area. The outgrowing cells form a distinct monolayer. They do not exhibit AP activity. Scale bar ≙ 200 μm.

After the described fruitless culture approaches, it was my goal to analyse at which point the PGCs vanish. Since the PGCs as well as the desired EGCs should express pluripotency factors, I decided to culture GR and MN fragments for a varying number of days and test for the presence of pluripotency factor mRNA expression, namely *OCT4* and *NANOG*, via qPCR. As a positive control for the detectability of the genes of interest, whole GR were collected directly after isolation (Day 0), and the measured expression levels in the GR-cultures were related to feeders-only controls cultured for the same amount of time. The results of this culture timeline are shown in **Figure 52**. As expected, high abundance of *OCT4* and *NANOG* transcripts were detected in the fresh GR tissue. Surprisingly, low levels of both pluripotency factors could be detected in the culture over the period covered by this experiment, indicating that some PGCs survive and are detectable in the culture.
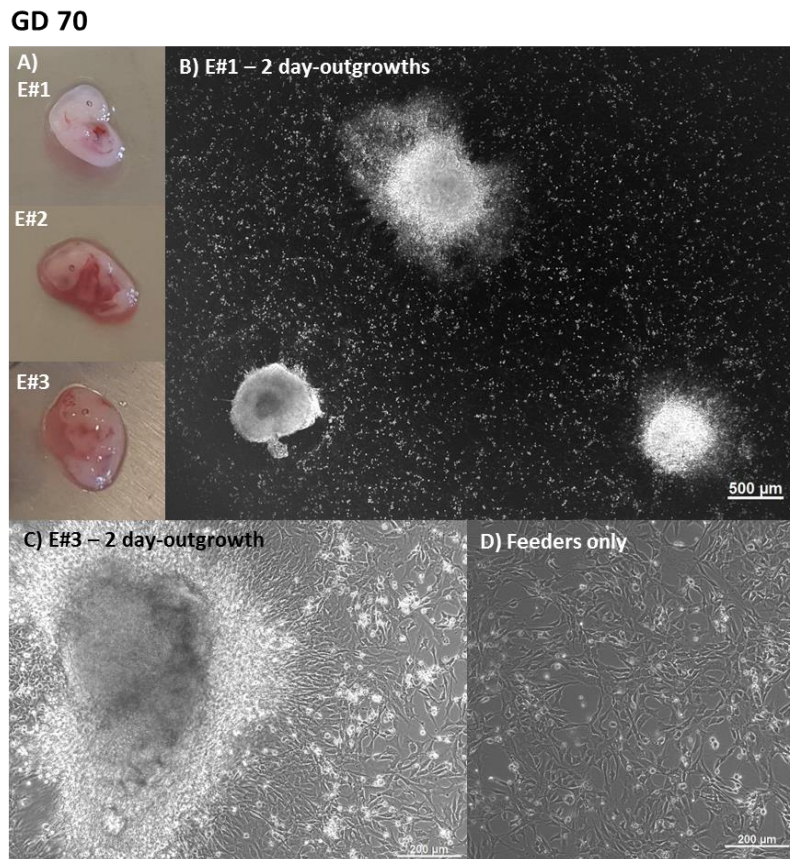
GD 70

Figure 51 | Tissue fragment culture of marmoset GD 70 embryo UGR. Marmoset monkey urogenital ridges were manually disrupted and plated as tissue fragment explants. **A)** Images of the intact embryos before dissection. **B) + C)** Microscopy images of tissue fragments taken after 2 days of culture. **D)** Feeders-only control culture plate after 2 culture days. Scale bar ≙ 500 µm (B), 200 µm (C+D).
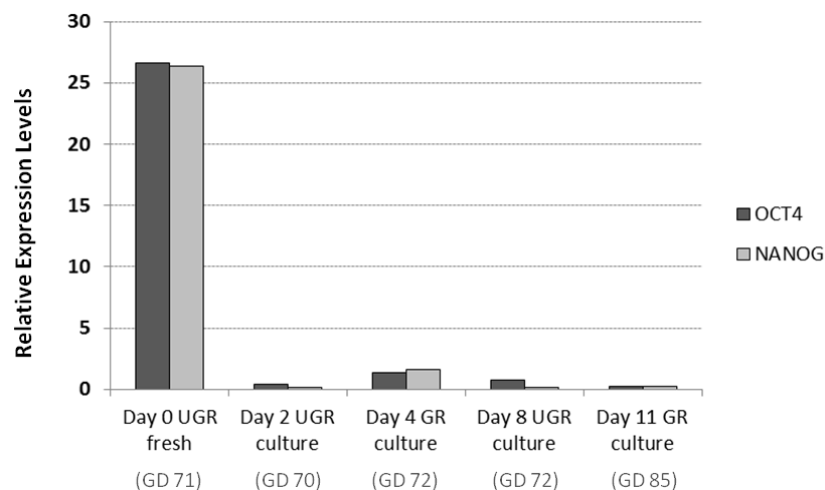
Figure 52 | Pluripotency factor expression in (U)GR cell culture. (Uro)genital ridge cells of marmoset embryos of indicated age were cultured for 2, 4, 8 or 11 days and then collected for qPCR analysis. 18S rRNA was used as housekeeping gene and the measured pluripotency factor expression was normalised to feeder cells-only controls cultured under the respective same conditions. Whole urogenital ridges were collected for comparison (Day 0).

3. Discussion

This study set out to investigate germ cell development in a non-human primate, the common marmoset monkey (*Callithrix jacchus*), via immunohistochemical *in situ* characterisation of marmoset primordial germ cells (PGCs), and attempted PGC culture to derive pluripotent marmoset embryonic germ cells (EGCs). Following my investigations, ANPEP and CD31 could be confirmed as novel marmoset PGC surface markers. The expression of transcription factors PAX5 and SOX17 in early marmoset PGCs could not conclusively be demonstrated, however SOX17 staining in adult primate gonads resulted in differential staining patterns. NLRP7 could not be confirmed as a primate pre-meiotic germ cell marker, but was detected in post-natal oocytes. Analysing PGC migration in mouse and marmoset embryos falsified the hypothesis that mammalian PGC migration is generally guided by neurons. The culture attempts of marmoset PGCs according to published protocols did not result in the establishment of EGCs, leading to the conclusion that protocols for successful mouse and human EGC derivation are not suitable using marmoset PGCs.

3.1 Part I – *In situ* studies of PGC development

3.1.1 PGCs do not migrate along nerve fibres in marmoset monkey and mouse embryos

The current comparative analysis of PGC translocation in the marmoset embryo extends and quantitates previous observations in the marmoset embryo by Aeckerle *et al.*, 2015, which described a wide spatio-temporal (diffuse) distribution of PGCs in the embryo over a large portion of the migration period[16]. Furthermore, I included mouse embryos in this comparative analysis as a non-primate reference species. In contrast to the marmoset, in the mouse embryos the PGCs can be followed during their translocation almost like a regular wave or homogenous cohort of cells with predictable locations at different embryonic days.

As described in the results, the onset of intense PGC proliferation in the mouse embryo can be determined histologically by the appearance of clusters of multiple PGCs around the gonad on E 11.5, where at the same location only single cells could be observed at E 10.5. At the same time the proportion of PGCs found less than 50 µm away from the closest neuron

increases from < 2 % on E 10.5 to approx. 5 % on E 11.5. This can be explained by the appearance of neurons in the peri-aortic space close to the gonads. Importantly, the data indicate that the neurons only appear in the vicinity of the gonad when the PGCs are already present in the gonad rather than the other way round.

Neither in the mouse nor in the marmoset embryos I detected any innervation of the gonad before the PGCs arrived there, which is in contrast to the observations in human embryos. This is probably the most important finding in this study, since it clearly speaks against the hypothesis of peripheral nerves acting as guiding structures for migrating PGCs – as it has been described for humans. Published data by Hoyer *et al.*[93] and Møllgard *et al.*[94], and those presented here rather suggest that nerve fibre-mediated guidance of PGCs is not a conserved phenomenon in mammals and may have developed only very recently in primate evolution. In this context it is important to mention a study performed by Sasaki *et al.*[7] on cynomolgus monkey (*Macaca fascicularis*) embryos, which belong to the group of Old World monkeys and are therefore evolutionarily even closer related to humans. They investigated this question as well by double-staining of migratory PGCs and neurons and came to the same conclusion that no structural associations were detectable.

The markers for the visualisation of PGCs (OCT4) and neurons (TUBB3) were chosen carefully. Most importantly, the same markers were used in the human embryo study[94] as well as the study in cynomolgus monkey embryos[7], facilitating comparison between the different species. As shown several times in this thesis OCT4A can be used to reliably identify PGCs. In the study on human embryos by Møllgard *et al.*, TUBB3 was shown to reliably detect neurons even in the earliest developmental stages. In the present study, using TUBB3 resulted in high-quality immunohistochemical stainings with very sensitive and clear signals in both investigated species. In fact, the TUBB3 protein sequence between human and marmoset TUBB3 is 99.8 % (449/450 amino acids) identical (BLASTP alignment of human TUBB3 sequence (Transcript ID ENST00000315491.11) with marmoset sequence (Transcript ID ENSCJAT00000009328.3) using *Ensembl* database (https://www.ensembl.org/Multi/Tools/Blast?db=core)), further substantiating the comparability of my data and the published data. I therefore feel confident that the selected markers and antibodies are well suited to answer the study question.

One could argue that inclusion of the PGCs that are already found in the gonads into the analysis may bias the results, since they make up a considerable percentage of total cells but are no longer migratory. However, looking at the individual developmental days in both marmoset and mouse embryos, I see no difference in the percentage of cells that are closely associated with neurons, independent of the PGCs' localisation. For example, on mouse embryonic day 9.5, ~ 92 % of PGCs are still migratory outside the gonad, and not a single PGC was detected close to a neuron (see Figures 6 and 8). On marmoset gestational day 65, only approx. 14 % of PGCs have reached the gonads, but more than 96 % of total cells were found in the > 50 μm-distance category (see Figures 2 and 4). From this, I can only draw the conclusion that my data set suitably answers the study question, and that PGC migration and translocation in the marmoset and mouse embryo are not dependent on peripheral nerve guidance to reach the gonad.

I am aware of the limitations of histological sections as they only allow two-dimensional analysis. A closer association between PGCs and nerve cells in the third dimension cannot be completely excluded. In order to minimize this problem, consecutive sections of the same embryos were analysed to obtain a better spatial resolution, and sagittal as well as transversal sections were used to cover all three dimensions. However, to analyse in detail and finally prove the spatial relationships between peripheral nerves and PGCs it would be favourable to have a three-dimensional representation of the tissues of interest.

Importantly, however, in the paper by Møllgard *et al*. a three dimensional representation of the embryos was not required to illustrate the close spatial association between neurons and PGCs. If these findings would be true also for the marmoset and the mouse it would be reasonable to assume that also the same or at least highly comparable methods would be sufficient to detect them.

Using this visualisation method, the possibility that the TUBB3 signal intensity lies under the detection threshold, and present neurons might therefore not be visible, can also not be excluded. However, I think this is unlikely since (I) another neuronal marker, MAP2, results in the same staining pattern via IHC as TUBB3, and (II), again, the findings in the human embryos were obtained by the same method and Møllgard and colleagues describe clearly detectable nerve fibres[94].

In summary of this part, I find a discrepancy between the published data for the human and the data presented here for the marmoset and the mouse. My current conclusion is that the reported differences between the marmoset and the mouse on the one hand and the human on the other hand represent an evolutionary very recent development in primate PGC migration.

3.1.2 SOX17 shows differential expression patterns in germ cells of non-human primates

SOX17 is a transcription factor that during embryonic development is important for the formation of the endodermal lineage, such as the definitive gut endoderm[83]. But it was also shown to be a key regulator of human PGC specification and is expressed even before BLIMP-1[76]. In order to test co-expression of both factors in the earliest marmoset PGCs available to me, marmoset embryos of GD 49 and GD 53 were stained for OCT4A and SOX17 to detect cells in sequential tissue sections that probably express both proteins. Indeed, on two sets of sequential GD 49 tissue sections, corresponding staining signals could be detected in several spots, likely deriving from the same cells. This can however not be ultimately confirmed, since the tissue shape on one section deviates slightly from that of its neighbouring section due to the embedding, sectioning and staining process. SOX17 staining of the GD 53 embryo did not reveal any SOX17-positive cells.

This method is not suitable to make statements about PGC specification in the marmoset, since (I) OCT4A is needed to visually identify the PGCs and OCT4A expression might only start downstream of SOX17 expression, and (II) the available marmoset embryos are too old. We do not know when PGC specification occurs in the marmoset, but a study in the cynomolgus macaque[7] indicates that it occurs as early as GD 11. It is therefore likely that SOX17 is expressed in early marmoset PGCs, but that the expression is possibly already downregulated when I looked at it. It might also be possible that SOX17 is not at all expressed in marmoset PGCs, which would explain why I did not detect it in GD 53 and older embryos. Since SOX17 has been implicated in germ cell specification in human and cynomolgus monkey, however, I think the first explanation is more likely.

SOX17 could not be detected in marmoset PGCs at GD 65 and GD 75. Indeed, SOX17 germ cell expression must start much later, since new-born marmoset testes and ovaries also show no SOX17 staining signal, but adult spermatogonia do. It would be interesting to stain

juvenile gonads in order to determine whether SOX17 expression in the germ cells starts before or after puberty.

According to UniProt (https://www.uniprot.org/uniprot/Q9H6I2), after inference of function by sequence similarity, SOX17 is a probable transcriptional activator in pre-meiotic germ cells. This would fit the expression pattern found in the adult marmoset testis, where SOX17 was detected in a subset of spermatogonia. Since there is still no known marker to identify the spermatogonial stem cells, which is an important goal for reproduction research, SOX17 might be a candidate and warrants further investigation in that direction. In contrast to this, SOX17 was detected in the meiotic and post-meiotic germ cells of the adult marmoset ovary and the testes of two investigated macaque species. This is an interesting finding that I currently have no explanation for. It might reflect the evolutionary divergence between New World and Old World monkeys, since the same staining pattern observed in the macaques was also obtained when human testis was stained for SOX17 in our lab (data not shown) and in the Human Protein Atlas (HPA; https://www.proteinatlas.org/ENSG00000164736-SOX17/tissue/testis#img).

In contrast to its role as transcription factor, SOX17 in the investigated NHP gonads was primarily found in the cytoplasm, not the nuclei of the cells. I hypothesised that this might be due to a change or the absence of a nuclear localisation sequence (NLS). Testing the SOX17 sequences using the cNLS Mapper tool (http://nls-mapper.iab.keio.ac.jp/cgi-bin/NLS_Mapper_form.cgi) revealed that indeed in the marmoset sequence no NLS could be detected, even if the providers of the tool claim that there might be other NLS's that are not yet recognised by the program. However, the rhesus macaque SOX17 sequence contains the same NLS as the human sequence and SOX17 is nevertheless found in the cytoplasm of the germ cells, so the subcellular localisation has probably something to do with the protein function and not the NLS in the first place. Moreover, there was clear nuclear staining for SOX17 in the colon, further supporting the specificity of the antibody (https://www.proteinatlas.org/ENSG00000164736-SOX17/tissue/colon#img).

I wanted to rule out the possibility that the used SOX17 antibody recognises other proteins than SOX17 in the tested primate species, which would result in the observed differential staining pattern. According to the data sheet, the used SOX17 antibody was raised against an epitope of 19 amino acids that in the human is only found in SOX17. A BLASTP of the human

SOX17 protein sequence against marmoset and rhesus monkey SOX17 revealed a sequence identity of 86 % and 97 %, respectively, with both monkey sequences containing the epitope which the antibody recognises. I therefore assume that the SOX17 staining observed by IHC is specific.

3.1.3 Analysis of NLRP7 and miscellaneous potential marker proteins in marmoset germ cells

NLRP7 is thought to be involved in the imprinting process of maternal genes in oocytes, and mutations in NLRP7 are associated with pregnancy loss through recurrent hydatiform mole[118]. Beside its expression in oocytes, published data of my lab[14] and those of collaboration partners[115] have shown high NLRP7 expression in the marmoset pre-implantation embryo and marmoset ESCs, suggesting potential germ line-significance, which is why I tested marmoset embryonic as well as gonadal tissues for presence of NLRP7. Looking at the testes tissues, male germ cells do not seem to express NLRP7, whereas it could be detected in oocytes in moderate levels already at birth and at high levels in the adult. This finding is in accordance with the reported expression of NLRP7 and its role in maternal imprinting in human oocytes[119]. However, human spermatozoa have also been reported to express *NLRP7* on the mRNA level[120], which is in contrast to what I see in the marmoset. I did observe some NLRP7 staining signal in the acrosome of marmoset spermatozoa; however, a phenomenon that was observed before is that the acrosome unspecifically binds to different antibodies (personal communication by R. Behr), so I evaluated the observed staining signal as unspecific. To further clarify NLRP7 expression in male marmoset germ cells, it would be possible to perform RT-PCR for NLRP7 on sperm samples. In embryonic PGCs of both sexes as well as germ cells in the male foetal gonad, no NLRP7 was detected. Unfortunately, no female foetus was available for analysis to further investigate the timepoint of the onset NLRP7 expression in oocytes. Since the NLRP7 signal in neonatal oocytes was rather low, I speculate however that it does not start long before birth. In mice, there is no *NLRP7* orthologue, and *NLRP7* in the human seems to have developed as a homologue to *NLRP2* after gene duplication[121]. Therefore, depending on the timepoint of this duplication, *NLRP7* might be a primate-specific gene and could account for developmental differences between mice and primates.

PAX5 was investigated in the marmoset because data shown at a conference talk in 2015 claimed that OCT4 dimerises with PAX5 in mouse PGCs. However, this could not be confirmed by the data that I obtained, neither in marmoset PGCs nor in the PGCs of mouse embryos (data not shown), and the original mouse data has so far not been published.

SSEA-5 was first detected as a cell surface glycan on human pluripotent stem cells in 2011[112], and has since mainly been used for selection and cell sorting[122]. As far as I can judge, its biological function is not yet properly investigated. In our group, it has been shown to be expressed on undifferentiated marmoset ESCs (unpublished data). Since the absence of SSEA-5 from marmoset PGCs has already been confirmed previously by our group (unpublished data), it was no primary epitope of interest for me. However, as this side project has revealed, SSEA-5 staining leads to interesting detection patterns in the marmoset gonad that do not fit its role as a pluripotency marker. For example, it could be detected also in primary spermatocytes in the adult marmoset testis, cells which are not associated with pluripotency. In the GD 70 and GD 74 embryos it was detected for example on the epithelia of stomach, gut, mesonephros and the developing mouth (data not shown).

I would also like to leave a note for coming experimenters: following antibodies were tested at length via IHC (dilution ranges, different tissues) but do not seem to recognise or specifically stain the respective protein in *Callithrix jacchus*:

Antibody	Source	Company, Article #
ANPEP-FITC	rHuman	Miltenyi #130-103-732
CD9	Mouse	AbD serotec #MCA469GA
c-Kit	Goat	Santa Cruz #sc-1494 (M-14)
c-Kit	Mouse	ThermoFisher #MA5-12944 (K45)
D2-40	Mouse	Dako #M3619
DAZL	Rabbit	Biozol #34139
DAZL	Rabbit	Cell Signaling #8042
DAZL	Rabbit	Cell Signaling #13057
ENO2	Rabbit	Abcam # ab53025
GCTM-2	Mouse	ThermoFisher #433140
OCT4	Rabbit	Cell Signaling #2750
SOX17	Mouse	Origene #TA500281
TNAP	Mouse	Santa Cruz #sc-166261

3.2 Part II – Cell culture studies

3.2.1 Development of the PGC culture protocol

Protocols for the derivation of mouse and human EGCs are available in the literature and describe a multi-step but rather uncomplicated cell line establishment[97, 98, 104]. I therefore started the mouse PGC culture approaches to establish this method in our lab and to practice GR isolation and culture before beginning experiments with the rare marmoset embryo samples. The obstacles encountered and the results of the protocol adaptations are described in detail in chapters 2.2.1 and 2.2.2. Especially the low feeder cell quality could not be overcome, even by changing the medium composition several times, increasing the feeder cell number or mixing different kinds of feeder cells. Adding foetal calve serum (FCS) had a beneficial effect on the feeder cells, and should be suitable for mouse EGC derivation as described in the protocols. However, FCS did not help in deriving mouse EGCs, and FCS was not used for the marmoset PGC culture since experience with marmoset ESCs shows that they differentiate as soon as the cells get in contact with FCS. It was stressed in the available literature that normal mouse embryonic fibroblasts (MEFs) are not suitable for culture, since they do not express the membrane-bound form of stem cell factor (SCF, or kit-ligand), which is essential for PGC reprogramming to pluripotency. This is also the reason why feeder-free culture was not attempted in this project.

Apart from the cytokine SCF in its membrane-bound as well as soluble form, the initial mouse PGC culture medium that I used contained the cytokine leukaemia inhibitory factor (LIF), basic fibroblast growth factor (bFGF) and forskolin[68, 101, 104]. LIF is expressed by the trophectoderm and its receptor on the cells of the inner cell mass (ICM)[123], and in culture promotes pluripotent cell renewal and inhibits differentiation[124]. bFGF via gremlin induction inhibits differentiation signals of bone morphogenic proteins (BMPs)[125], proteins which are induced during PGC specification[62], and in culture bFGF induces proliferation in pluripotent stem cells[126-128]. Forskolin increases levels of the second messenger cyclic AMP[129]. While some available EGC-derivation protocols claim that forskolin is dispensable, the addition of the other factors is – understandably – crucial for PGC conversion to the pluripotent state. All of these factors were also contained in the medium of the more sophisticated culture protocol that was implemented after my visit to the lab of Prof Schorle in Bonn[102]. One

difference was that their concentration was initially high in the culture medium and then slowly decreased over time as fresh culture medium was added, until finally only LIF, CHIR99021 and PD0325901 were added to the medium. The other main difference was the addition of two small molecule inhibitors (2i). CHIR99021 is an inhibitor of GSK3 and therefore an activator of the beta-catenin/Wnt-signalling-cascade, which induces cell division and proliferation[130]. PD0325901 is an inhibitor of MEK and therefore of the MAPK-pathway, which usually leads to reduced cell proliferation[131, 132]. While it may seem contradictory to use both compounds in the same culture, the so-called 2i medium is widely used in different cell culture and differentiation studies[133-135] and has been proven to be sufficient for naïve pluripotency in mouse cells[136].

Another remaining problem is that AP activity on marmoset PGCs could not yet be confirmed, this would however be important as an indicator of PGC culture success. AP-live stain of single cells or a GR cell suspension to verify AP expression and identify PGCs was not feasible due to autofluorescence. Using the AP-stain on fixed cells would wash away the single or unattached PGCs during the staining process, and for IHC of GR in the embryo no suitable antibody was available.

After the failed attempts of marmoset EGC derivation, I wanted to at least roughly analyse at which point of the culture the PGCs vanish in order to find new starting points for improvement of the culture strategy. As described in chapter 2.2.2.3, GR and MN fragments were cultured for a varying number of days and then tested for the presence of pluripotency factor expression via qPCR. If EGCs would form and proliferate, I expected to see an increase of OCT4 and NANOG expression over time, but since I never saw any colonies I did not expect to detect any pluripotent cells remaining in the culture. Surprisingly, there was neither an increase nor a decrease of expression levels over time. From this I have to draw the conclusion that at least some PGCs remain in the culture, and the problem is getting them to properly attach and proliferate, as speculated above. What has to be kept in mind when looking at the qPCR-data is that the "Day 0"-amount of cells is not comparable to the cultured cells. It was necessary to obtain fresh GR as positive control for the detectability of the pluripotency factors, but additionally I should have made a Day 0 culture which would also have contained the feeder cells and the appropriate "dilution" of GR cells, as it occurred in the other culture samples. Also, due to the rarity of the material, no biological duplicates or better triplicates were available. This experiment definitely would have to be repeated in

100

order to make reliable statements about the trajectory of pluripotency factor expression levels and hence PGC/EGC culture over time.

3.2.2 EGCs in the context of germ cell culture

The failed attempts to culture marmoset primordial germ cells in this study can be seen in a wider context of germ cell culture experiments. As elaborated in chapter 1.2, apart from the culture of mouse foetal germ cells, namely PGCs, there are also studies that show derivation of pluripotent stem cells from neonatal and adult mouse germ cells[51-53]. These reports show the potential of post-natal germ cells to convert back into a pluripotent state. Vice versa, functional mouse germ cells can now be derived in culture from pluripotent stem cells[137]. Therefore, at least in the mouse, trans-differentiation between germ cells and pluripotent cells is possible. Studies on the derivation of pluripotent cells from human spermatogonia followed soon after the reports on mice[54-57, 138]. The existence of human germ cell-derived pluripotent cells is however still debated today. One study was retracted[138] and even the persons who initially published such reports have now doubts about the true pluripotent state and the identity of the cultured cells[139, 140]. Looking at the situation in non-human primates, the culture of adult marmoset spermatogonia did not result in the derivation of pluripotent cells[59], and even the culture of younger spermatogonia with supposedly higher proliferative potential from neonatal marmoset testes did not yield pluripotent cell lines (unpublished data of our lab). The same can be said for the culture of neonatal marmoset oogonia[60]. Therefore, the next step for marmoset germ cell culture was to use even younger germ cells and thus marmoset PGC culture was attempted in this study. It seems, however, that while mouse germ cell culture works relatively well and is widely accepted, the derivation of true pluripotent stem cells from human and non-human primate (adult) germ cells remains to be demonstrated.

After performing all these culture experiments I feel that the description of EGC-line derivations in the literature is possibly slightly exaggerated. As I have seen in the lab of Prof Hubert Schorle, mouse EGC derivation is possible and reproducible, even if I do not think a (permanent) cell line in the actual sense can be established. If I should speculate, compared to the cells of the blastocyst's ICM and deriving ESCs, PGCs probably already carry some somatic epigenetic marks that do not vanish after spontaneous reprogramming in culture

and will therefore at some point reduce the proliferative potential of the EGCs. The same is probably true for human EGCs, since no human EGC line is available. This was confirmed through personal communication with Prof Neil A. Hanley (Division of Diabetes, Endocrinology & Gastroenterology, School of Medical Sciences, University of Manchester, UK), who is one of the few who reported human EGC derivation[105, 141]. While this disqualifies from my point of view at least human EGCs as true pluripotent stem cells, the limited proliferation might still be a valuable feature of these cells and advantage over other pluripotent stem cells. One of the biggest problems of pluripotent stem cells for their use in regenerative therapy is their unlimited proliferative potential and their potential to form specific tumours, namely teratoma. This means that even after differentiation into the target tissue, e.g. heart muscle cells, some undifferentiated cells might remain and after transplantation into the patients start to form teratoma. EGCs theoretically could be expanded over a certain time before they cease proliferation until the cell number is high enough, and then safely be differentiated into the target cells.

3.2.3 The importance of finding a marmoset PGC surface marker

From the beginning, it was my goal to identify a marmoset PGC-specific surface protein to be able to enrich the PGCs in the fraction of cultured cells. This would allow making more precise statements about the cells in culture, and additionally help to perform more efficient single cell transcriptome analyses. As mentioned before, marmoset PGCs do not seem to express any of the known surface markers of human and mouse PGCs or ESCs (SSEA-1, -3, -4, -5; TRA-1-60, Tra-1-81), and the task to identify a novel surface marker proved rather difficult. I was therefore quite confident when finally PGC surface-specific localisation of ANPEP was detected.

One rather disappointing finding was that ANPEP cannot be used to select and purify live PGCs. One possible explanation for this would be that ANPEP is enzymatically active on live cells but not Bouin-fixed tissues, so it is detectable via IHC, but the peptidase might cut the antibody when it is not fixed. As stated on https://pubchem.ncbi.nlm.nih.gov/target/gene/ANPEP/cattle#section=Orthologous-Genes, ANPEP is a *"Broad specificity aminopeptidase which plays a role in the final digestion of peptides generated from hydrolysis of proteins by gastric and pancreatic proteases. Also involved in the processing of various peptides*

including peptide hormones, such as angiotensin III and IV, neuropeptides, and chemokines. May also be involved the cleavage of peptides bound to major histocompatibility complex class II molecules of antigen presenting cells." This hypothesis was confirmed by immunofluorescence, where ANPEP was detectable on fixed but not on intact non-fixed cells.

This leaves the task of finding another PGC-specific surface protein. Unfortunately, CD31 (PECAM) expression on marmoset PGCs could only be confirmed via IHC very late in the course of this project, so that I was not able to test it *in vivo* on GR cells. This finding forms a good starting point for further PGC purification attempts using this surface marker. In the original publication, it is shown that CD31 expression on mouse PGCs starts around E 9, marking the onset of PGC migration, and ceases after E 13, which is associated with sex determination[114]. Since in the marmoset it is not clear at which stage the gonadal PGCs start their differentiation into gonocytes, CD31 might potentially be used as a marker for this process. Also, mouse PGCs are usually not used for EGC derivation after E 12.5 due to sex determination and subsequent loss of EGC-forming potential[68, 101]. Loss of CD31 expression in the marmoset could therefore also indicate the point after which the PGCs lose their potential for reprogramming in culture. Since I detected CD31 presence on marmoset PGCs in the embryonic gonad at GD 74 as well as GD 85, but PGC culture attempts were mostly performed with younger embryos of GD 70-74, I am now confident that the used PGCs should at least have had the potential to regain pluripotency in culture.

Indeed, it is not clear whether the age of the used embryos was ideal for EGC derivation. I attempted to reach a balance between having as many PGCs as possible in the genital ridges at the point of isolation, but isolating them before they start the sex differentiation process. In the mouse, this balance point is usually reached at E 10.5 and E 11.5. In the marmoset, I judged because of morphological shape and PGC numbers in the GR and decided that GD 70-74 should be suitable. I have however no data to confirm this.

This leaves several potential candidates of surface proteins that are expressed on mouse or human PGCs or germ cells, and that remain to be tested on marmoset PGCs: CD38[76], CXCR4b[142], CXCR7[143], FGFR3[144] and Ep-CAM[145] were not yet tested. GCTM-2 (Podocalyxin)[146-148] as well as c-Kit[93], D2-40[149] and CD9[150] were tested, however the

available antibodies do not seem to recognise the marmoset proteins, so until a suitable antibody can be found, their presence on marmoset PGCs remains unknown.

3.3 Outlook

Further marmoset PGC culture attempts are planned. However, to test a new and hopefully more promising approach, refined cell culture conditions will be tested. In collaboration with Dr Ufuk Günesdogan, marmoset ESCs will first be differentiated into PGC-like cells *in vitro* in order to identify the underlying molecular mechanisms and cell culture requirements for PGC differentiation, and then have a better idea how to reverse the germ cell differentiation process from PGCs to pluripotent stem cells.

I also contributed pre-natal marmoset tissue samples to a large EU consolidator grant project on comparative developmental genomics coordinated by Prof Henrik Kaessmann (Research group *Evolution of Mammalian Genomics*, ZMBH, University of Heidelberg, Germany). We are still waiting for the single cell transcriptome data of the PGCs that will also be obtained in the context of this project. With this data, we hope to verify the protein expression results obtained in this study by IHC. It might also help to unveil the expression of the candidate surface proteins mentioned above, for which no suitable antibody is available. If a successful isolation of PGCs with a surface protein can be established, it could also be possible to isolate migratory PGCs, and compare the transcriptome of migratory versus gonadal PGCs and gonocytes/oogonia after sex differentiation. It would also be desirable to compare the transcriptome of mouse and marmoset PGCs to identify additional primate-specific characteristics of germ cell development[151].

Germ cell development is accompanied by epigenetic reprogramming, and the methylation status of promoters of various genes (for example *OCT4, VASA, MAGEA4* and the imprinted genes *MEST* and *H19*) might give new insights into the onset of sex differentiation. Therefore, when purification of PGCs is finally possible, a promoter-methylation study could be performed as initially intended to determine when the potential for reprogramming of PGCs to EGCs is lost.

3.4 Summary & Conclusions

In summary, no spatial association between PGC migration and nerve fibres could be observed, neither in the mouse nor the marmoset monkey embryo as a non-human primate. This finding falsifies the hypothesis that PGC guidance by developing peripheral nerves is a conserved mechanism in mammalian embryonic development. When I compare my findings to those obtained in the human embryos, I conclude that the observations by Møllgard *et al*. – other than representing a general mammalian strategy – rather reflect a species-specific trait of human PGC development. This must have emerged late in primate evolution.

Via IHC, I could not confirm NLRP7 as a marker for pre-meiotic germ cells, thereby falsifying my hypothesis that NLRP7 could be a primate-specific pre-meiotic germ cell marker. Neither could the expression of the transcription factor PAX5 be detected in marmoset PGCs, nor could the presence of SOX17 in early marmoset PGCs be definitely demonstrated. Staining of SOX17 on adult non-human primate gonads however revealed differential protein expression patterns in the primate germ cells that might reflect the evolutionary divergence between New World and Old World monkeys. ANPEP and CD31 were confirmed as surface proteins of marmoset PGCs via IHC. However, ANPEP was not suitable for purification of live PGCs, and CD31 remains to be tested.

Finally, the attempted derivation of a marmoset EGC line was not successful and I have to conclude that the published protocols for human and mouse EGC derivation are not effective for marmoset PGCs.

4. Materials and Methods

4.1 Materials

4.1.1 Solutions and Media

Bouin's fixative:
15 parts Picric acid 1.2 %
5 parts Formaldehyde 35 %
1 part Acetic acid 100 %

M10 medium:
DMEM
10 % FCS
0.1 % (v/v) AmpB
1 % P/S
2 mM GlutaMAX
1x NEAA

ESM:
KO-DMEM
20 % KO-Serum replacement
1 % P/S
2 mM Glutamax
1 mM MEM-NEAA
50 µM β-Mercaptoethanol

PGC culture medium (N2B27):
Equal parts DMEM-F12 + Neurobasal medium
N2 supplement
B27 supplement
0.3 % BSA
1% P/S
1x Glutamax
1x NEAA
100 µM β-Mercaptoethanol

EGC culture medium (2i):
DMEM-Glutamax
10 % FCS
1 % P/S
200 mM Glutamin
1x NEAA
1x EAA

FACS/MACS buffer:
1x PBS
0.5 % BSA
2 mM EDTA

4x SDS sample buffer:
8 % (w/v) SDS
200 mM Tris/HCl pH 6,8
50 % (v/v) Glycerol
4 % (v/v) β-Mercaptoethanol
0.04 % (w/v) Bromphenol blue

10x SDS running buffer:
250 mM Tris
1 % (w/v) SDS
1.92 M Glycin

TBS washing buffer:
0.05 M Tris
0.15 M NaCl
pH 7.6

TBS-Tween:
TBS + 0.1 % (v/v) Tween

Anode buffer I:
0.3 M Tris/HCl pH 10.4
20 % (v/v) Methanol

Anode buffer II:
0.025 M Tris/HCl pH 10.4
20 % (v/v) Methanol

Cathode buffer:
0.025 M Tris/HCl pH 9.4
0.04 M Glycine
20 % (v/v) Methanol

4.1.2 Antibodies

Table I | List of antibodies used for immunohistochemistry

Antibody	Source	Dilution	Company, Article #
ANPEP (CD13)	Mouse	1:50	R&D Systems #498001
CD31	Mouse	1:100	Dako #M0823
LIN28	Rabbit	1:200	Cell Signaling #3978
MAP2	Rabbit	1:150	Sigma HPA012828
NANOG	Rabbit	1:100	Cell Signaling #4903
Nestin	Mouse	1:400	Santa Cruz #sc377380
NLRP7	Rabbit	1:1000	Abcam #ab117732
OCT3/4	Rabbit	1:150	Santa Cruz #9081 (H-134)
OCT4A	Rabbit	1:300	Cell Signaling #2890
PAX5	Mouse	1:150	Dako #M7307
SALL4	Mouse	1:200	Abcam #ab57577
SOX17	Rabbit	1:300	ThermoFisher #PA5-23352
SOX9	Rabbit	1:500	Millipore #AB5535
SSEA-5	Mouse	1.1000	GeneTex GTX70019
TUBB3	Mouse	1:2000	Sigma #T8660
VASA	Goat	1:200	R&D #AF2030

Table II | List of antibodies used for Western Blot

Antibody	Source	Dilution	Company
OCT4A	Rabbit	1:500	Cell Signaling #2890
α-Rabbit-HRP	Goat	1:1000	R&D Systems #HAF008
TUBB3	Mouse	1:2000	Sigma #T8660
α-Mouse-HRP	Goat	1:1000	R&D Systems #HAF007

Table III | List of antibodies used for immunofluorescence, FACS and MACS

Antibody	Source	Dilution	Company
ANPEP (CD13)	Mouse IgG	1:50	R&D Systems #498001
α-Mouse-IgG-AF488	Goat	1:1000	Invitrogen A10680
TRA-1-81	Mouse IgM	1:100	eBioscience #14-8883
SSEA-1	Mouse IgM	1:50	eBiosciences #14-8813
α-Mouse-IgM-AF488	Goat	1:1000	Invitrogen A10680

4.2 Methods

4.2.1 Obtaining staged marmoset monkey embryos

All animal studies were performed in accordance with the German Animal Protection Law and approved by the ethics committee of the animal welfare office of the Lower Saxony State Office for Consumer Protection and Food Safety (Niedersächsisches Landesamt für Verbraucherschutz und Lebensmittelsicherheit, LAVES), which is in charge of this approval. The animals were obtained from the common marmoset (*Callithrix jacchus*) breeding colony of the German Primate Center (Deutsches Primatenzentrum, DPZ). The institutional guidelines on housing and care of marmosets were strictly followed.

Monitoring progesterone levels in female marmosets:

Marmoset monkeys were kept in breeding pairs. After set-up of the mating, blood samples of the female were obtained twice a week in order to measure the blood progesterone level. The hormone assay was performed by the Hormone Laboratory Service Unit of the DPZ. During the natural cycle, blood progesterone levels lie distinctly below 10 ng/ml during the follicular phase. After ovulation the progesterone levels increase significantly to values > 20 ng/ml. The day when progesterone levels exceed the 10 ng/ml-threshold is defined as the day of ovulation or gestational day (GD) 0. In case of pregnancy, progesterone levels will remain high throughout pregnancy even after the luteal phase, and the exact age of the embryos can be calculated. When the females are not pregnant, after the luteal phase progesterone levels will decrease again until they reach the baseline.

Retrieval of embryos via caesarean section or hysterotomy:

The embryos were obtained at a defined gestational day (GD) via caesarean section or hysterotomy typically with survival of the mother animal as described previously[16]. All surgical procedures on the animals were performed by a specialised and experienced veterinarian. Surgery was performed under anaesthesia under sterile conditions. Appropriate analgesic and antibiotic therapy was administered to all animals after surgery.

The embryos were extracted from the placenta in ice cold PBS (Gibco), weighed and measured and the tail frozen for subsequent DNA analysis. The embryos were then either fixed *in toto* for immunohistochemical analysis, or further dissected for cell culture

experiments. Marmoset Embryos of GD 49, 50 and 53 and the embryos used for the PGC migration study have been previously obtained by our group under license #42502-04-12/0708, and were available for histological analysis.

4.2.2 Retrieval of mouse embryos, gonads and other reference tissues

Female CD1 mice were obtained from the animal facility of the European Neuroscience Institute (ENI; Göttingen, Germany); female C57BL/6 mice were obtained from the animal facility of the Max-Planck-Institute for biophysical Chemistry (MPI BPC, Göttingen, Germany), at a defined number of days after vaginal plug detection. The mice were sacrificed by cervical dislocation and the uterus removed for embryo collection. Embryos for this study were obtained at embryonic day (E) 8.5, E 9.5, E 10.5 and E 11.5, respectively.

Testes and ovaries of different non-human primate (NHP) and rodent species as well as other reference tissues for immunohistochemistry were taken from the tissue bank of the Platform Degenerative Diseases. All tissues were obtained from animals that had to be sacrificed for veterinarian purposes or within the scope of other projects where these tissues were not needed and therefore given to us for histological analyses. Additionally, the German Animal Protection Law (Tierschutzgesetz) states in §7 Section 2 that the sacrifice of an animal for the collection of organs for scientific purposes only is not defined as an animal experiment. Thus, scientific organ collection has to be registered with, but not approved by, the responsible authorities.

109

4.2.3 Immunohistochemistry & Immunofluorescence

Tissue processing:

The embryos were fixed directly after retrieval in Bouin's solution for 4 – 24 hours depending on the embryo size. Fixation was followed by several washing steps with 70 % EtOH over at least 2 days. Then tissues were embedded in paraffin and sectioned at 5 μm. The embryos were positioned in order to obtain either transversal or sagittal sections.

Immunohistochemical staining:

Slides for immunohistochemistry were stained using the EnVision^{TM} Flex Kit by Dako (#K8024). Briefly, the slides were deparaffinised in Xylol, rehydrated in a graded Ethanol

series and antigen retrieval was performed by heating the slides in 10 µM Na-Citrate buffer pH 6.0 (Merck) in the microwave for 10 minutes. Subsequently, endogenous phosphatase and peroxidase enzymes were blocked using the blocking agent provided in the kit. Slides were washed in TBS and incubated with the primary antibody over night at 4°C in a humidified chamber. The antibody signal was visualised the next day using the 3,3'-diaminobenzidine (DAB+) chromogen. Subsequently, the slides were counter-stained for 10 – 15 seconds in Mayer's Hematoxylin Solution, the reaction stopped in 0.1 M HCl, washed with tap water and mounted with coverslips using Glycergel (Dako #C0563). Control stainings using IgG antibodies at the same protein concentration as the primary antibodies were performed in order to exclude unspecific antibody binding. Antibodies used for this project are listed in **Table I**.

Double-staining:

Immunohistochemical double-staining was performed in a three-day process using the EnVision™ Doublestain System Kit by Dako (#K5361). The slides were deparaffinised, rehydrated and antigen retrieval was performed as described above. The first primary antibody directed against OCT4 in mice and OCT4A in marmoset was incubated over night at 4°C and stained the next day using the 3,3'-diaminobenzidine (DAB+) chromogen. After washing and blocking with an agent to prevent double staining of the same antigen, the slides were incubated with the second primary antibody against TUBB3 over night at 4°C. All incubation steps were performed using a humidified chamber. On the third day, the second antibody-signal was visualised using PermanentRed chromogen. The slides were counter-stained for 10 – 15 seconds in Mayer's Hematoxylin Solution. Immunohistochemical images were taken using the Leica Aperio CS2 Digital Slide Scanner and morphometrically analysed with the Aperio ImageScope© software.

Immunofluorescence staining of cultured cells:

Marmoset embryonic stem cells (ESCs) were grown in a 6-well plate on glass coverslips. For comparison of the staining results of live versus fixed cells, cells were washed twice with PBS and then either fixed in Bouin's solution for 30 minutes at room temperature (RT) or kept intact in PBS for the same time. Fixation was followed by blocking the cells with 1 % BSA in PBS for 20 minutes at RT. For incubation with the primary antibody, the coverslips were

placed in a humidified chamber for 1 hour at 37°C. This was followed by incubation with the secondary antibody for 1 hour at 37°C. Primary and secondary antibodies were diluted in PBS + 1 % BSA. After each of the previous steps the cells were washed twice with PBS. Cells were then incubated with DAPI (0.5 μg/ml diluted in PBS + 1 % BSA for 10 minutes at RT), followed by washing with PBS and finally water to remove any salt residues. Coverslips were mounted on glass slides in Glycerol/PBS solution AF1 mounting medium (Citifluor #AF1-100). Fluorescence microscopy images were taken with a Zeiss Observer Z1 and analysed using the AxioVision software (Zeiss). The used primary and respective secondary antibodies can be found in **Table III**.

4.2.4 Western Blot

Protein isolation:

Proteins were isolated from tissues using the Qproteome Kit by QIAGEN (#37582) according to manufacturer's instructions. Using this kit resulted in two fractions: cytosolic and nuclear proteins. Protein concentration in the samples was measured using the Bradford assay. Briefly, protein samples are incubated with the dye Coomassie Brilliant Blue (BioRad #500-0006) and the absorbance at 595 nm is measured in a spectrophotometer. The absorbance is proportional to the protein concentration and can be calculated using a standard calibration curve of defined BSA concentrations. The calibration curve was established using the Nano Photometer Pearl (IMPLEN, Munich) according to the manufacturer's instructions.

SDS-Polyacrylamide gel electrophoresis:

The appropriate volume of SDS-sample buffer was added to a sample volume containing 25 μg of protein and the samples heated at 95°C for 10 minutes to denature the proteins. The proteins were then separated according to their molecular weight via gel electrophoresis in 10 % polyacrylamide gels using a Minigel-Twin-chamber (Biometra) filled with 1x SDS-running buffer. A constant current of 20 mA was provided by the Biometra Standard Power Pack P25 for approx. 2 hours. Two size standards were used: the NovexR Sharp Prestained Protein Standard (LifeTechnologies #LC5800) for visualisation in the gel and on the membrane as well as the MagicMark XP (LifeTechnologies #LC5602), which only becomes visible during chemiluminescence detection.

Semi-dry protein transfer:

After gel electrophoresis, the proteins were transferred onto a PVDF membrane (Amersham Hybond^{TM}-P, GE Healthcare) using a V20 Semi-Dry Blotter Unit (Scie-Plas) for 40 minutes at 2.4 mA/cm^2 gel area (approx. 150 mA/gel). Before the transfer, the membrane had to be activated by incubation in Methanol for 5 minutes and the Whatman filter papers had to be equilibrated in the respective buffers. A scheme of the transfer set-up is shown below.
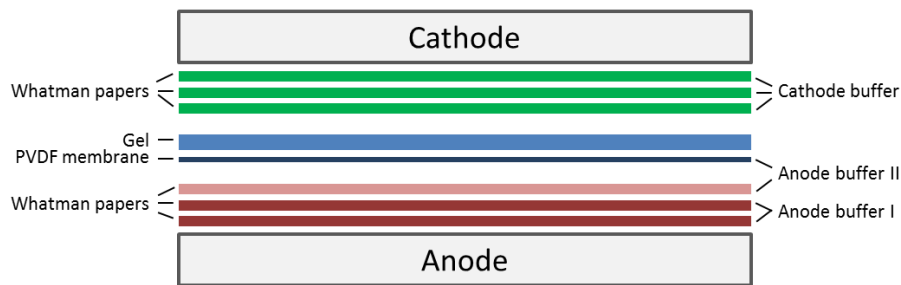
Immunodetection:

After proteins were transferred onto the membrane, it was blocked in TBS-Tween/5 % Milk (Tween 20: Sigma-Aldrich #P1379, Milk powder: Roth) for 1 hour at RT on a shaker. Incubation with the primary antibody was performed over night at 4°C. On the next day, the membrane was washed twice for 5 minutes with TBS-Tween before incubation with an HRP-linked secondary antibody for 1 hour at RT and again washed twice with TBS-Tween. Primary and secondary antibodies were diluted in TBS-Tween/5 % Milk. Antibodies used for western blot analysis are given in **Table II**. Detection was performed using an Enhanced Chemiluminescent solution (Amersham^{TM} ECL^{TM} Western Blotting Analysis System, GE Healthcare #RPN2109). The membrane was incubated with 2 ml of ECL solution for 1 min ute before detection of the luminescent signal via Intas Chemo Cam and the Chemo Star software (INTAS, Göttingen).

4.2.5 Culture of embryonic stem cells (ESCs)

Culture of mouse ESCs:

A commercial mouse embryonic stem cell line (Merck #SCR011, C57BL/6 background) was maintained in culture on a feeder cell layer of mouse embryonic fibroblasts (MEFs). MEFs were produced by our technical assistants according to established protocols[13] and

γ-irradiated to prevent cell proliferation. Embryonic stem cell medium (ESM, all ingredients by Gibco) containing 1000 U/ml of mLIF (Gibco #PMC9484) was used to maintain undifferentiated ESCs. Medium was changed every other day and cells had to be split every 2-4 days before the plates became too confluent. For this purpose, cells were detached from the plate via incubation in Accutase enzyme solution (Gibco #11599686) for 3 minutes at 37°C, centrifuged at 200 g for 5 minutes, the resulting pellet resuspended in ESM and transferred onto fresh feeder cells.

Feeder-free cell culture of marmoset ESCs:

Marmoset ESCs were cultured on Geltrex (ThermoFisher Scientific #A1413302) coated 6 cm-dishes or 6-well plates with ESC feeder-free culture medium (iPS-Brew XF (Miltenyi Biotech #130-107-086) supplemented with 1 µM CHIR99021 (LC Labs #C-6556) and 1 µM IWR1 (Sigma #I0161)) at 37°C under 5 % CO_2. For Geltrex coating, 2 ml of Geltrex (0.16 mg/ml in DMEM (Gibco)) were distributed on the dish and plates were incubated at 37°C for 1 hour. To maintain ESCs in an undifferentiated state, medium had to be changed every day and they had to be split regularly before the plates became too confluent. For this purpose, cells were either manually picked under the stereo microscope using a glass tip and transferred onto a new plate, or split using Versene solution (Gibco #15040-033). To avoid contamination after manual picking, 1 µl/ml penicillin-streptomycin (Gibco #15140-122) was added to the medium. 2 mM Prosurvival compund (Merck #529659) was added on the first day after splitting or picking of the cells to promote ESC survival.

All cell culture work was performed under sterile conditions in a flow cabinet. Unless stated otherwise, cells were incubated at 37°C and 5 % CO_2.

4.2.6 Culture of primordial germ cells (PGCs)

Embryo dissection:

Genital ridges (GR) were dissected from mouse and marmoset embryos of varying developmental stages directly after their extraction from the placenta. Embryos were placed in ice cold PBS (Gibco) in a plastic petri dish under a stereo microscope. Head, tail and heart were removed and frozen in liquid nitrogen for different purposes. The remaining embryo fragment was placed on the back and an incision made on the ventral midline. Organs were

removed and frozen in liquid nitrogen if they could be identified, then the lateral body wall was cut away until the urogenital ridges were visible. The tissue complex of aorta/GR/mesonephros (MN) was extracted using micro-scissors. If the developmental stage allowed separation, the GR were separated from the MN with fine insulin needles (B. Braun Omnican 40). Otherwise the whole urogenital ridge was taken for further culture experiments.

Digestion:

Depending on the respective protocol, genital ridges were enzymatically digested using either trypsin (dilution of 0.5 % Trypsin/EDTA-stock solution (Gibco #15400-054) to final concentration of 0.05 % - 0.25 %) or an enzyme mix of 1 mg/ml hyaluronidase (Sigma #H2126), 1 mg/ml collagenase IV (Sigma #C5138) and 15 U/ml DNase I (Roche #11284932001) diluted in equal parts DMEM-Glutamax and F-12 (Gibco). Digestion was performed in wells of a 96-well round bottom plate at 37°C for 5-10 minutes depending on the dissociation efficiency. Tissues were dissociated by gentle pipetting, then the cell suspension was washed via centrifugation at 200 g for 5 minutes and the resulting pellet resuspended in the respective culture medium.

Depending on the respective protocol, GR and MN were sometimes cultured as tissue explants, meaning that they were placed in the culture plate as whole tissues or mechanically disrupted to obtain smaller fragments, but not enzymatically digested.

Culture:

The obtained GR/MN cell suspension or the tissue explants were plated on 6-well or 12-well culture dishes on feeder cells, with the (U)GR cells of 1 embryo per well. Depending on the protocol, SNLP-feeder[98] (ATCC #SCRC-1050) or Sl^4-m220 cells[97] (Gift of Prof H. Schorle, Bonn) were used. The plates had to be prepared 1-2 days prior to culture initiation. For this purpose, plates were coated with gelatine for 15 minutes at 37°C, then gelatine was removed and plates air-dried. Γ-irradiated feeder cells were thawed in M10-medium and distributed on the culture dish to achieve a 90-95 % confluency (approx. $10x10^4$ cells/cm^2). After 24 hours, the feeder cells had attached to the plate and the M10 medium could be replaced with PGC culture medium. Ideally, the culture medium should be placed on the feeder cells at least 4 hours prior to the GR cells to allow "conditioning" of the milieu.

The development of the culture protocol is illustrated more detailed in the results part. However, there are roughly two different protocols that were followed:

(1) Protocol based on publications by Durcova (2008)[101] and De Miguel (2011)[68]

(2) Protocol based on publication by Leitch, Surani, Smith *et al*. (2013)[102]

Protocol (1) was initially used for culture of mouse PGCs. Cells were cultured on SNLP-feeder cells in ESM containing mLIF (1000 U/ml, Gibco #PMC9484), bFGF (20 ng/ml, Prospec #CYT-386), mSCF (10 ng/ml, Prospec #CYT-275) and forskolin (10 µM, LC Labs #F-9929). Medium was changed daily, wherein 2/3 of the old medium were removed and replaced with new medium containing freshly added growth factors. Plates were observed regularly for the appearance of embryonic germ cell (EGC) colonies. Colony formation was expected to start after 7 days. Appearing colonies were manually picked under a stereo microscope using a fine glass tip and transferred onto a fresh plate with mouse embryonic fibroblast (MEF) feeder cells. MEF-feeder cells were produced by our technical assistants according to established protocols[13] and were plated as described above. The sub-cultured EGC colonies were cultured in ESM containing 1000 U/ml of mLIF.

Protocol (2) was recommended for EGC derivation by Prof H. Schorle and was tested for mouse and marmoset PGC culture. Cells were cultured on Sl^4-m220 feeders in N2B27-medium (all ingredients by Gibco) with dynamic concentrations of growth factors. Initially the following components were added to the N2B27-stock medium: bFGF (25 ng/ml, Prospec #CYT-275 (m)/#CYT-218 (h)), LIF (1000 U/ml, Gibco #PMC9484 (m)/Peprotech #300-05 (h)), SCF (100 ng/ml, Prospec #CYT-275 (m)/#CYT-255 (h)), forskolin (10 µM, LC Labs #F-9929), retinoic acid (2 µM, Sigma #R2625) and GSK3-Inhibitor CHIR99021 (LC Labs #C-6556, 3 µM for mouse, 1 µM for marmoset PGCs). After 48 hours, one volume of freshly prepared PGC growth medium (N2B27-stock medium with LIF (1000 U/ml), CHIR99021 (3 µM/1 µM) and MEK-Inhibitor PD0325901 (1 µM)) was added. After 4 days, half of the old medium was replaced with fresh PGC growth medium, thus continually diluting the initial growth factor concentrations. After 6 days, medium was changed completely and fresh PGC growth medium was supplied every two days. EGC colonies were expected to form 12-16 days after culture initiation. Appearing colonies were manually picked under the stereo microscope and transferred into wells of a 96-well round bottom plate for digestion with 0.05 % Trypsin/EDTA (Gibco #15400-054) for 3-5 minutes at 37°C. After pipetting up and

down to dissociate the colonies, cells were transferred onto fresh 48-well plates with MEFs and cultured in 2i-medium, which was changed every 2-3 days.

All cell culture work was performed under sterile conditions in a flow cabinet. Unless stated otherwise, cells were incubated at 37°C and 5 % CO_2.

4.2.7 Alkaline Phosphatase staining

Alkaline Phosphatase (AP) expression is considered a hallmark of pluripotent stem cells and used as a means to verify EGC identity[97]. AP enzymatic activity can be detected via substrate formation using commercially available kits either on PFA-fixed cells (Merck #SCR004) or on live cells (Molecular Probes #A14353). Kits were used according to manufacturer's instructions.

4.2.8 Flow cytometry and cell sorting

Fluorescence associated cell sorting:

Flow cytometry and fluorescence associated cell sorting (FACS) requires single cell suspensions. For this purpose, genital ridge tissue was digested using an enzyme solution (Equal parts DMEM-Glutamax and F-12 (Gibco) containing 1 mg/ml hyaluronidase (Sigma #H2126), 1 mg/ml collagenase IV (Sigma #C5138) and 15 U/ml DNase I (Roche #11284932001)). After 10 minutes at 37°C, tissues were carefully pipetted up and down to dissociate the cells, and finally passed through a 35 µm-cell strainer (Corning #352235) to create single cells. Marmoset ESCs were detached from their culture plates using Accutase enzyme solution (Gibco #11599686) for 4 minutes at 37°C and passed through a 35 µm-cell strainer to create a single cell suspension. After washing the cells with FACS buffer and centrifugation at 200 g for 5 minutes, cells were counted and distributed to FACS tubes (Corning #352235) with at least $1x10^5$ cells/tube. Cells were incubated with the primary antibody for 1 hour at 4°C if not indicated otherwise, washed twice with FACS buffer and incubated with a fluorochrome-coupled secondary antibody for 30 minutes at 4°C if not indicated otherwise. Primary and secondary antibodies were diluted in a total volume of 50 µl FACS buffer per tube. Antibodies used for this project are given in **Table III**. After staining the cells were washed, resuspended in 200 µl FACS buffer and either analysed using

a LSR II flow cytometer (BD Biosciences) or sorted using the SH800S Cell Sorter (Sony Biotechnology). Flow cytometry plots were analysed using the *FlowJo* software (*FlowJo, LLC*).

Magnetism associated cell sorting:

Magnetism associated cell sorting (MACS) was used to purify mouse PGCs from total genital ridge cells. A single cell suspension was created as described above. After counting the cells, MACS was performed according to manufacturer's instructions (Miltenyi Biotec). Briefly, cells were incubated in MACS buffer containing the primary antibody against the target surface protein for 30 minutes at 4°C, washed twice and incubated at 4°C for 15 minutes with magnetic microbeads directed against the primary antibody (Miltenyi #130047302). The cells were then passed through a magnetic column (Miltenyi #130-042-201) to retain the magnetically-labelled target cells and after removal of the magnet flushed out of the column. Target cells were then cultured as described in chapter 4.2.6. A list of antibodies used for this project is given in **Table III**.

4.2.9 PCR for sex determination of marmoset embryos

Isolation of genomic DNA:

Genomic DNA (gDNA) from marmoset embryo tissue was isolated using the DNeasy Blood and Tissue Kit (Qiagen # 69506) according to manufacturer's instructions.

Photometric quantification of nucleic acids:

Photometric quantification of nucleic acids was carried out with the Nano Photometer Pearl (IMPLEN, Munich) according to the manufacturer's instructions.

Amplification of target genes:

The target genes were amplified via polymerase chain reaction (PCR) using Taq Polymerase (NEB #M0273S) according to manufacturer's instructions. One PCR preparation of 25 µl total volume contained 200 ng of gDNA as well as 1x Taq standard buffer, 200 µM dNTPs (NEB #N0447S), 0.2 µM of each primer and 1.25 units of Taq polymerase. PCR reaction was carried out in a Biometra T300 Thermocycler under following conditions: Initial denaturation at 95°C for 30 seconds, followed by 35 cycles of denaturation at 95°C for 30 seconds, annealing at the respective appropriate temperature for 15 seconds and elongation at 68°C for

1 minute/kilobasepair. After a final extension at 68°C for 5 minutes samples were cooled down to 8°C. Primer sequences and annealing temperatures are given in **Table IV**. Annealing temperatures were calculated using the T_m calculator tool by ThermoFisher (https://www.thermofisher.com/de/de/home/brands/thermo-scientific/molecular-biology/molecular-biology-learning-center/molecular-biology-resource-library/thermo-scientific-web-tools/tm-calculator.html).

Table IV | Primer sequences for gDNA amplification

Target	Primer Name, Sequence (5' → 3')	PCR-Product	Annealing Temp.
Beta-Actin	G0334 fwd.: CAC TCT TCC AGC CTT CTT TCC G0335 rev.: GTG ATC TCC TTC TGC ATC CTG	177 bp	51°C
DDX3	G2108 fwd.: GGW CGR ACT CTA GAY CGG T G2109 rev.: GTR CAG ATC TAY GAG GAA GC	X = 176 bp Y = 137 bp	49°C

Agarose gel electrophoresis:

The amplified DNA fragments were separated according to their size in a 2 % (w/v) agarose gel. The agarose (Biozym) was boiled in 1x TAE buffer (Roth) until completely dissolved, and after cooling ethidium bromide was added to a final concentration of 1 µg/ml. The solution was poured into a tray and left to solidify for 15-30 minutes. The appropriate volume of loading dye (NEB #B7024S) was added to the DNA samples. As a size standard the Quick-Load 100 bp DNA Ladder (NEB #N0467S) was used. Electrophoresis was performed in 1x TAE buffer (Roth) at 100 V for 45 min in a Mupid$^©$-ex electrophoresis system. DNA bands were visualised under UV light (302 nm) in the Intas Gel Documentation Station (INTAS, Göttingen).

4.2.10 Analysis of gene expression of cultured cells

RNA isolation:

RNA was isolated from frozen cell pellets using the TRIzol/Chloroform method. All working steps were performed on ice. Briefly, 1 ml of TRIzol solution (Ambion by life technologies #15596026) was used to lyse the cell pellet in a Tissue Lyser LT (Qiagen) for 1 minute. 200 µl Chloroform (Merck) was added, the sample vortexed and incubated on ice for 10-15 minutes. Following centrifugation at 12000 g for 15 minutes, three phases had formed in the reaction tube. The upper phase containing the RNA was transferred to a new tube, 1 ml of

75 % EtOH was added and the sample incubated at -20°C for 30 minutes. After centrifugation at 12000 g for 10 minutes the resulting RNA-pellet was washed twice with 1 ml 75 % EtOH, dried and resuspended in 30 µl nuclease-free water (Qiagen #129115). To remove any traces of remaining DNA, the DNA-free kit (Invitrogen #AM1906) was used according to manufacturer's instructions.

cDNA generation:

To generate cDNA from isolated RNA, the Omniscript RT Kit (Qiagen, #205113) was used according to manufacturer's instructions. Additionally to the Oligo-dT primers from the kit, Random Hexamer Primers (Thermo Scientific #SO142) were added to a final concentration of 1 µM. For the reverse transcriptase (RT) reaction 1 µg of RNA was used, resulting in a final cDNA concentration of 50 ng/ml.

Real-time quantitative PCR:

Real-time quantitative PCR (qPCR) was performed on the StepOnePlus System (Applied Biosystems). For each qPCR reaction, 10 ng of template cDNA was mixed with Power SYBR green master mix (Applied Biosystems #4367659) and respective pimers with a final concentration of 600 nM. Sequences of the used primers can be found in **Table V**. All qPCR reactions were measured in technical triplicates to reduce technical measurement errors. The obtained data for each gene of interest was normalised against the housekeeping gene 18S rRNA. The collected qPCR data was analysed using *Microsoft Excel.*

Table V | Primer sequences for qPCR

Target	Primer Name, Sequence (5' → 3')
NANOG	G0883 fwd.: TCTTCAGCAGATGCAAGAACTTT
	G0884 rev.: GGTTTTGGAACCAGGTCTTCAC
OCT4	G0963 fwd.: GCCAGGGCTTTTAGGATTAAGTT
	G0964 rev.: TGCCCTCACCCTTTGTGTTC
18s rRNA	G1197 fwd.: CACCAAGAGGGCAGGAGAAC
	G1198 rev.: TGGATTCTGCATAATGGTGATCA

5. References

Note: This reference list was generated with the literature software *EndNote X8.*

1. Pinheiro, H.L.N. and A.R. Mendes Pontes, *Home Range, Diet, and Activity Patterns of Common Marmosets (Callithrix jacchus) in Very Small and Isolated Fragments of the Atlantic Forest of Northeastern Brazil.* International Journal of Ecology, 2015. **2015**: p. 13.

2. Ferrari, S.F. and M.A. Lopes Ferrari, *A re-evaluation of the social organisation of the Callitrichidae, with reference to the ecological differences between genera.* Folia Primatol (Basel), 1989. **52**(3-4): p. 132-47.

3. Ross, C.N., J.A. French, and G. Orti, *Germ-line chimerism and paternal care in marmosets (Callithrix kuhlii).* Proc Natl Acad Sci U S A, 2007. **104**(15): p. 6278-82.

4. O'Rahilly, R. and F. Muller, *Developmental stages in human embryos: revised and new measurements.* Cells Tissues Organs, 2010. **192**(2): p. 73-84.

5. Phillips, I.R., *The embryology of the common marmoset (Callithrix jacchus).* Adv Anat Embryol Cell Biol, 1976. **52**(5): p. 3-47.

6. Merker, H.-J., et al., *The Embryology of Callithrix jacchus*, in *Non-Human Primates - Developmental Biology and Toxicology*, D. Neubert, H.-J. Merker, and A.G. Hendrickx, Editors. 1988, Ueberreuter Wissenschaft: Wien; Berlin. p. 217 - 242.

7. Sasaki, K., et al., *The Germ Cell Fate of Cynomolgus Monkeys Is Specified in the Nascent Amnion.* Dev Cell, 2016. **39**(2): p. 169-185.

8. Chandolia, R.K., et al., *Changes in endocrine profile and reproductive organs during puberty in the male marmoset monkey (Callithrix jacchus).* Reproduction, 2006. **132**(2): p. 355-63.

9. Sasaki, E., et al., *Generation of transgenic non-human primates with germline transmission.* Nature, 2009. **459**(7246): p. 523-7.

10. Seferovic, M., et al., *Experimental Zika Virus Infection in the Pregnant Common Marmoset Induces Spontaneous Fetal Loss and Neurodevelopmental Abnormalities.* Sci Rep, 2018. **8**(1): p. 6851.

11. Hikishima, K., et al., *Atlas of the developing brain of the marmoset monkey constructed using magnetic resonance histology.* Neuroscience, 2013. **230**: p. 102-13.

12. Wu, A., et al., *Characterization of mammary epithelial stem/progenitor cells and their changes with aging in common marmosets.* Sci Rep, 2016. **6**: p. 32190.

13. Debowski, K., et al., *Non-viral generation of marmoset monkey iPS cells by a six-factor-in-one-vector approach.* PLoS One, 2015. **10**(3): p. e0118424.

14. Debowski, K., et al., *The transcriptomes of novel marmoset monkey embryonic stem cell lines reflect distinct genomic features.* Sci Rep, 2016. **6**: p. 29122.

15. Takahashi, T., et al., *Birth of healthy offspring following ICSI in in vitro-matured common marmoset (Callithrix jacchus) oocytes.* PLoS One, 2014. **9**(4): p. e95560.

16. Aeckerle, N., et al., *Primordial germ cell development in the marmoset monkey as revealed by pluripotency factor expression: suggestion of a novel model of embryonic germ cell translocation.* Mol Hum Reprod, 2015. **21**(1): p. 66-80.

17. Abbott, D.H., et al., *Aspects of common marmoset basic biology and life history important for biomedical research.* Comp Med, 2003. **53**(4): p. 339-50.

18. Vijaykumar, T., et al., *Bisphenol A-induced ultrastructural changes in the testes of common marmoset.* Indian J Med Res, 2017. **146**(1): p. 126-137.

19. Philippens, I.H., et al., *Acceleration of Amyloidosis by Inflammation in the Amyloid-Beta Marmoset Monkey Model of Alzheimer's Disease.* J Alzheimers Dis, 2017. **55**(1): p. 101-113.

20. Yasue, M., et al., *Inequity aversion is observed in common marmosets but not in marmoset models of autism induced by prenatal exposure to valproic acid.* Behav Brain Res, 2018. **343**: p. 36-40.

21. *The common marmoset genome provides insight into primate biology and evolution.* Nat Genet, 2014. **46**(8): p. 850-7.

22. Liu, Z., et al., *Cloning of Macaque Monkeys by Somatic Cell Nuclear Transfer.* Cell, 2018. **172**(4): p. 881-887.e7.

23.   Phillips, K.A., et al., *Why primate models matter.* Am J Primatol, 2014. **76**(9): p. 801-27.

24.   Hummeler, K., et al., *Encephalomyelitis due to infection with Herpesvirus simiae (herpes B virus); a report of two fatal, laboratory-acquired cases.* N Engl J Med, 1959. **261**(2): p. 64-8.

25.   Sariol, C.A., et al., *Herpes B-virus seroreactivity in a colony of Macaca mulatta: data from the Sabana Seca Field Station, a new specific pathogen-free program.* J Med Primatol, 2005. **34**(1): p. 13-9.

26.   Oatley, J.M. and R.L. Brinster, *[11] - Spermatogonial Stem Cells*, in *Methods in Enzymology*, I. Klimanskaya and R. Lanza, Editors. 2006, Academic Press. p. 259-282.

27.   Hermo, L., et al., *Surfing the wave, cycle, life history, and genes/proteins expressed by testicular germ cells. Part 1: background to spermatogenesis, spermatogonia, and spermatocytes.* Microsc Res Tech, 2010. **73**(4): p. 241-78.

28.   Gupta, G., et al., *Seasonal variations in daily sperm production rate of rhesus and bonnet monkeys.* J Med Primatol, 2000. **29**(6): p. 411-4.

29.   Fereydouni, B., et al., *The neonatal marmoset monkey ovary is very primitive exhibiting many oogonia.* Reproduction, 2014. **148**(2): p. 237-47.

30.   Johnson, W.H., et al., *Production of four identical calves by the separation of blastomeres from an in vitro derived four-cell embryo.* Vet Rec, 1995. **137**(1): p. 15-6.

31.   Tarkowski, A.K., *Experiments on the development of isolated blastomers of mouse eggs.* Nature, 1959. **184**: p. 1286-7.

32.   Mitalipov, S.M., et al., *Monozygotic twinning in rhesus monkeys by manipulation of in vitro-derived embryos.* Biol Reprod, 2002. **66**(5): p. 1449-55.

33.   Mitalipov, S. and D. Wolf, *Totipotency, Pluripotency and Nuclear Reprogramming.* Advances in biochemical engineering/biotechnology, 2009. **114**: p. 185-199.

34.   Gardner, R.L. and J. Rossant, *Investigation of the fate of 4-5 day post-coitum mouse inner cell mass cells by blastocyst injection.* J Embryol Exp Morphol, 1979. **52**: p. 141-52.

35.   Evans, M.J. and M.H. Kaufman, *Establishment in culture of pluripotential cells from mouse embryos.* Nature, 1981. **292**(5819): p. 154-6.

36.   Martin, G.R., *Isolation of a pluripotent cell line from early mouse embryos cultured in medium conditioned by teratocarcinoma stem cells.* Proc Natl Acad Sci U S A, 1981. **78**(12): p. 7634-8.

37.   Thomson, J.A., et al., *Isolation of a primate embryonic stem cell line.* Proc Natl Acad Sci U S A, 1995. **92**(17): p. 7844-8.

38.   Thomson, J.A., et al., *Pluripotent cell lines derived from common marmoset (Callithrix jacchus) blastocysts.* Biol Reprod, 1996. **55**(2): p. 254-9.

39.   Thomson, J.A., et al., *Embryonic stem cell lines derived from human blastocysts.* Science, 1998. **282**(5391): p. 1145-7.

40.   Hartman, M.E., D.F. Dai, and M.A. Laflamme, *Human pluripotent stem cells: Prospects and challenges as a source of cardiomyocytes for in vitro modeling and cell-based cardiac repair.* Adv Drug Deliv Rev, 2016. **96**: p. 3-17.

41.   Loring, J.F., *Autologous Induced Pluripotent Stem Cell-Derived Neurons to Treat Parkinson's Disease.* Stem Cells Dev, 2018. **27**(14): p. 958-959.

42.   Farrer, L.A. and M.M. DeAngelis, *Human induced pluripotent stem cells illuminate pathways and novel treatment targets for age-related macular degeneration.* Stem Cell Investig, 2017. **4**: p. 92.

43.   Simonson, O.E., et al., *The safety of human pluripotent stem cells in clinical treatment.* Ann Med, 2015. **47**(5): p. 370-80.

44.   Takahashi, K. and S. Yamanaka, *Induction of pluripotent stem cells from mouse embryonic and adult fibroblast cultures by defined factors.* Cell, 2006. **126**(4): p. 663-76.

45.   Okita, K., T. Ichisaka, and S. Yamanaka, *Generation of germline-competent induced pluripotent stem cells.* Nature, 2007. **448**(7151): p. 313-7.

46.   Kang, L. and S. Gao, *Generation of Viable Mice from Induced Pluripotent Stem Cells (iPSCs) Through Tetraploid Complementation.* Methods Mol Biol, 2015. **1330**: p. 125-32.

47.   Takahashi, K., et al., *Induction of pluripotent stem cells from adult human fibroblasts by defined factors.* Cell, 2007. **131**(5): p. 861-72.

48.   Yu, J., et al., *Induced pluripotent stem cell lines derived from human somatic cells.* Science, 2007. **318**(5858): p. 1917-20.

49. Staerk, J., et al., *Reprogramming of human peripheral blood cells to induced pluripotent stem cells.* Cell Stem Cell, 2010. **7**(1): p. 20-4.

50. Zhou, T., et al., *Generation of human induced pluripotent stem cells from urine samples.* Nat Protoc, 2012. **7**(12): p. 2080-9.

51. Kanatsu-Shinohara, M., et al., *Generation of pluripotent stem cells from neonatal mouse testis.* Cell, 2004. **119**(7): p. 1001-12.

52. Guan, K., et al., *Pluripotency of spermatogonial stem cells from adult mouse testis.* Nature, 2006. **440**(7088): p. 1199-203.

53. Ko, K., et al., *Induction of pluripotency in adult unipotent germline stem cells.* Cell Stem Cell, 2009. **5**(1): p. 87-96.

54. Kossack, N., et al., *Isolation and characterization of pluripotent human spermatogonial stem cell-derived cells.* Stem Cells, 2009. **27**(1): p. 138-49.

55. Golestaneh, N., et al., *Pluripotent stem cells derived from adult human testes.* Stem Cells Dev, 2009. **18**(8): p. 1115-26.

56. Mizrak, S.C., et al., *Embryonic stem cell-like cells derived from adult human testis.* Hum Reprod, 2010. **25**(1): p. 158-67.

57. Lim, J.J., et al., *In vitro culture-induced pluripotency of human spermatogonial stem cells.* Biomed Res Int, 2013. **2013**: p. 143028.

58. Stimpfel, M., et al., *Isolation, characterization and differentiation of cells expressing pluripotent/multipotent markers from adult human ovaries.* Cell Tissue Res, 2013. **354**(2): p. 593-607.

59. Eildermann, K., J. Gromoll, and R. Behr, *Misleading and reliable markers to differentiate between primate testis-derived multipotent stromal cells and spermatogonia in culture.* Hum Reprod, 2012. **27**(6): p. 1754-67.

60. Fereydouni, B., et al., *Long-Term Oocyte-Like Cell Development in Cultures Derived from Neonatal Marmoset Monkey Ovary.* Stem Cells Int, 2016. **2016**: p. 2480298.

61. Witschi, E., *Migration of the germ cells of human embryos from the yolk sac to the primitive gonadal folds.* Contributions to embryology, 1948. **209**.

62. Lawson, K.A., et al., *Bmp4 is required for the generation of primordial germ cells in the mouse embryo.* Genes Dev, 1999. **13**(4): p. 424-36.

63. Saitou, M., S. Kagiwada, and K. Kurimoto, *Epigenetic reprogramming in mouse pre-implantation development and primordial germ cells.* Development, 2012. **139**(1): p. 15-31.

64. Kehler, J., et al., *Oct4 is required for primordial germ cell survival.* EMBO Rep, 2004. **5**(11): p. 1078-83.

65. Chambers, I., et al., *Nanog safeguards pluripotency and mediates germline development.* Nature, 2007. **450**(7173): p. 1230-4.

66. Campolo, F., et al., *Essential role of Sox2 for the establishment and maintenance of the germ cell line.* Stem Cells, 2013. **31**(7): p. 1408-21.

67. Leitch, H.G. and A. Smith, *The mammalian germline as a pluripotency cycle.* Development, 2013. **140**(12): p. 2495-501.

68. De Miguel, M., et al., *Techniques and Conditions for Embryonic Germ Cell Derivation and Culture*, in *Embryonic Stem Cells - Basic Biology to Bioengineering*, M. Kallos, Editor. 2011, InTech.

69. Sharova, L.V., et al., *Global gene expression profiling reveals similarities and differences among mouse pluripotent stem cells of different origins and strains.* Dev Biol, 2007. **307**(2): p. 446-59.

70. Felix, W., *Entwicklung der Harn- und Geschlechtsorgane*, in *Keibel-Malls Handbuch der Entwicklungsgeschichte des Menschen*. 1911: Leipzig.

71. Fuss, A., *Über die Geschlechtszellen des Menschen und der Säugetiere*. 1912: Cohen.

72. Politzer, G., *Die Keimbahn des Menschen.* Zeitschr Anat Entwicklungsgesch, 1933(100): p. 331-361.

73. McKay, D., et al., *Histochemical observations on the germ cells of human embryos*, H.M.S. Department of Pathology, Editor. 1953: Boston.

74. Kerr, C.L., et al., *Expression of pluripotent stem cell markers in the human fetal ovary.* Hum Reprod, 2008. **23**(3): p. 589-99.

75. De Felici, M., *Origin, migration, and proliferation of human primordial germ cells*, in *Oogenesis*, G. Coticchio, D. Albertini, and L. DeSantis, Editors. 2013, Springer-Verlag: London.

76. Irie, N., et al., *SOX17 is a critical specifier of human primordial germ cell fate.* Cell, 2015. **160**(1-2): p. 253-68.

77. Sugawa, F., et al., *Human primordial germ cell commitment in vitro associates with a unique PRDM14 expression profile.* Embo j, 2015. **34**(8): p. 1009-24.

78. de Jong, J., et al., *Differential expression of SOX17 and SOX2 in germ cells and stem cells has biological and clinical implications.* J Pathol, 2008. **215**(1): p. 21-30.

79. Perrett, R.M., et al., *The early human germ cell lineage does not express SOX2 during in vivo development or upon in vitro culture.* Biol Reprod, 2008. **78**(5): p. 852-8.

80. Evans, T., et al., *Acquisition of germ plasm accelerates vertebrate evolution.* Science, 2014. **344**(6180): p. 200-3.

81. Ginsburg, M., M.H. Snow, and A. McLaren, *Primordial germ cells in the mouse embryo during gastrulation.* Development, 1990. **110**(2): p. 521-8.

82. Saitou, M. and M. Yamaji, *Germ cell specification in mice: signaling, transcription regulation, and epigenetic consequences.* Reproduction, 2010. **139**(6): p. 931-42.

83. Kanai-Azuma, M., et al., *Depletion of definitive gut endoderm in Sox17-null mutant mice.* Development, 2002. **129**(10): p. 2367-79.

84. Niakan, K.K., et al., *Sox17 promotes differentiation in mouse embryonic stem cells by directly regulating extraembryonic gene expression and indirectly antagonizing self-renewal.* Genes Dev, 2010. **24**(3): p. 312-26.

85. Ohinata, Y., et al., *Blimp1 is a critical determinant of the germ cell lineage in mice.* Nature, 2005. **436**(7048): p. 207-13.

86. McLaren, A., *Primordial germ cells in the mouse.* Dev Biol, 2003. **262**(1): p. 1-15.

87. Freeman, B., *The active migration of germ cells in the embryos of mice and men is a myth.* Reproduction, 2003. **125**(5): p. 635-43.

88. Molyneaux, K.A., et al., *Time-lapse analysis of living mouse germ cell migration.* Dev Biol, 2001. **240**(2): p. 488-98.

89. Godin, I. and C.C. Wylie, *TGF beta 1 inhibits proliferation and has a chemotropic effect on mouse primordial germ cells in culture.* Development, 1991. **113**(4): p. 1451-7.

90. Bucay, N., et al., *A novel approach for the derivation of putative primordial germ cells and sertoli cells from human embryonic stem cells.* Stem Cells, 2009. **27**(1): p. 68-77.

91. Doitsidou, M., et al., *Guidance of primordial germ cell migration by the chemokine SDF-1.* Cell, 2002. **111**(5): p. 647-59.

92. Farini, D., et al., *Chemoattractant action and molecular signaling pathways of Kit ligand on mouse primordial germ cells.* Dev Biol, 2007. **306**(2): p. 572-83.

93. Hoyer, P.E., A.G. Byskov, and K. Mollgard, *Stem cell factor and c-Kit in human primordial germ cells and fetal ovaries.* Mol Cell Endocrinol, 2005. **234**(1-2): p. 1-10.

94. Mollgard, K., et al., *Human primordial germ cells migrate along nerve fibers and Schwann cells from the dorsal hind gut mesentery to the gonadal ridge.* Mol Hum Reprod, 2010. **16**(9): p. 621-31.

95. Matsui, Y., et al., *Effect of Steel factor and leukaemia inhibitory factor on murine primordial germ cells in culture.* Nature, 1991. **353**(6346): p. 750-2.

96. Donovan, P.J., et al., *Migratory and postmigratory mouse primordial germ cells behave differently in culture.* Cell, 1986. **44**(6): p. 831-8.

97. Matsui, Y., K. Zsebo, and B.L. Hogan, *Derivation of pluripotential embryonic stem cells from murine primordial germ cells in culture.* Cell, 1992. **70**(5): p. 841-7.

98. Resnick, J.L., et al., *Long-term proliferation of mouse primordial germ cells in culture.* Nature, 1992. **359**(6395): p. 550-1.

99. Dolci, S., et al., *Requirement for mast cell growth factor for primordial germ cell survival in culture.* Nature, 1991. **352**(6338): p. 809-11.

100. Godin, I., et al., *Effects of the steel gene product on mouse primordial germ cells in culture.* Nature, 1991. **352**(6338): p. 807-9.

101. Durcova-Hills, G. and A. Surani, *Reprogramming primordial germ cells (PGC) to embryonic germ (EG) cells.* Curr Protoc Stem Cell Biol, 2008. **Chapter 1**: p. Unit1A.3.

102. Leitch, H.G., et al., *Rebuilding pluripotency from primordial germ cells.* Stem Cell Reports, 2013. **1**(1): p. 66-78.

103. Stewart, C.L., I. Gadi, and H. Bhatt, *Stem cells from primordial germ cells can reenter the germ line.* Dev Biol, 1994. **161**(2): p. 626-8.

104. Shamblott, M.J., et al., *Derivation of pluripotent stem cells from cultured human primordial germ cells.* Proc Natl Acad Sci U S A, 1998. **95**(23): p. 13726-31.

105. Turnpenny, L., et al., *Derivation of human embryonic germ cells: an alternative source of pluripotent stem cells.* Stem Cells, 2003. **21**(5): p. 598-609.

106. Liu, S., et al., *Human embryonic germ cells isolation from early stages of post-implantation embryos.* Cell Tissue Res, 2004. **318**(3): p. 525-31.

107. Kerr, D.A., et al., *Human embryonic germ cell derivatives facilitate motor recovery of rats with diffuse motor neuron injury.* J Neurosci, 2003. **23**(12): p. 5131-40.

108. Frimberger, D., et al., *Human embryoid body-derived stem cells in bladder regeneration using rodent model.* Urology, 2005. **65**(4): p. 827-32.

109. Yu, S., et al., *Differentiation of human embryonic germ cells and transplantation in rats with acute myocardial infarction.* Exp Ther Med, 2014. **7**(3): p. 615-620.

110. Zhang, L., et al., *SOX17 Regulates Conversion of Human Fibroblasts Into Endothelial Cells and Erythroblasts by Dedifferentiation Into CD34(+) Progenitor Cells.* Circulation, 2017. **135**(25): p. 2505-2523.

111. Saito, K., et al., *Maintenance of hematopoietic stem and progenitor cells in fetal intra-aortic hematopoietic clusters by the Sox17-Notch1-Hes1 axis.* Exp Cell Res, 2018. **365**(1): p. 145-155.

112. Tang, C., et al., *An antibody against SSEA-5 glycan on human pluripotent stem cells enables removal of teratoma-forming cells.* Nat Biotechnol, 2011. **29**(9): p. 829-34.

113. Ezeh, U.I., et al., *Human embryonic stem cell genes OCT4, NANOG, STELLAR, and GDF3 are expressed in both seminoma and breast carcinoma.* Cancer, 2005. **104**(10): p. 2255-65.

114. Wakayama, T., et al., *The expression of platelet endothelial cell adhesion molecule-1 in mouse primordial germ cells during their migration and early gonadal formation.* Histochem Cell Biol, 2003. **119**(5): p. 355-62.

115. Boroviak, T., et al., *Lineage-Specific Profiling Delineates the Emergence and Progression of Naive Pluripotency in Mammalian Embryogenesis.* Dev Cell, 2015. **35**(3): p. 366-82.

116. Neubert, D., et al., *Variability and Speed of Development in Marmosets as Compared to Man*, in *Non-Human Primates - Developmental Biology and Toxicology*, D. Neubert, H.-J. Merker, and A.G. Hendrickx, Editors. 1988, Ueberreuter Wissenschaft: Wien, Berlin.

117. Perfetto, S.P., et al., *Amine-reactive dyes for dead cell discrimination in fixed samples.* Curr Protoc Cytom, 2010. **Chapter 9**: p. Unit 9.34.

118. Murdoch, S., et al., *Mutations in NALP7 cause recurrent hydatidiform moles and reproductive wastage in humans.* Nat Genet, 2006. **38**(3): p. 300-2.

119. Sanchez-Delgado, M., et al., *Absence of Maternal Methylation in Biparental Hydatidiform Moles from Women with NLRP7 Maternal-Effect Mutations Reveals Widespread Placenta-Specific Imprinting.* PLoS Genet, 2015. **11**(11): p. e1005644.

120. Zhang, P., et al., *Expression analysis of the NLRP gene family suggests a role in human preimplantation development.* PLoS One, 2008. **3**(7): p. e2755.

121. Duenez-Guzman, E.A. and D. Haig, *The evolution of reproduction-related NLRP genes.* J Mol Evol, 2014. **78**(3-4): p. 194-201.

122. Rampoldi, A., et al., *Targeted Elimination of Tumorigenic Human Pluripotent Stem Cells Using Suicide-Inducing Virus-like Particles.* ACS Chem Biol, 2018. **13**(8): p. 2329-2338.

123. Stewart, C.L., et al., *Blastocyst implantation depends on maternal expression of leukaemia inhibitory factor.* Nature, 1992. **359**: p. 76.

124. Xu, J., et al., *Role of leukaemia inhibitory factor in the induction of pluripotent stem cells in mice.* Cell Biol Int, 2010. **34**(8): p. 791-7.

125. Pereira, R.C., A.N. Economides, and E. Canalis, *Bone Morphogenetic Proteins Induce Gremlin, a Protein That Limits Their Activity in Osteoblasts**This work was supported by NIAMSD Grant AR-21707.* Endocrinology, 2000. **141**(12): p. 4558-4563.

126. Liu, Y., et al., *A novel chemical-defined medium with bFGF and N2B27 supplements supports undifferentiated growth in human embryonic stem cells.* Biochemical and Biophysical Research Communications, 2006. **346**(1): p. 131-139.

127. Choi, K.H., et al., *FGF2 Signaling Plays an Important Role in Maintaining Pluripotent State of Pig Embryonic Germ Cells.* Cell Reprogram, 2018.

128.   Tienari, J., et al., *Fibroblast growth factor-mediated stimulation of differentiating teratocarcinoma cells: evidence for paracrine growth regulation.* Differentiation, 1995. **59**(3): p. 193-9.

129.   Alasbahi, R.H. and M.F. Melzig, *Forskolin and derivatives as tools for studying the role of cAMP.* Pharmazie, 2012. **67**(1): p. 5-13.

130.   Naujok, O., et al., *Cytotoxicity and activation of the Wnt/beta-catenin pathway in mouse embryonic stem cells treated with four GSK3 inhibitors.* BMC Res Notes, 2014. **7**: p. 273.

131.   Brown, A.P., et al., *Pharmacodynamic and toxicokinetic evaluation of the novel MEK inhibitor, PD0325901, in the rat following oral and intravenous administration.* Cancer Chemother Pharmacol, 2007. **59**(5): p. 671-9.

132.   Sebolt-Leopold, J.S., *Advances in the development of cancer therapeutics directed against the RAS-mitogen-activated protein kinase pathway.* Clin Cancer Res, 2008. **14**(12): p. 3651-6.

133.   Hastreiter, S., et al., *Inductive and Selective Effects of GSK3 and MEK Inhibition on Nanog Heterogeneity in Embryonic Stem Cells.* Stem Cell Reports, 2018. **11**(1): p. 58-69.

134.   Verma, V., et al., *Dual kinase inhibition promotes pluripotency in finite bovine embryonic cell lines.* Stem Cells Dev, 2013. **22**(11): p. 1728-42.

135.   Van der Jeught, M., et al., *Application Of Small Molecules Favoring Naive Pluripotency during Human Embryonic Stem Cell Derivation.* Cell Reprogram, 2015. **17**(3): p. 170-80.

136.   Ying, Q.-L., et al., *The ground state of embryonic stem cell self-renewal.* Nature, 2008. **453**: p. 519.

137.   Zhou, Q., et al., *Complete Meiosis from Embryonic Stem Cell-Derived Germ Cells In Vitro.* Cell Stem Cell, 2016. **18**(3): p. 330-40.

138.   Conrad, S., et al., *Generation of pluripotent stem cells from adult human testis.* Nature, 2008. **456**(7220): p. 344-9.

139.   Chikhovskaya, J.V., et al., *Human testis-derived embryonic stem cell-like cells are not pluripotent, but possess potential of mesenchymal progenitors.* Hum Reprod, 2012. **27**(1): p. 210-21.

140.   Tapia, N., et al., *Concise review: challenging the pluripotency of human testis-derived ESC-like cells.* Stem Cells, 2011. **29**(8): p. 1165-9.

141.   Turnpenny, L. and N. Hanley, *Culture of the Human Germ Cell Lineage*, in *Culture of Human Stem Cells*, I. Freshney, G. Stacey, and J. Auerbach, Editors. 2007, John Wiley & Sons, Inc.

142.   Knaut, H., et al., *A zebrafish homologue of the chemokine receptor Cxcr4 is a germ-cell guidance receptor.* Nature, 2003. **421**(6920): p. 279-82.

143.   Mahabaleshwar, H., B. Boldajipour, and E. Raz, *Killing the messenger: The role of CXCR7 in regulating primordial germ cell migration.* Cell Adh Migr, 2008. **2**(2): p. 69-70.

144.   Durcova-Hills, G., et al., *The role of exogenous fibroblast growth factor-2 on the reprogramming of primordial germ cells into pluripotent stem cells.* Stem Cells, 2006. **24**(6): p. 1441-9.

145.   Anderson, R., et al., *Expression of the homophilic adhesion molecule, Ep-CAM, in the mammalian germ line.* J Reprod Fertil, 1999. **116**(2): p. 379-84.

146.   Polanco, J.C., et al., *Enrichment and purging of human embryonic stem cells by detection of cell surface antigens using the monoclonal antibodies TG30 and GCTM-2.* J Vis Exp, 2013(82): p. 50856.

147.   Schopperle, W.M., D.B. Kershaw, and W.C. DeWolf, *Human embryonal carcinoma tumor antigen, Gp200/GCTM-2, is podocalyxin.* Biochem Biophys Res Commun, 2003. **300**(2): p. 285-90.

148.   Kang, L., et al., *The Universal 3D3 Antibody of Human PODXL Is Pluripotent Cytotoxic, and Identifies a Residual Population After Extended Differentiation of Pluripotent Stem Cells.* Stem Cells Dev, 2016. **25**(7): p. 556-68.

149.   Jin, Z.W., et al., *A comparison between D2-40 and c-KIT immunohistochemistry for the human fetal testis and ovary at the second trimester of gestation.* Okajimas Folia Anat Jpn, 2010. **87**(1): p. 1-4.

150.   Kanatsu-Shinohara, M., S. Toyokuni, and T. Shinohara, *CD9 is a surface marker on mouse and rat male germline stem cells.* Biol Reprod, 2004. **70**(1): p. 70-5.

151.   Behr, R., *Characteristic Features of Male Germline Development in Primates*, in *Genetics of Human Infertility*, P. Vogt, Editor. 2017, S. Karger AG: Basel.